

A Computational and Theoretical Study of Conductance in Hydrogen-bonded
Molecular Junctions

by

Micah Wimmer

A Dissertation Presented in Partial Fulfillment
of the Requirements for the Degree
Doctor of Philosophy

Approved April 2017 by the
Graduate Supervisory Committee:

Vladimiro Mujica, Chair
George Wolf
Andrew Chizmeshya

ARIZONA STATE UNIVERSITY

May 2017

ABSTRACT

This thesis is devoted to the theoretical and computational study of electron transport in molecular junctions where one or more hydrogen bonds are involved in the process. While electron transport through covalent bonds has been extensively studied, in recent work the focus has been shifted towards hydrogen-bonded systems due to their ubiquitous presence in biological systems and their potential in forming nano-junctions between molecular electronic devices and biological systems.

This analysis allows us to significantly expand our comprehension of the experimentally observed result that the inclusion of hydrogen bonding in a molecular junction significantly impacts its transport properties, a fact that has important implications for our understanding of transport through DNA, and nano-biological interfaces in general. In part of this work I have explored the implications of quasideviant transport in short chains of weakly-bonded molecular junctions involving hydrogen bonds. I used theoretical and computational analysis to interpret recent experiments and explain the role of Fano resonances in the transmission properties of the junction.

In a different direction, I have undertaken the study of the transversal conduction through nucleotide chains that involve a variable number of different hydrogen bonds, e.g. $\text{NH}\cdots\text{O}$, $\text{OH}\cdots\text{O}$, and $\text{NH}\cdots\text{N}$, which are the three most prevalent hydrogen bonds in biological systems and organic electronics. My effort here has focused on the analysis of electronic descriptors that allow a simplified conceptual and computational understanding of transport properties. Specifically, I have expanded our previous work where the molecular polarizability was used as a conductance descriptor to include the possibility of atomic and bond partitions of the molecular polarizability. This is important because it affords an alternative molecular description of conductance that is not based on the conventional view of molecular orbitals as transport channels. My findings suggest that the hydrogen-bond networks are crucial

in understanding the conductance of these junctions.

A broader impact of this work pertains the fact that characterizing transport through hydrogen bonding networks may help in developing faster and cost-effective approaches to personalized medicine, to advance DNA sequencing and implantable electronics, and to progress in the design and application of new drugs.

To Dziadzia.

ACKNOWLEDGMENTS

*“I believe, that as the methods of structural chemistry are further applied to physiological problems it will be found that the significance of the hydrogen bond for physiology is greater than that of any other single structural feature.”*¹

This work would not have been possible without the professional and personal support of my advisor and friend, Dr. Vladimiro Mujica who promoted a free-thinking environment and thoughtful discussions both domestically and internationally. I am also indebted to Dr. Tarakeshwar Pilarisetty, Dr. Julio Palma, Dr. Shobeir Mazinani, and Reza Vatan Meidanshahi for their advice, support, and guidance during my PhD program.

I am also grateful to those with whom I have had the pleasure of working with during my program, including visiting professors and students. Each of the members of my Dissertation Committee provided me with extensive personal and professional guidance (both in my undergraduate studies and graduate work). Their contributions have helped to further craft my scientific discipline and I have learned how to be a better researcher as a result of their patience and guidance.

My time at Arizona State University has been made more enjoyable through my relationships with the unsung heroes of the School of Molecular Sciences - the various support staff that have come and gone throughout the years. I am thankful for my many conversations with Jo Anne Sercl, the unwavering support of Mary Ann Bucciarelli, and the many smiles of Waunita Parrill. I also wouldn't be graduating without the support of my undergraduate advisor Amber Soergel. Last, the business

¹Linus Pauling - The Nature of the Chemical Bond, 1939

aspects of research would have been more complicated if not for the assistance of Ziva Lackoff and Sarah Montgomery.

I am also eternally grateful to those that showed me that the field of chemistry could be as thrilling as mathematics and helped me transition my undergraduate major early in my academic career. While there are too many to mention, I would like to specially thank Dr. Ron Briggs, Dr. Jennifer Morgan, and Dr. Sarah Staton.

There were also those that have been vitally important to my sanity during graduate school. I don't know if I would have completed my degree without the wise counsel of Dr. Anne Jones, the comedy of Gabi Montañez and Curtis Pettit, the support of Eric and Rachel Hannah, the critiques of Hagit Levin, the whimsy of Maura, and the professional opportunities offered by Dr. James Klemaszewski. I am also thankful to my Brothers of Masonry who stood by me during the highs and lows (they specifically know who they are!).

I simply would not have made it to graduate school without the input of three amazing people. The first is my grandfather who raised me to understand that there is no path in life but that of hard work and perseverance. Without him and my late grandmother I would not have had the privilege of academic pursuit. Next, I would never have believed in my abilities if not for my high school geometry teacher Ms. Gail Tibbals who took a chance on me and gave me an opportunity that forever changed my life.

Nobody has been more important to me in the pursuit of this project than my wife, Andrea. If not for her eternal love (and patience!), I may not have completed this endeavor. She has inspired me to be better every day and I simply owe her more than a few sentences could ever convey.

∴

TABLE OF CONTENTS

| | Page |
|--|------|
| LIST OF TABLES | ix |
| LIST OF FIGURES | x |
| CHAPTER | |
| 1 INTRODUCTION | 1 |
| 1.1 A Brief History of Molecular Electronics | 1 |
| 1.2 From Electron Transfer to Electron Transport | 6 |
| 1.3 Electron Transport in Molecular Junctions | 9 |
| 1.4 Potential Barriers and Tunneling | 11 |
| 1.5 Transport Through Weak Bonds | 14 |
| 1.6 Quality of Bonds | 15 |
| 1.7 Hydrogen Bonding | 15 |
| 1.8 Polarizability as a Descriptor for Conductance | 22 |
| 2 THEORETICAL AND COMPUTATIONAL METHODOLOGY | 25 |
| 2.1 Standard Electron Transfer Theory | 25 |
| 2.2 Transmission Between Conducting Leads | 28 |
| 2.3 The Landauer Formula | 30 |
| 2.4 Molecular Conduction | 32 |
| 2.5 Conduction Channels | 34 |
| 2.6 Quantum Interference and Fano Resonances | 39 |
| 2.7 Polarizability | 43 |
| 3 CALCULATED PROPERTIES OF SELECTED MONOMERS | 48 |
| 3.1 Introduction | 48 |
| 3.2 Computational Methods | 48 |
| 3.3 Results and Discussion | 51 |

| CHAPTER | Page |
|---|------|
| 4 SINGLE-MOLECULE CONDUCTANCE THROUGH HYDROGEN BONDS. THE ROLE OF RESONANCES. | 59 |
| 4.1 Abstract | 59 |
| 4.2 Introduction..... | 60 |
| 4.3 Theory..... | 61 |
| 4.4 Computational Methods..... | 62 |
| 4.5 Results and Discussion | 65 |
| 5 CALCULATED PROPERTIES OF SELECTED DIMERS AND DNA/RNA BASE PAIRS | 72 |
| 5.1 Introduction..... | 72 |
| 5.2 Methods | 73 |
| 5.3 Results & Discussion | 74 |
| 6 CONCLUSIONS AND FUTURE WORK | 85 |
| 6.1 Future Work | 87 |
| REFERENCES | 89 |
| APPENDIX | |
| A COMPUTATION: THE NITTY-GRITTY | 100 |
| A.1 Computational Details | 101 |
| A.2 Relating to the Electrode..... | 101 |
| A.2.1 Sample Structure | 101 |
| A.2.2 XYZ Files -Electrode..... | 102 |
| A.3 Relating to Hydrogen Bonded Dimers | 103 |
| A.3.1 Sample Structure | 103 |
| A.3.2 XYZ Files - H4 Dimer..... | 104 |

| APPENDIX | Page |
|--|------|
| A.3.3 ORCA Input File - H4 Dimer Optimization | 105 |
| A.3.4 SIESTA Input FDF File - H4 Dimer | 106 |
| A.3.5 Gaussian 09 Input File - H4 Dimer Polarizability | 107 |
| A.4 Relating to Alkanes | 108 |
| A.4.1 Sample Structure | 108 |
| A.4.2 XYZ Files - A6 Alkane | 109 |
| A.4.3 ORCA Input File - A6 Optimization | 110 |
| A.4.4 SIESTA Input FDF File - A6 Alkane | 111 |
| A.5 Relating to Monomers | 112 |
| A.5.1 Sample Structure | 112 |
| A.5.2 XYZ File - Adenine | 112 |
| A.5.3 Gaussian 09 Input File - Adenine | 113 |
| A.6 Relating to DNA/RNA Base Pairs | 114 |
| A.6.1 Sample Structure | 114 |
| A.6.2 XYZ File - A-T Base Pair | 115 |
| A.6.3 Gaussian 09 Input File - A-T Base Pair | 117 |
| A.6.4 SIESTA Input FDF File - A-T Base Pair | 118 |
| A.6.5 Gaussian 09 Input File - A-T Base Pair | 119 |
| B REPRINT PERMISSIONS | 120 |
| B.1 Chapter 1 | 121 |
| B.2 Chapter 2 | 123 |
| B.3 Chapter 4 | 125 |

LIST OF TABLES

| Table | Page |
|---|------|
| 1.1 Hydrogen Bond Strengths Defined By Jeffrey [1] and Adapted from Steiner <i>et al.</i> [2] | 21 |
| 3.1 HOMO-LUMO Gap Energies of Considered Systems. | 51 |
| 3.2 Calculated Atomic Polarizability and Other Geometric Parameters in Comparison to Their $NH \cdots O$ Bond. | 54 |
| 3.3 Calculated Atomic Polarizability and Other Geometric Parameters in Comparison to Their $NH \cdots N$ Bond. | 54 |
| 3.4 Calculated Polarizabilities of Purine and Derivatives. | 56 |
| 3.5 Calculated Polarizabilities of Pyrimidine - Different Levels of Theory. ... | 57 |
| 3.6 Calculated Polarizabilities of Pyrimidine and Derivatives. | 58 |
| 5.1 Atomic Polarizability of the Hydrogen Acceptor Atom (α_O) in the Presence of EDG and EDW Groups. | 77 |
| 5.2 HOMO-LUMO Gap Energies of Considered Systems. | 79 |
| 5.3 Calculated Atomic Polarizability, Conductance, and Other Geometric Parameters of Different Systems from the Perspective of Their $NH \cdots O$ Bond. | 81 |
| 5.4 Calculated Atomic Polarizability, Conductance, and Other Geometric Parameters of Different Systems from the Perspective of Their $NH \cdots N$ Bond. | 82 |

LIST OF FIGURES

| Figure | Page |
|---|------|
| 1.1 Overview of Multimodal AFM and STM Techniques. Figure and Caption Reproduced from Ref. [3]. | 3 |
| 1.2 Comparison: Molecular Wire Transport and Nonadiabatic Intramolecular Electron Transfer. Figure Reproduced and Modified from Ref. [4] | 7 |
| 1.3 A Potential Barrier. | 12 |
| 1.4 Electron Tunneling Through a Barrier. | 14 |
| 1.5 Classical View of the Hydrogen Bond. Here, $d = \text{H} \cdots \text{O}$ Distance, and $D = \text{O} \cdots \text{O}$ Distance. Figure Reproduced from Ref. [2]. | 16 |
| 1.6 Comparing Hydrogen Bond Bridges. a) A Normal Hydrogen Bond with a Single Acceptor. b) Bifurcated Hydrogen Bond. c) Trifurcated Hydrogen Bond. Figure Reproduced from Ref. [2]. | 19 |
| 1.7 Electrostatic Potential Profile of a Molecular Junction for a) No Molecule Present, and b) Molecule Present. | 23 |
| 2.1 Common Types of Molecular Junctions with Transmission Profiles. (a) 2-Site, (b) T-Shaped, (c) Cyclic, and (d) Odd-membered Molecular Junctions. Figure Reproduced from Nozaki <i>et al.</i> [5]. | 40 |
| 2.2 Illustration of the Fano Formula (Equation 2.65) as a Superposition of the Lorentzian Line Shape of the Discrete Level with a Flat Continuous Background. Caption and Figure Adopted From Ref. [6]. | 43 |
| 2.3 Normalized Fano Profiles (1) with the Prefactor $1/(1 + q^2)$ (2) for Various Values of the Asymmetry Parameter q . Caption and Figure Adopted From Ref. [6] | 44 |

| Figure | Page |
|---|------|
| 3.1 (a) Measured Conductance (G) [7] Versus Total Polarizability. (b) Measured Conductance (G) [7] Versus the Polarizability of the Proton Acceptor Atom in the $\text{NH}\cdots\text{O}$ Bond. Here, O is the Proton Acceptor. | 53 |
| 3.2 Purine and Its Derivatives. Nitrogen Atoms in the 6-Membered Ring are Labeled A and B; All Nitrogen Atoms in the 5-Membered Ring are Labeled C and D. | 55 |
| 3.3 Pyrimidine and Derivatives. | 57 |
| 3.4 Summary of Results for Monomer Structures. | 58 |
| 4.1 Original TOC Graphic. | 59 |
| 4.2 Considered Systems and Electrode Setup | 64 |
| 4.3 Natural Log of Conductance Verses S-S Distance of H-bonded (Pink Circles) and Alkane Systems (Blue Squares). The H-bonded Systems Have an Increased Conductance Over the Alkanes Until the Turnover Regime at Approximately 17 Å. The Beta Decay Factor is $1.32 \pm 0.18 \text{ \AA}^{-1}$ for the H-bonded Systems and $0.95 \pm 0.15 \text{ \AA}^{-1}$ for the Alkanes.... | 66 |
| 4.4 Panel A - Log of the Transmission as a Function of Energy of the H-bonded Systems Showing a Distinct Peak at the Fermi Energy. Panel B - Log of the Transmission as a Function of Energy of the Alkane Systems. | 67 |
| 4.5 Density of States for the Shortest H-bonded Structure (H4). Red Line - DOS Including Gold Atoms of the Electrodes. Black Line - DOS Excluding Gold Atoms of the Electrodes. | 68 |

| Figure | Page |
|--|------|
| 4.6 Panel A - DOS of the H-bonded Systems. Inset Shows the Region Around the Fermi Energy Magnified. Panel B - DOS of the Alkane Systems. | 69 |
| 4.7 Transmission Function Comparing the Modified H-bond Lengths..... | 70 |
| 5.1 H-bonded Dimers Considered in This Section | 75 |
| 5.2 Conductance (G) Versus Total (a) and Acceptor Atom (b) Atomic Polarizabilities for the H-Bonded Systems. | 76 |
| 5.3 H4 and CH ₃ Modified Terminal Groups. | 77 |
| 5.4 Transmission Curves for the A-T, A-U, and G-C Systems. | 78 |
| 5.5 Calculated Conductance (G) Versus Total Polarizability for A-T, A-U, and C-G. | 80 |
| 5.6 Atomic Polarizabilities of Atoms Participating in the Junction Between Nucleotides. The Images Located on the Left of each Panel Shows the Values of Each Atom in the Junction When the Base Pairs are Analyzed Together. Images on the Left of Each Panel are the Values of the Same Structures as Monomers. | 81 |
| 5.7 Summary of Results - Hydrogen Bonded Dimers. | 83 |
| 5.8 Summary of Results - DNA/RNA Basepairs..... | 84 |
| 6.1 Summary of Polarizability Studies. | 87 |
| A.1 Structure of the Electrode | 101 |
| A.2 Electrode Structure's XYZ Files | 102 |
| A.3 Structure of H4 | 103 |
| A.4 H4 Between Electrodes | 103 |
| A.5 H4 Structure's XYZ Files | 104 |

| Figure | Page |
|---|------|
| A.6 H4 ORCA Input File | 105 |
| A.7 H4 FDF File for Electronic Structure Calculations..... | 106 |
| A.8 H4 Gaussian 09 Input File | 107 |
| A.9 Structure of A6 | 108 |
| A.10 A6 Between Electrodes | 108 |
| A.11 A6 Structure's XYZ Files | 109 |
| A.12 A6 ORCA Input File | 110 |
| A.13 A6 FDF File for Electronic Structure Calculations..... | 111 |
| A.14 Structure of Adenine | 112 |
| A.15 Adenine Structure's XYZ File..... | 112 |
| A.16 Adenine Optimization and Polarizability Input File..... | 113 |
| A.17 Structure of Adenine-Thymine | 114 |
| A.18 A-T Between Electrodes | 114 |
| A.19 A-T Structure's XYZ File | 115 |
| A.20 A-T Structure's XYZ Files | 116 |
| A.21 A-T Optimization Input File..... | 117 |
| A.22 A-T FDF File for Electronic Structure Calculations | 118 |
| A.23 A-T Polarizability Input File | 119 |
| B.1 Reprint Permission for Used Figure | 121 |
| B.2 Reprint Permission for Used Table | 122 |
| B.3 Reprint Permission for Used Figure | 123 |
| B.4 Reprint Permission for Used Figures..... | 124 |
| B.5 Reprint Permission for Original Work | 125 |

Chapter 1

INTRODUCTION

1.1 A Brief History of Molecular Electronics

An interesting topic in chemistry and physics regards trying to answer the question, how do electrons move through molecules? One method to investigate this topic deals with molecular charge transport where current is passed through a molecule sandwiched between two electrodes. The other deals with electron transfer which is a charge moving from an electron donating moiety to an electron accepting one. In this introduction, a brief history of molecular electronics and a few interesting experimental and theoretical techniques used in this field will be explored. The chapter will then conclude with an explanation of an often overlooked (but an unquestionably important) aspect of molecular electronics and its importance to today's research in this area.

The field of molecular electronics emerged in the early 1970's with the work of many researchers including Arie Aviram, Mark Ratner, Hans Kuhn, Bernhard Mann, and others [8, 9]. In 1971, Kuhn and Mann reported conductance measurements through monolayers of cadmium salts. Their measurements revealed that conductance decreases exponentially with the thickness of the layer. This meant that electron tunneling was taking place through the organic monolayer. Tunneling is a quantum mechanical feature where particles (in this case, electrons), are sent through a classically forbidden region where there is a probability that they will pass through the region. Since then, another major advancement in molecular electronics took place - using a single molecule as an electrical component whereby a single molecule was

sandwiched between two electrodes and a bias applied. In fact, Aviram and Ratner first proposed the construction of a specific type of electronic device, a rectifier, in 1974 [9, 10].

One of the most important advancements in molecular electronics occurred in the 1980's with the development of the scanning tunneling microscope (STM) by IBM laboratories in Zurich [11]. Later, the atomic force microscope (AFM) was invented by the same. Both of these advancements allowed for the direct measurement of conductance through single molecules. Figure 1.1 demonstrates some of the differences between AFM and STM. STM has played an important role in our understanding of transport phenomena and remains important due to its dual use in microscopy and tunneling spectroscopy [10]. However, STM requires well-defined surfaces (such as single crystals) and is thus not suitable for many experimental setups [10]. Here is where AFM plays a role as another useful structural characterization tool. While AFM typically has lower resolution than STM, it allows for the combined force and conductance measurements providing information concerning the bonding nature of the molecule-electrode contacts [10, 12].

Mark Reed's group at Yale University was the first to make significant progress in measuring single molecule transport. This was done in collaboration with James Tour and resulted in publications in the 1990's and early 2000's which provided insights into the transport properties of different molecules [13]. Their work resulted in collaborations across many different disciplines.

One of the first challenges in obtaining conductance measurements through single molecules is the number of different fields involved. To properly characterize conductance through a molecule, the combined effort of synthetic chemists, experimental physicists and physical chemists, and theoreticians was needed [14]. The synthetic chemists faced the problem of attaching a single molecule to electrodes. They found

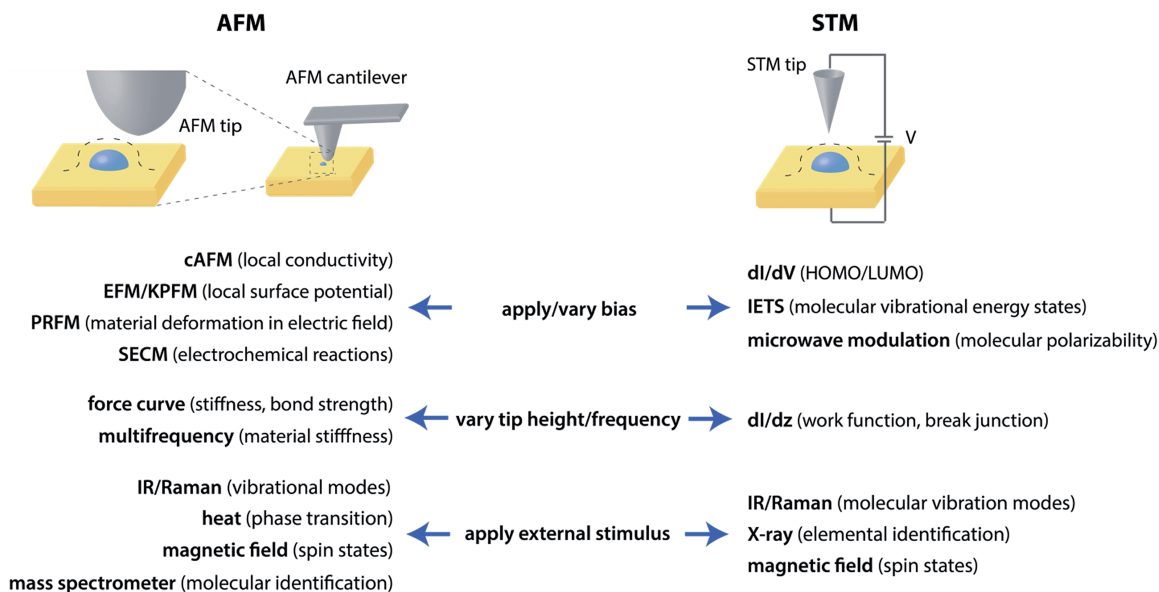


Figure 1.1: Overview of Multimodal AFM and STM Techniques. Figure and Caption Reproduced from Ref. [3].

that it was reasonable to attach the molecule to preferably gold or platinum electrodes (to reduce oxidation and degradation) and that sulphur, amine, or other lone-pair species could be used as anchoring groups for the molecule to the gold electrode and lone-pair species as anchoring groups for attaching a molecule to platinum electrodes [15].

Experimentalists faced the problem of accurately measuring the single molecule conductance of the systems previously developed. Often, large fluctuations in experimental data would lead experimentalists to create new schemes for better measurements. In order to not only measure the current accurately, but to also create a useful physical device, molecules needed to be electrically wired reliably to its electrodes [10]. The conductance of a molecule is sensitive to not only the chemical bonds [16] between itself and the electrodes but also to the atomic-scale details of the molecule-electrode contact geometry [17]. Having precise control over the contact

geometry has been a challenge for many research groups [18]. One available method for reliably attaching a molecule to an electrode is to functionalize the molecule with a thiol group and then connecting it to gold electrodes. This approach works well but comes with its own disadvantage, for example, high metal-atom mobility and a large polarization field at the contact interface [10]. Researchers have explored other ‘linker groups’ outside of thiols. Some groups have used linker groups comprised of C-C [19, 20], C-Si [21], and other bond arrangements [22, 23] to differing degrees of success.

Another challenge faced by experimentalists that has been observed is stochastic fluctuations where unwanted random telegraphic switching of conductance has been observed in metal-molecule-metal junctions [24, 10]. Explanations for this behavior include molecular motion due to conformational changes and bond fluctuation due to molecules tethered to the gold surface becoming attached or detached randomly [10]. This behavior has been reported in the conductance measurements of many systems, for example, Si-metal-oxide field effect transistors [24]. Similar stochastic fluctuations have been observed in the optical spectroscopy of single molecules. While not a severe limitation in the actualization of nanoscale devices, this type of challenge should be understood [10].

Another important topic for consideration is the current-induced instability and local heating experienced by the molecule during these experiments. Electromigration and local heating are well known in conventional electronics and become even more important at the nanoscale [25]. Current-induced instability and local heating effects arise from the energy exchanged between electrons and phonons [26, 10]. While in a nanoscale junction the inelastic electron mean free path is relatively large compared to the junction size, substantial effects still often arise due to the large current density in the nanojunction [10]. Local heating can be assessed by measuring

the force required to detach molecules bound to their electrodes [27]. Detachment in this case is thermally activated and directly related to the force required to separate the molecule from its electrodes. By measuring this force requirement, one can get an idea of the effective temperature of the molecular junction as a function of the applied bias voltage [27].

Theoreticians approached the question concerning the movement of electrons through molecules using a modified technique originally developed by Rolf Landauer, Markus Buttiker, Yigal Meir and Ned Wingreen [8, 28, 29]. This technique, referred to as the non-equilibrium Green's function, is a type of correlation function that demonstrates excellent agreement between computational work and experiment [8, 28, 29]. Much of this work was expanded by Mujica and coworkers later with this inclusion of scattering methods to calculate conductance in molecular wires [29]. Another theoretical technique is based on the Simmons model from the early 1960's and takes into account the concept of barrier tunneling and the dependence of the tunneling process on the shape and size of the barrier [8, 30]. Useful predictions based on this model come in the form, ' π systems will conduct better than σ systems', 'current decays exponentially with the length of the molecule', and 'frontier molecular orbitals and their structures will determine molecular conductance' [8]. Still, elegant and striking measurements have been made on a number of designed organic molecular systems where these rules of thumb hold true. For example, the Simmons analysis and the HOMO/LUMO (Highest Occupied Molecular Orbital / Lowest Unoccupied Molecular Orbital) analysis are standard for explaining molecular transport [8].

While these simple predictions have been useful, research has moved beyond the simple transport model and now incorporates more advanced areas of molecular electronics such as molecular spintronics (closed-shell and odd-spin molecular species), the investigation of vibronic effects (interaction between electronic and vibrational de-

degrees of freedom), excitation of the molecular junction using polarized light, quantum interference and decoherence, molecular chirality, molecular stretching and distortion, and thermoelectric response in junctions [8, 31].

As we can see, from 1971 to present much advancement has been made in the field and techniques of molecular electronics. This field is still relatively new when we consider the vast number of systems still to be analyzed (there are estimated to be about 10^{60} organic compounds with 15 atoms or fewer) and the types of systems that exist - from single molecule to complex organic structures like those of DNA and RNA [8]. This ends our brief overview on the history of molecular electronics. Next, we will discuss more on the theory behind how molecules and electrons interact with each other in a nanojunction.

1.2 From Electron Transfer to Electron Transport

Intramolecular electron transfer and charge transport in molecular wires are closely related areas [4, 8]. In the case of intramolecular electron transfer, reactions are either photo-induced or initially deposited non-equilibrium electron density transfers, in a rate process between sites linked by a molecular bridge. These types of electron transfer reactions are exceptionally important in areas of investigation such as chemical corrosion and photosynthesis and have been of interest to physical chemists for decades [4]. Since intramolecular electron transfer takes place by an electron tunneling from an initial state to a final state through a bridging medium, it is directly related to transport through a molecular wire [4]. We can see the equivalent concepts between these two ideas in Figure 1.2. The individual concepts behind encapsulated in this figure including the underlying mathematics are discussed later in Chapter 2.

The simplest example of a molecular junction analyzed for transport is the molecular wire. This wire simply serves to convey either charge or excitation energy from one

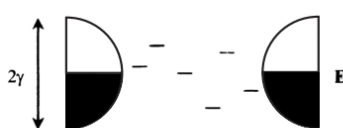
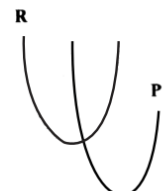
| <u>Aspect</u> | <u>Molecular Wire</u> | <u>Nonadiabatic Intramolecular Electron Transfer</u> |
|--------------------------|---|--|
| Potential Energy Diagram |  |  |
| Observable | Current | Rate Constant |
| Continuum | Electronic States | Vibronic States |
| Initial State | Electrode | Vibronic Levels |
| Process | Electron Tunneling | Electron Tunneling |

Figure 1.2: Comparison: Molecular Wire Transport and Nonadiabatic Intramolecular Electron Transfer. Figure Reproduced and Modified from Ref. [4]

electrode to another [4]. The two types of molecular wires that have been widely investigated are photonic molecular wires that transfer excitation and electronic molecular wires which move either electrons or hole charges. Molecular wires differ from macroscopic conductive wires in size which in turn changes the nature of its energy levels and transport processes. Varying conditions have been explored to study molecular wires from synthetic techniques based on molecular self-assembly, to nano-assembled circuitry.

One way of computing the conductance across a molecular wire in a simple way is via the Landauer approach. In a steady state, the Landauer formalism states that the conductance is proportional to the transmission probability t^2 of the electronic states around the Fermi energy level (the energy up to which states are occupied) [32, 33, 4].

$$g \propto \frac{2e^2}{\pi\hbar} t^2 \quad (1.1)$$

Equation 1.1 assumes that an electron in the donor electrode moves to the acceptor electrode via an elastic scattering medium (a molecule or system of molecules). Landauer observed that even in the absence of inelastic mechanisms that the system will still have a well defined conductance and noted that the traveling electron arrives in the acceptor electrode in a hot state that then thermalizes to the Fermi level of the second electrode through scattering [4]. Landauer's formula has been accepted among theoretical calculations as robust due to its expressing a connection between the transmission probability and the conductance. His formula also shows that minimal resistance (optimal conductance), is finite. Since the number of conduction channels is discrete, the maximum possible conductance in a system is an integer multiple of the quantum of conductance [4]. The quantum of conductance is defined as [34]:

$$G_0 = \frac{2e^2}{h} = 7.748\,091\,7310(18) \times 10^{-5} \text{ S} \quad (1.2)$$

Though Landauer's expression is fundamental, other approaches such as cluster analysis have been useful from a computational standpoint [4, 35, 36, 37]. For example, based on Bardeen's analysis of tunneling, in the case of low voltage we can obtain an expression for one-dimensional conductance in a form similar to Landauer's

$$g \propto \frac{2e^2}{\pi\hbar} \Delta_D \Delta_A |G_{1N}|^2 \quad (1.3)$$

where the Δ s are chemisorption couplings to the donor and acceptor electrodes, and G_{1N} is the 1, N element of the total molecular Green's function. G_{1N} is the relevant matrix element of the Green's function whereby conductance is calculated. It is defined as

$$G_{1N} = \frac{(-1)^{N-1} \prod_{i=1}^{N-1} V_{i,i+1}}{D_{1,N} - D_{2,N} \sum_N + D_{2,N-1} \sum_1 \sum_N} \quad (1.4)$$

where N is the number of sites in the wire (tight-binding approximation), and $V_{i,i+1}$ is the interaction between neighboring sites. The D components of the above equation are determinants constructed from the wire Hamiltonian matrix [29].

Equation 1.3 demonstrates, just like Landauer's, that the conductance depends on the transmission probability [4]. However, 1.3 takes into account factors that can influence the transmission probability. The chemisorption couplings Δ_D and Δ_A enter here separately and also the conductance maxima relates to the poles of the molecular Green's function. This therefore takes into account the molecular orbital (MO) energies of the isolated molecule [4].

By extending this formalism to cases with finite voltage, the current is given by:

$$I = \int_{-eV}^0 dE f_D(E)(1 - f_A(E + eV))g(E)/e \quad (1.5)$$

where $g(E)$ is the conductance corresponding to transmission at an energy E , and where the Fermi level of the donor reservoir defines the zero of energy [4].

The interpretation of 1.5 can be explained simply as the total current as the sum of all conductance coming from all energy states between both Fermi levels [4]. Due to this, the current is linear for small voltages. Another result from this formalism is that when any of the molecular energies cross one of the Fermi levels, the current increases and will remain constant until the next energy crossing resulting in a current-voltage curve resembling a staircase function [4]. This is due to the resonance-like structure of the conductance spectrum $g(E)$. [4]

1.3 Electron Transport in Molecular Junctions

As we mentioned earlier, the simplest setup for molecular electronics is a single molecule transport junction where a molecule is connected to a source and a drain electrode [38]. When the length of the molecule bridging the electrodes is relatively

short and the gap between the injection energy and molecular eigenstates is large, transport will occur via elastic tunneling. If stochastic switching occurs, the vibronic signature can be found using a technique called inelastic electron tunneling spectroscopy (IETS).

One of the first concerns in using single molecule electronics was whether the current passing through a single molecule was a measurable quantity [38, 39]. The first pioneering experiments in this field revealed immediately that the current/voltage (I/V) characteristics of a molecular junction revealed little about the particular molecule being employed in the junction [38, 40]. The role of the molecule in the junction acts as a tunneling barrier between the electrodes [38, 41]. Molecules can reveal their individual presence in the junction when we couple electron transport with nuclear motions. While the conductance through a single molecule was observed, it was learned that the nature of the electrode-molecule contact and the geometry of the interface were the least controllable aspects of the experiment and it was these considerations that affected the measured current the most [38, 18, 42, 10].

We can observe inelastic tunneling of the electrons in the junction if, during the coherent tunneling transport process, they exchange energy with one or more of the available vibrational levels of the junction [38, 43]. At low temperatures (<10 K), it is assumed that all of the vibrational modes are in their ground state. In this state, the electron can only lose a vibrational quanta of energy $\hbar\omega_a$. Here ω_a is the frequency of the molecular vibrational mode a . We can see that the inelastic channel that causes the excitation of mode a is available only when the bias V is such that $|V| > \hbar\omega_a/e$. This can be visualized by a small and sharp increase in conductance (dI/dV) every time a new inelastic channel becomes available as a peak in a plot of d^2I/dV^2 at $|V| > \hbar\omega_a/e$. Only a small percentage ($< 2\%$) of electrons happen to cross the junction inelastically. The measurement of d^2I/dV^2 is what constitutes

the methodology behind inelastic electron tunneling spectroscopy [38, 44]. It mainly provides information on the vibrational levels of the junction and its applicability remains in showing that a molecule is indeed bridging the two electrodes and forming a junction [38].

Molecular junction transport can occur in different transport regimes and can be distinguished by different energy scales. These regimes consider the injection gap energy E_G between the frontier molecular orbitals and the injection energy from the molecule, the spectral density Γ (the coupling between the molecule and electrode) which characterizes the orbital mixing at the molecule-electrode interface, the vibronic coupling strength which is a measure of the energy associated with nuclear reorganization, on-molecule Coulomb repulsion, and thermal energy [38].

The electrode-molecule electronic coupling is characterized by Γ . The transmission peaks are broadened and the off-resonance injection is relatively easy when Γ is large. We see sharper peaks and greatly reduced off-resonant injection when Γ is small. It's also necessary to note that vibronic couplings can change the transport mechanism in both small and large Γ regimes [38, 45, 46].

1.4 Potential Barriers and Tunneling

Let us consider electrons in contact with a potential barrier such as one in Figure 1.3. Here we assume that electrons are approaching the barrier from the left and has some probability of being reflected by the barrier. However, there is also the probability that the electron will be transmitted through the barrier even though its energy might be less than the barrier height. Transmission through this type of barrier is referred to a tunneling. In later Chapters we will see that our systems are in junctions where tunneling is the dominant method for electron transport. In much longer systems, ‘hopping’ may occur - a multistep electron transport process [47].

To address this model, we turn to the time-independent Schrodinger Equation. If

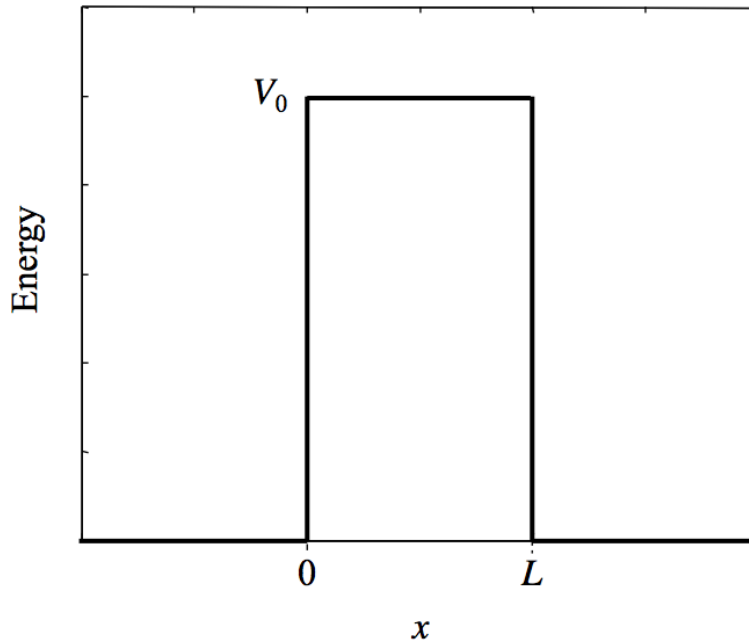


Figure 1.3: A Potential Barrier.

we look at either the left or right of the barrier, we can see that the electron is in a classically allowed region. We can model the electron in this region using plane waves. However, when the electron is within the barrier, if the energy E of the electron is below that of the barrier potential V_0 , the barrier becomes a classically forbidden region. The solution is described by expanding and decaying exponentials. We can assume a solution in the form

$$\psi(x) = \begin{cases} e^{ikx} + re^{-ikx}, & \text{for } x \leq 0 \\ ae^{\alpha x} + be^{-\alpha x}, & \text{for } 0 \leq x \leq L \\ te^{ikx}, & \text{for } x \geq L \end{cases} \quad (1.6)$$

where we have

$$k = \sqrt{\frac{2mE}{\hbar^2}} \quad (1.7)$$

and

$$\alpha = \sqrt{\frac{2m(V_0 - E)}{\hbar^2}} \quad (1.8)$$

Here, the intensity of the incoming plane wave is unity where the amplitude of the reflected wave r is the reflection coefficient and the amplitude of the transmitted wave t is the transmission coefficient. The reflectivity is $|r|^2$ and the transmissivity is $|t|^2$. We can now match the piecewise solutions at the left edge of the barrier by equating the amplitude of the wavefunction to give

$$\psi(0) = 1 + r = a + b \quad (1.9)$$

where equating the slope of the wavefunction gives

$$\psi'(0) = ik - ikr = \alpha a - \alpha b \quad (1.10)$$

At the right edge of the barrier

$$\psi(L) = ae^{\alpha L} + be^{-\alpha L} = te^{ikL} \quad (1.11)$$

and

$$\psi'(L) = a\alpha e^{\alpha L} - b\alpha e^{-\alpha L} = ikte^{ikL} \quad (1.12)$$

It is important to note here that the tunneling probability is enhanced when the approaching electron has an energy close to that of the barrier height. Also, the reflection of electrons off the barrier can lead to interference with electrons in contact with the barrier. In the instance where the electron energy is much less than the barrier height, the wavefunction within the barrier can be modeled as a decaying exponential. The transmission probability is then approximately

$$T \approx e^{-2\alpha L} \quad (1.13)$$

Figure 1.4 shows the plot of a wavefunction for an electron approaching the barrier from the left. When the electron energy is lower than the barrier height, tunneling

is possible, but the probability is small. When the energy of the electron is close to that of the barrier height, there is a non-zero transmission probability through the barrier.

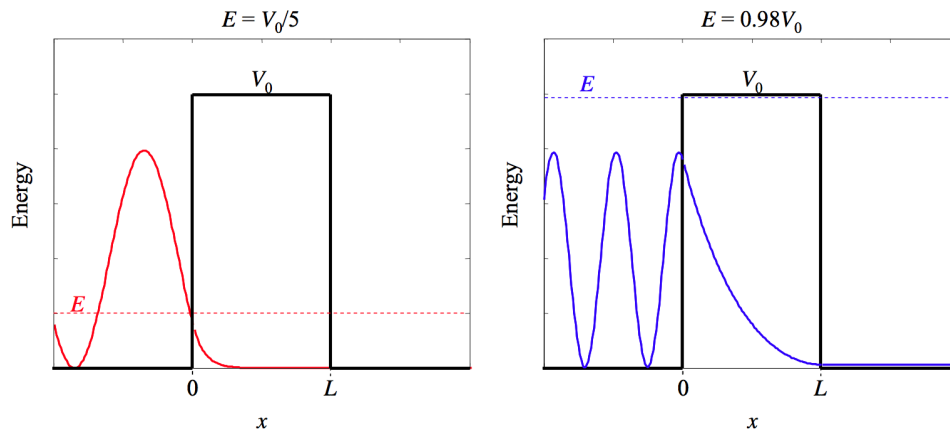


Figure 1.4: Electron Tunneling Through a Barrier.

1.5 Transport Through Weak Bonds

While time has been taken to discuss the history behind molecular electronics, the relevance of this work in respect to this history has not yet been addressed. We have seen how experimentalists and theorists alike have spent decades trying to devise methods to not only sandwich a single molecule between electrodes but to also measure its conductance. However, most of these researchers have focused on molecular systems that resembled 'wires' in order to accomplish this purpose. Systems such as alkanes, alkenes, and alkynes have been used, as have systems more complex like DNA and RNA. Intuitively this makes sense. However, if we are to consider electrons moving through these types of systems, the question comes to mind concerning the quality of bonds. What bond type is the best for transport? In this work transport through a much less discussed medium: the hydrogen bond is considered.

1.6 Quality of Bonds

This work focuses on a type of bond typically considered a 'weak link'. Weak links are of the nature of hydrogen bonds and bonds arising from van der Waal-like interactions (through-space) and may be important for nanoscale devices. One reason for this is that the pathways model assumes that through-bond connections (covalent-like bonds), being much stronger than van der Waals contacts, should in principle yield a weaker decay with the length of the junction for electron tunneling [48, 49, 50]. Therefore, it is assumed that tunneling should preferentially occur through bonded connections [48].

A study by Kurlancheek *et al.* found that at most, there existed a modest difference observed between tunneling via H-bonded contacts and tunneling via van der Waals contacts [48]. Also, Therien and co-workers previously studied the effect of H-bonds on the coupling between a donor and acceptor atoms and found that the coupling strength is comparable to that of some covalent bonds [48]. While this is consistent with the pathways model, it brings to question the exact role that transport through hydrogen bonds can play. Last, of particular relevance to our work, Nishino *et al.* found that conductance through hydrogen bonds was actually higher than through covalent σ bonds (alkanes) for short chains. This calls into question whether there is a *better* bond for transport. This work seeks to explore the role of transport through hydrogen bonds.

1.7 Hydrogen Bonding

The hydrogen bond was discovered almost 100 years ago and yet is still a hot topic of discussion today. The long lasting interest in hydrogen bonding is due to its importance for the structure, function, and dynamics of a large number of chemical

systems ranging from inorganic to biological chemistry [2, 51]. Interest in hydrogen bonding can be found in many disciplines including mineralogy, material science, inorganic and organic chemistry, supramolecular chemistry, biochemistry, molecular medicine, and pharmaceuticals [2, 52, 53]. When we compare hydrogen bonds to other chemical bonds, the hydrogen bond is typically considered “weak” and is one of the most important bonds in the chemistry of life [52]. Hydrogen bonds can be made and broken at ambient temperatures, are important in determining the tertiary structure of proteins and nucleic acids, dictate the thermal properties of polymers like nylon, and participate in vital drug-receptor interactions [52]. Before we begin a systematic overview of the hydrogen bond, let’s first review the classical definition of the hydrogen bond.

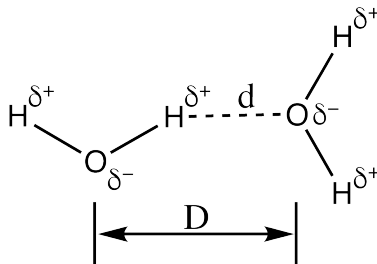


Figure 1.5: Classical View of the Hydrogen Bond. Here, $d = \text{H} \cdots \text{O}$ Distance, and $D = \text{O} \cdots \text{O}$ Distance. Figure Reproduced from Ref. [2].

The semi-classical view of hydrogen bonding can be visualized in Figure 1.5 where we can see the interaction between two water molecules. This two-water system is the classical basis where we see directional interaction between the molecules [2]. Differences in electronegativity between the hydrogen (H) and oxygen (O) atoms makes the resulting O-H bond in the water molecule polar [2, 52]. There exists a partial atomic charge of approximately +0.4 on each H atom and approximately -0.8 on the O atom [2]. We can see here that the local dipoles resulting from these

partial charges ($O^{\delta-} - H^{\delta+}$) point towards the negative partial charge ($O^{\delta-}$) [2]. In the resulting bond ($O - H \cdots O$), the intermolecular bond distance is shorter by around 1 Å when compared to the sum of the van der Waal radii for the H and O atoms [52]. This indicates that there is substantial overlap of the electron orbitals to form a three-center four-electron bond. The total interaction in this bond is mostly electrostatic with a dissociation energy around 3.5 kcal mol⁻¹ [2]. This classical picture of the hydrogen bond can be extended with small changes to include similar interaction of the type $X - H \cdots A$. This bond is formed with strongly polar groups ($X^{\delta-} - H^{\delta+}$) on one side of the bond and electronegative atoms ($A^{\delta-}$) on the other side. In this example, $X=O, N$, or a halogen and $A=O, N, S$, halide, etc.

While the hydrogen bond can in some instances be thought of in this classical sense, we now know that the hydrogen bond can be much more complicated and requires a quantum model. For example, there exists hydrogen bonds so strong that they more closely resemble covalent bonding while in other examples the bond is so weak that it more closely resembles van der Waal's interactions [2]. The hydrogen bond actually exists on a spectrum consisting of continuous transition regions representing effects ranging from covalent-like bonding, purely ionic bonding, the cation- π bonding, and the van der Waal's interaction-type bonding [2, 53]. The traditional view encompassing the electrostatic dominance of the hydrogen bond is only accurate for a subset of occasions while other times it behaves differently [2]. Whereas we mentioned above in the classical view, the hydrogen bond ($H \cdots A$) distance is not necessarily shorter than the sum of the van der Waal's radii [2]. Also, for an X-H group to form a hydrogen bond, X does not need to be especially electronegative; it is only necessary for X-H to be slightly polar [2].

Now that we have briefly discussed an overview on the some of the complexities demonstrated by a hydrogen bond, it would be prudent to define what a hydrogen

bond actually is. An early definition proposed by Pimentel and McClellan posited that a hydrogen bond exists if two conditions were present: 1) that there was evidence of a bond in general, and 2) that there is evidence that the bond sterically involves hydrogen already bonded to another atom [2, 54]. This definition clearly leaves out any chemical information concerning the other atoms involved in the bond including their polarities or net charges. Also, nothing is specified concerning the interaction geometry of the hydrogen atom; only that the hydrogen atom must be present in or around the bond. Another drawback of this definition is the fact that pure van der Waal interactions (which do form bonds) are included in this definition. A better definition proposed by Steiner *et al.* states, “An $X - H \cdots A$ interaction is called a *hydrogen bond*, if 1. it constitutes a local bond, and 2. $X - H$ acts as a proton donor to A.” [2, 52] We can immediately see that the second requirement is related to the acid/base properties of the bond and also implies a proton-transfer reaction from $X - H$ to A. This definition also serves to exclude pure van der Waals contacts and agostic interactions [2]. Point 2 of this definition also serves to include symmetric hydrogen bonds ($X - H - X$) where the donor and acceptor atoms cannot be distinguished, but nevertheless, the hydrogen bond exists [2].

In a hydrogen bond of the type $X - H \cdots A$, the group $X - H$ is referred to as the donor while A is called the acceptor [2, 53, 52]. In this nomenclature it is understood that donor and acceptor means *proton donor* and *proton acceptor*, respectively. There are cases in the literature where some authors prefer nomenclature where $X - H$ is the electron acceptor while A is the electron donor [2]. Both sets of nomenclature are accepted. For the purpose of this thesis I will be using the former definitions of donor and acceptor - referring exclusively to the proton.

Now that we have a sense of what a hydrogen bond is and the terminology, we can discuss different types of hydrogen bond bridges - that is, a molecular systems contain-

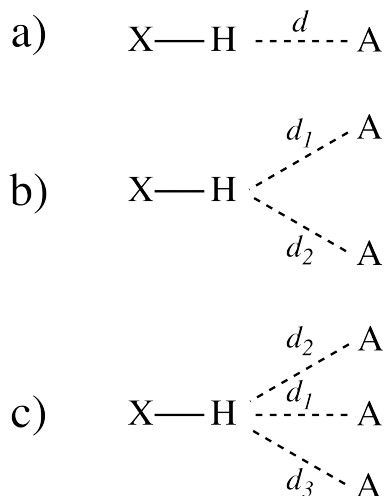


Figure 1.6: Comparing Hydrogen Bond Bridges. a) A Normal hydrogen Bond with a Single Acceptor. b) Bifurcated Hydrogen Bond. c) Trifurcated Hydrogen Bond. Figure Reproduced from Ref. [2].

ing more than one hydrogen bond. Figure 1.6 shows the different types of hydrogen bond bridges. In a simple hydrogen bond, the proton donor interacts with only one acceptor atom. However, systems exist where a donor can interact with two or three acceptors at the same time [2]. Hydrogen bonds with more than three acceptors are possible but rare due to the very high spatial densities of the acceptors. In the case where the proton is bonded to two acceptors simultaneously, the term “bifurcated” is often used [52]. The term “two-centered” can also be used in this scenario. Last, we can see that “trifurcated” systems also exist. While some authors have also used the terminology “non-bonded interactions”, or “through-space interactions”, I will be focusing on referring to hydrogen bonds as H-bond or through-space interactions, as I have just shown that “non-bonded interactions” may cause confusion going forward.

Let us now focus on constituent interactions in the hydrogen bond. The hydrogen bond is a complex interaction with multiple constituents, different in nature, playing an important role [2]. The total energy of a hydrogen bond (E_{tot}) is comprised of con-

tributions from electrostatics (E_{el}), polarization (E_{pol}), charge transfer (E_{ct}), dispersion (E_{disp}), and exchange repulsion (E_{er}) [2, 52]. The individual distance and angular characteristics of these constituents are different from each other. The electrostatic term is highly directional and distance dependant. For example, the electrostatic term diminishes slowly as $-r^{-3}$ for dipole-dipole interactions and $-r^{-2}$ for dipole-monopole interactions. The polarization constituent decreases even faster as $-r^{-4}$ and the charge-transfer constituent term decreases even faster than that as approximately e^{-r} . If we consider natural bond orbital analysis [55], charge transfer occurs from an electron lone pair on atom A to an antibonding orbital of X-H ($n_A \rightarrow \sigma_{XH}^*$). The dispersion constituent is isotropic and has a distance dependance of $-r^{-6}$ while the exchange-repulsion constituent term increases sharply with reducing distance as $+r^{-12}$. The prior two terms (dispersion and exchange-repulsion) are typically combined into an isotropic “van der Waals” contribution term that is approximately described by the widely known Lennard-Jones potential ($E_{vdW} \sim Ar^{-12} - Br^{-6}$). While we can characterize the energy of a hydrogen bond with these constituent terms, each term is weighted differently depending on the donor-acceptor combination and the details surrounding the bond geometry. Therefore, no one term dominates the total energy of the hydrogen bond (E_{tot}). Due to these many constituents and the varying types of hydrogen bond configurations discussed, it is not easy to pin down an average hydrogen bond energy. Actually, the energy of the hydrogen bond covers more than two orders of magnitude in experimental studies (-0.2 to -40 kcal mol $^{-1}$) [2, 52].

Another interesting way of considering hydrogen bonds is to regard them as proton-transfer chemical reactions. If we consider the hydrogen bond in this light, then the notation X-H \cdots Y serves to illustrate a “picture” of the bond in the reaction where: X-H \cdots Y \rightleftharpoons X $^-$ \cdots H $^-$ - Y $^+$ or X $^+$ - H \cdots Y \rightleftharpoons X \cdots H $^-$ - Y $^+$. This means that a partial X-H bond already exists and it is understood that the proton

is “floating” between the other atoms forming the bond. Treating the hydrogen bond as a proton-transfer reaction is complementary to electrostatic views on hydrogen bonding and allows us to consider aspects such as acid/base affects, proton affinities, and will allow us to address later the partially covalent nature of the bond.

A hydrogen bond is often considered to be “weak”, “strong”, and some cases “in-between” depending on many factors. Here, we follow Jeffrey [1] to consider “moderate” hydrogen bonding if the bond resembles those between water molecules or in simple carbohydrates have bond energies in the range of 4 – 15 kcal mol⁻¹. Hydrogen bonds with energies above or below this range are considered strong or weak, respectively. Steiner *et al.* created a simple table for reference which I have reproduced here in part.

| | Strong | Moderate | Weak |
|-------------------------------------|-----------------------|----------------------|-------------------|
| Interaction Type | Strongly Covalent | Mostly Electrostatic | Electro./Dispers. |
| Bond Lengths [Å] | | | |
| H...A | 1.2 – 1.5 | 1.5 – 2.2 | > 2.2 |
| $\Delta X - H$ [Å] | 0.08 – 0.25 | 0.02 – 0.08 | < 0.02 |
| X – H vs. H...A | X – H \approx H...A | X – H < H...A | X – H \ll H...A |
| X...A [Å] | 2.2 – 2.5 | 2.5 – 3.2 | > 3.2 |
| Directionality | Strong | Moderate | Weak |
| Bond Angles [°] | 170 – 180 | > 130 | > 90 |
| E_{tot} [kcal mol ⁻¹] | 15 – 40 | 4 – 15 | < 4 |

Table 1.1: Hydrogen Bond Strengths Defined By Jeffrey [1] and Adapted from Steiner *et al.* [2]

Since hydrogen bonding interactions are dynamic and ubiquitous in nature, re-

searchers have begun to study the use of H-bonded organic semiconductors [53]. For example, Glowacki *et al.* has identified three main avenues of research for utilizing H-bonding in organic electronics and consists of the following: investigating the conduction mechanism of the H-bond in biological materials like DNA, investigating H-bonded organic pigments, and supramolecular H-bonded mediated self-assembly of conducting moieties [53]. In my research I have investigated some of these avenues. Specifically, I have looked at conduction through dimers and DNA base-pairs while also looking for an easier and more cost effective molecular descriptor in order to generalize conductance trends without the computational cost of full-scale conductance calculations.

1.8 Polarizability as a Descriptor for Conductance

Since the start of the field of molecular electronics many experimentalists have tried to use molecular properties of the bridge as a way to make a quick judgment about the transport properties of a molecular junction. Some of the most commonly used properties are length [56], and the energy gap between HOMO (highest occupied molecular orbital) and LUMO (lowest unoccupied molecular orbital [57]. Because of the complex nature of transport, these rules have been proven ineffective in many cases - particularly when the quantum effects become more dominant [58, 12]. Mazinani *et al.* have suggested the use of molecular polarizability as a descriptor that can capture the essence of transport through molecular junctions.

Mujica and coworker's have shown that by self-consistently solving the Schrödinger and Poisson equations, one can connect the quantum electronic density to the electrostatic potential and therefor obtain the spatial profile of the electrostatic potential [59]. The interesting result of this model is that molecules in the junction behave mostly as a dielectric - that their polarization response counteracts the driving field.

This is, in fact, a very different profile from the spatial profile of a vacuum junction. Figure 1.7 schematically portrays the difference.

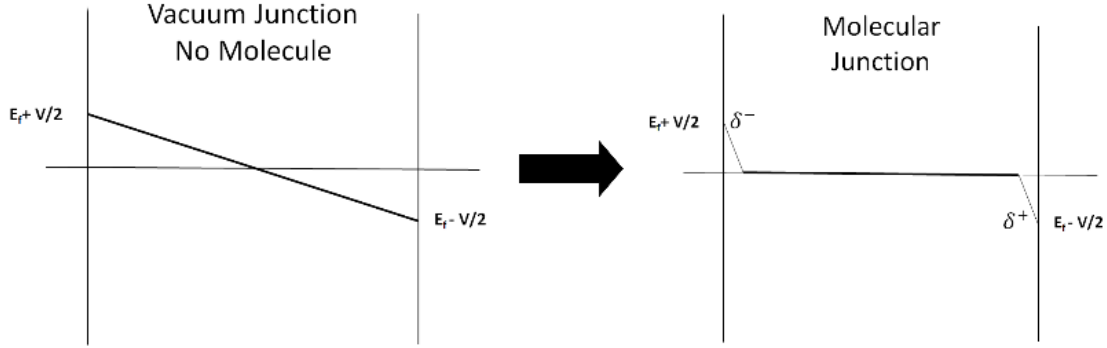


Figure 1.7: Electrostatic Potential Profile of a Molecular Junction for a) No Molecule Present, and b) Molecule Present.

This picture, establishes the paramount role of the molecular bridge in determining the local dielectric properties of the molecular junction. The connection between molecular polarizability and dielectric constant can be set, in its simplest form, by the Clausius- Mossotti relation

$$\frac{\epsilon_r - 1}{\epsilon_r + 2} = \frac{N\alpha}{3\epsilon_0} \quad (1.14)$$

where $\epsilon_r = \epsilon/\epsilon_0$ is the dielectric constant of the material, ϵ_0 is the permittivity of free space, N is the number density of the molecules (number of molecules per cubic meter), and α is the molecular polarizability.

Mazinani *et al.* have approached this problem in its simplest form and showed that the following relation between conductance and polarizability can be established [60]

$$g = g_1 e^{-\beta_1 \alpha} \left(C - \frac{\beta_1}{2} \alpha + \dots \right) \quad (1.15)$$

where β_1 is the decay constant, g_1 is the quantum of conductance, C is an expansion constant, and α is the molecular polarizability.

It is worth noting that increase in polarizability of the bridge results in a decrease of the molecular conductance. In later chapters, we show that this connection works even in systems with multiple hydrogen bonds.

Thus far, the history and importance of molecular electronics and the potential role of hydrogen bonding within this framework has been reviewed. It is now necessary to review the methodology behind the results contained in this work. Computational chemists have many tools at their disposal to calculate a variety of molecular properties. In this work, computational packages such as ORCA, TranSIESTA, Gaussian, and others were used. These programs use the same, or very similar mathematics in their calculations. In the next chapter, the mathematics behind this work are introduced.

THEORETICAL AND COMPUTATIONAL METHODOLOGY

2.1 Standard Electron Transfer Theory

This chapter begins by first focusing on a review of electron transfer processes. The following equations and derivations are provided by Nitzan and coworkers [61]. To start, the expression for the electron transfer rate in the limit of non-adiabatic transfer is given by the equation

$$k_{et} = \frac{2\pi}{h} |V_{DA}|^2 F \quad (2.1)$$

where V_{DA} is the coupling between the donor (D) and acceptor (A) electronic states and where

$$F = F(E_{AD}) = \sum_{V_D} \sum_{V_A} P_{th}(\varepsilon_D(V_D)) |\langle V_D | V_A \rangle|^2 \delta(\varepsilon_A(V_A) - \varepsilon_D(V_D) + E_{AD}) \quad (2.2)$$

is the thermally averaged Franck Condon (FC) weighted density of states. In Equation 2.2, V_D and V_A are the donor and acceptor states, P_{th} is the Boltzmann distribution over donor states, $\varepsilon_D(V_D)$ and $\varepsilon_A(V_A)$ are nuclear energies above the corresponding electronic origin and $E_{AD} = E_A - E_D$ is the electronic energy gap between the donor and acceptor states. In the classical limit, F is given by,

$$F(E_{AD}) = \frac{e^{-(\lambda + E_{AD})^2 / 4\lambda k_B \Theta}}{\sqrt{4\pi\lambda k_B \Theta}} \quad (2.3)$$

where k_B is the Boltzmann constant, Θ is the temperature, and where λ is the reorganization energy. If the donor is replaced by an electrode, we have to sum over all occupied electrode states

$$|V_{DA}|^2 F \Rightarrow \sum_k f(\varepsilon_k) F(\varepsilon_k - e\Theta) |V_{kA}|^2 = \int d\varepsilon f(\varepsilon) F(\varepsilon - e\Theta) \sum_k \delta(\varepsilon - \varepsilon_k) |V_{kA}|^2 \quad (2.4)$$

where

$$f(\varepsilon) = \frac{1}{1 + e^{\varepsilon/k_B\Theta}} \quad (2.5)$$

is the Fermi-Dirac distribution function with ε measured relative to the electron chemical potential μ in the electrode and Θ which determines the position of the acceptor level relative to μ is the overpotential. Defining

$$\sum_k \delta(\varepsilon - \varepsilon_K) |V_{kA}|^2 \equiv |V(\varepsilon)|^2 \quad (2.6)$$

the electron transfer rate becomes

$$k_{et} = \frac{2\pi}{\hbar} \int d\varepsilon \frac{e^{-(\lambda - \varepsilon\Theta + \varepsilon)^2/4\lambda k_B\Theta}}{\sqrt{e\pi\lambda k_B\Theta}} |V(\varepsilon)|^2 f(\varepsilon) \quad (2.7)$$

Much of the early work on electron transfer have used equations like Equation 2.3 and Equation 2.7 with the electronic coupling term V_{DA} used as a fitting parameter. More recent work has focused on ways to characterize the dependence of this term on the electronic structure of the donor/acceptor pair and on the environment. Studies of bridge mediated electron transfer, where the donor and acceptor species are rigidly separated by molecular bridges of well defined structure and geometry have been valuable for characterizing the interrelationship between structure and functionality of the separating environment in electron transfer processes. As expected for tunneling processes, the rate is found to decrease exponentially with the donor-acceptor distance

$$k_{et} = k_0 e^{-\beta' R_{DA}} \quad (2.8)$$

where β' is the range parameter that characterizes the distance dependence of the electron transfer rate. The appearance of the term V_{DA} in Equation 2.1 is a low-order perturbation theory result. A more general expression is obtained by replacing V_{DA} by T_{DA} where the T operator is defined by $T(E) = V + VG(E)V$, with $G(E) = (E - H + (1/2)i\Gamma)^{-1}$, V is the electronic coupling between zero order molecular states,

and where Γ stands for the inverse lifetime matrix of bridge levels. If we assume for a moment that the donor level $|D\rangle$ is coupled only to bridge state $|1\rangle$ and that the acceptor level $|A\rangle$ is coupled only to the bridge level N , the effective coupling for a one dimensional bridge between the donor and acceptor now becomes

$$T_{DA}(E) = V_{DA} + V_{D1}G_{1N}(E)V_{NA} \quad (2.9)$$

This represents the transition amplitude as a sum of a direct contribution, V_{DA} , which is usually disregarded for long bridges, and a bridge mediated contribution. In using T_{DA} instead of V_{DA} in Equation 2.1 the energy parameter E in Equation 2.9 should be taken to equal $E_D = E_A$ at the point where the corresponding potential surfaces cross. Now, the Green's function element in Equation 2.9 is given by

$$G_{1N}(E) = \frac{1}{E - E_N} \prod_{n=1}^{N-1} \frac{V_{n,n+1}}{E - E_n} \quad (2.10)$$

For a model with identical bridge segments E_n and $V_{n,n+1}$ are independent of n and will be denoted $E_n = E_B$ and $V_{n,n+1} = V_B$. Using this in Equation 2.1 leads to

$$k_{et} = \frac{2\pi}{\hbar} \left| \frac{V_{1D}V_{NA}}{V_B} \right|^2 \left(\frac{V_B}{\Delta E_B} \right)^{2N} F \quad (2.11)$$

where $\Delta E_B = E_B - E$. Also, for a bridge assisted transfer between a molecule and an electrode, Equation 2.7 applies $|V(\varepsilon)|^2$ given by

$$|V(\varepsilon)|^2 = \left(\frac{V_B}{\Delta E_B} \right)^{2N} \sum_k \delta(\varepsilon - \varepsilon_k) \left| \frac{V_{1k}V_{NA}}{V_B} \right|^2 \quad (2.12)$$

These results imply a simple form for the distance parameter β' of Equation 2.8,

$$\beta' = \frac{2}{a} \ln \left(\frac{\Delta E_B}{V_B} \right) \quad (2.13)$$

where a measures the segment size, so that the bridge length is NA . The exponential dependence on the bridge length is a manifestation of the tunneling character of this process.

2.2 Transmission Between Conducting Leads

Equation 2.1, Equation 2.7, and Equation 2.11 are expressions for the rate of electron transfer between donor and acceptor molecules or between a molecule and a metal electrode. For electron transfer in metal-molecule-metal junctions, the primary observable is the current-voltage (I/V) characteristics of the system.

We will first consider a simple model for a metal-insulator-metal system where the insulator is represented by a continuum characterized by a dielectric constant ϵ . We will assume that the electrode surfaces are infinite parallel lines perpendicular to the x direction. In this case, the transmission problem is essentially 1-dimensional and depends only on the incident particle velocity in the x direction, $v_x = \sqrt{2E_x/m}$. In the WKB approximation (named after Wentzel-Kramers-Brillouin and also known as the Liouville-Green method) the transmission probability is given by

$$T(E_x) = \exp \left[-\frac{4\pi}{\hbar} \int_{s_1}^{s_2} [2m(U_B(x) - E_x)]^{1/2} dx \right] \quad (2.14)$$

where $U_B(x)$ is the barrier potential that determines the turning points s_1 and s_2 and m is the mass of the tunneling particle. The tunneling flux is given by $T(E_x)n(E_x)\sqrt{2E_x/m}$, where $n(E_x)$ is the density per unit volume of electrons of energy E_x in the x direction. $n(E_x)$ is obtained by integrating the Fermi-Dirac function with respect to E_y and E_z . When a potential Φ is applied so that the right electrode is positively biased, the net current density is obtained in the form,

$$J = \int_0^\infty dE_x T(E_x) \xi(E_x) \quad (2.15)$$

where

$$\begin{aligned} \xi(E_x) &= \frac{2m^2 e}{(2\pi\hbar)^3} \int_{-\infty}^{\infty} dv_y \int_{-\infty}^{\infty} dv_z [f(E) - f(E + e\Phi)] \\ &= \frac{4\pi m e}{(2\pi\hbar)^3} \int_0^\infty dE_r [f(E) - f(E + e\Phi)] \end{aligned} \quad (2.16)$$

and where $E_r = E - E_x = (1/2)m(v_y^2 - v_z^2)$ is the energy in the direction perpendicular to x . In obtaining this result it is assumed that the electrodes are chemically identical. At zero temperature and when $\Phi \rightarrow 0$, $f(E) - f(E_e\Phi) = e\Phi\delta(E - E_F)$. Equation 2.15 and Equation 2.16 then lead to an expression for the conduction per unit area (the conductivity per unit length)

$$\sigma_x = \frac{4\pi m e^2}{(2\pi\hbar)^2} \int_0^{E_F} dE_x T(E_x) \quad (2.17)$$

For finite Φ these expressions provide a framework for predicting the current-voltage characteristics of the junction where explicit approximate expressions were given by Simmons. Here, it has been emphasized that the dependence on Φ arises in part from the structure of Equation 2.15 and Equation 2.16. At zero temperature we have

$$J = \frac{4\pi m^2 e^2}{(2\pi\hbar)^3} \left[e\Phi \int_0^{E-F-e\Phi} dE_x T(E_x) + \int_{E_F-e\Phi}^{E_F} dE_x (E_F - E_x) T(E_x) \right] \quad (2.18)$$

but mainly from the voltage dependence of T . The simplest model for a metal-vacuum-metal barrier between two identical electrodes without an external field is a rectangular barrier of height above the Fermi energy given by the metal workfunction. When a uniform electric field is imposed between the two metal a linear potential drop from E_F on one electrode to $E_F - e\Phi$ on the other is often assumed. In addition, the image potential experienced by the electron between the two metals will considerably modify the potential barrier. For a point charge e , located at position x between two conducting parallel plates that are a distance d apart, the image potential is

$$V_1 = \left(-\frac{e^2}{4\pi\epsilon} \right) \left[\frac{1}{2x} + \sum_{n=1}^{\infty} \left\{ \frac{nd}{[(nd)^2 - x^2]} - \frac{1}{nd} \right\} \right] \quad (2.19)$$

where ϵ is the dielectric constant of the spacer. For $x = d/2$ this becomes

$$V_1 = \frac{e^2 \ln 2}{2\pi\epsilon d} \quad (2.20)$$

This negative contribution to the electron's energy reduces the barrier potential and has been invoked to explain the lower than expected barrier observed in STM experiments.

2.3 The Landauer Formula

Landauer's original result was obtained for a system of two 1-dimensional leads connecting two macroscopic electrodes (electron reservoirs) via a scattering object or a barrier characterized by a transmission function $T(E)$. The zero temperature conductance, measured as the limit $\Phi \rightarrow 0$ of the ration I/Φ between the current and the voltage drop between the reservoirs was found to be

$$g = \frac{e^2}{\pi\hbar} T(E_F) \quad (2.21)$$

This result is obtained by computing the total unidirectional current carried in an ideal lead by electrons in the energy range $(0, E) = (0, \hbar^2 k_e^2 / (2m))$. In a 1-dimensional system of length L the density of electrons, including spin, with wavevectors in the range between k and $k + dk$ is $n(k)dk = 2(1/L)(L/2\pi)f(E_k)dk = f(E_k)dk/\pi$. The corresponding velocity is $v = \hbar k/m$. Thus,

$$I(E) = e \int_0^{k_E} dk v(k) n(k) = e \int_0^{k_E} dk (\hbar k/m) f(E_k) / \pi = \frac{e}{\pi\hbar} \int_0^E dE' f(E') \quad (2.22)$$

At zero temperature, the net current carried under bias Φ is

$$I = \frac{e}{\pi\hbar} \int_0^\infty dE (f(E) - f(E + e\Phi)) \xrightarrow{\Theta \rightarrow 0} \frac{e^2}{\pi\hbar} \Phi \quad (2.23)$$

Thus the conductance of an ideal 1-dimensional lead is $I/\Phi = e^2/\pi\hbar = (12.9K\Omega)^{-1}$.

In the presence of the scatterer this is replaced by

$$I = \frac{e}{\pi\hbar} \int_0^\infty dE T(E) (f(E) - f(E + e\Phi)) \xrightarrow{\Theta \rightarrow 0, \Phi \rightarrow 0} \frac{e^2}{\pi\hbar} T(E_F) \Phi \quad (2.24)$$

which leads to Equation 2.25. This result is valid for 1-dimensional leads. When the leads have finite size in the direction normal to the propagation so that they support traversal modes, a generalization of Equation 2.21 to this case yields

$$g = \frac{e^2}{\pi\hbar} \sum_{i,j} T_{ij}(E_F) \quad (2.25)$$

where $T_{ij} = |S_{ij}|^2$ is the probability that a carrier coming from the left of the scatterer in transversal mode i will be transmitted to the right into transversal mode j . The sum in Equation 2.25 is over all traversal modes whose energy is smaller than E_F . More generally, the current for a voltage difference Φ between the electrodes is given by

$$I = \int_0^\infty dE [f(E) - f(E + e\Phi)] \frac{g(E)}{e} \quad (2.26)$$

and

$$g(E) = \frac{e^2}{\pi\hbar} \sum_{i,j} T_{ij}(E) \quad (2.27)$$

Next, we can replace the expression based on transmission coefficient T by an equivalent expression based on scattering amplitudes, or T matrix elements, between zero order states localized on the electrodes. This can be derived directly from Equation 2.25 or Equation 2.27 by using the identity

$$\sum_{i,j} T_{ij}(E) = 4\pi^2 \sum_{l,r} |T_{lr}|^2 \delta(E - E_l) \delta(E - E_r) \quad (2.28)$$

On the left side of Equation 2.28 a pair of indices (i, j) denote an exact scattering state of energy E , characterized by an incoming state i on the left electrode and an outgoing state j on the right electrode. On the right, l and r denote zero order states confined to the left and right electrodes, respectively. T is the corresponding transition operator whose particular form depends on the details of this confinement.

Alternatively, we can start from the golden-rule-like expression

$$\begin{aligned}
I &= e \frac{4\pi}{\hbar} \sum_{l,r} [f(E_l)(1 - f(E_r + e\Phi)) - f(E_r + e\Phi)(1 - f(E_l))] |T_{lr}|^2 \delta(E_l - E_r) \\
&= \frac{4\pi e}{\hbar} \sum_{l,r} [f(E_l) - f(E_r + e\Phi)] |T_{lr}|^2 \delta(E_l - E_r)
\end{aligned} \tag{2.29}$$

We can rewrite this in the form

$$\begin{aligned}
I &= \frac{4\pi e}{\hbar} \int_0^\infty dE [f(E) - f(E + e\Phi)] \sum_{l,r} |T_{lr}|^2 \delta(E - E_l) \delta(E - E_r) \\
&= \int_0^\infty dE [f(E) - f(E + e\Phi)] \frac{g(E)}{e}
\end{aligned} \tag{2.30}$$

where

$$g(E) \equiv \frac{4\pi e^2}{\hbar} \sum_{l,r} |T_{lr}|^2 \delta(E - E_l) \delta(E - E_r) \tag{2.31}$$

We can see here that Equation 2.28 and Equation 2.31 imply Equation 2.27. For $\Phi \rightarrow 0$ Equation 2.30 and Equation 2.31 lead to $I = g\Phi$ with

$$g = g(E_F) \tag{2.32}$$

2.4 Molecular Conduction

Equation 2.30, Equation 2.31, and Equation 2.32 provide a convenient starting point for most treatments of currents through molecular junctions where the coupling between two metal electrodes is weak. In this case it is convenient to write the system's Hamiltonian as the sum, $H = H_0 + V$, of a part H_0 that represents the uncoupled electrodes and spacer and the coupling V between them. As we have shown previously, in the weak coupling limit, the T operator

$$T(E) = V + VG(E)V; \quad G(E) = (E - H + i\varepsilon)^{-1} \tag{2.33}$$

is usually replaced by its second term only. The first 'direct' term V can be disregarded if we assume that V couples the states l and r only via states of the molecular

spacer. Consider now a simple model where this spacer is an N -site bridge connecting two electrodes so that site 1 of the bridge is attached to the left electrode and site N to right electrode. In this case we have $T_{lr} = V_{l1}G_{1N}V_{Nr}$, so that that at zero temperature

$$\sum_{i,j} T_{ij}(E) = |G_{1N}(E_F)|^2 \Gamma_1^{(L)}(E_F) \Gamma_N^{(R)}(E_F) \quad (2.34)$$

and by using Equation 2.30 and Equation 2.31,

$$I(\Phi) = \frac{e}{\pi\hbar} \int_{E_F - e\Phi}^{E_F} dE |G_{1N}(E, \Phi)|^2 \Gamma_1^{(L)}(E) \Gamma_N^{(R)}(E + e\Phi) \quad (2.35)$$

with

$$\Gamma_1^{(L)}(E) = 2\pi \sum_l |V_{l1}|^2 \delta(E_1 - E); \quad \Gamma_N^{(R)}(E) = 2\pi \sum_r |V_{Nr}|^2 \delta(E_N - E) \quad (2.36)$$

The Green's function in Equation 2.34 is itself reduced to the bridge's subspace by projecting out the degrees of freedom of the electrode. This results in a renormalization of the bridge Hamiltonian: in the bridge subspace

$$(E - H + i\eta)^{-1} \rightarrow (E - H_B - \Sigma_B(E))^{-1} \quad (2.37)$$

where $H_B = H_B^0 + V_B$ is the Hamiltonian of the isolated bridge entity with

$$H_B^0 = \sum_{n=1}^N E_n |n\rangle\langle n|; \quad V_B = \sum_{n=1}^N \sum_{n'=1}^N V_{n,n'} |n\rangle\langle n'| \quad (2.38)$$

and where in the basis of eigenstates of H_B^0

$$\Sigma_{nn'}(E) = \delta_{n,n'} (\delta_{n,1} + \delta_{n,N}) [\Lambda_n(E) - (1/2)i\Gamma_n(E)] \quad (2.39)$$

$$\Gamma_n(E) = 2\pi \sum_j |V_{nj}|^2 \delta(E - E_j) \quad (2.40)$$

$$\Lambda_n(E) = \frac{PP}{2\pi} \int_{-\infty}^{\infty} dE' \frac{\Lambda_n(E')}{(E - E')} \quad (2.41)$$

In Equation 2.42 the sum is over both the right and left manifolds (j goes over all states $\{l\}$ and $\{r\}$ in these manifolds) so that $\Gamma_n = \Gamma_n^{(L)} + \Gamma_n^{(R)}$; $n = 1, N$. The

transmission problem is thus reduced to evaluating a Green's function matrix element and two width parameters. The first calculation is a simple inversion of a finite (order N) matrix. The width Γ and the associated shift Λ , represent the finite lifetime of an electron on a molecule adsorbed on the metal surface, and can be estimated for example, using the Newns-Anderson model of chemisorption. In the simple tight binding model of the bridge and in the weak coupling limit, G_{1N} is given by Equation 2.10 modified by the inclusions of the self energy terms,

$$G_{1N}(E) = \frac{V_{1,2}}{(E - E_1 - \Sigma_1(E))(E - E_N - \Sigma_N(E))} \prod_{j=2}^{N-1} \frac{V_{j,j+1}}{E - E_j} \quad (2.42)$$

Equation 2.34 through Equation 2.42 thus provide a complete simple model for molecular conduction, equivalent to similar approximations used in theories of molecular electron transfer.

2.5 Conduction Channels

Next, molecular conduction is broken down into channels based on the work and derivations of Solomon and coworkers [62]. To start, the simplest form of the transmission as given by

$$T(E) = \mathbf{Tr} [\Gamma^L(E)G^r(E)\Gamma^R(E)G^a(E)] \quad (2.43)$$

where $G^r(E)$ and $G^a(E)$ are the retarded and advanced Green's function of the molecule. We can then write Γ^L and Γ^R matrices as

$$\Gamma_{ij}^L(E) = 2\pi \sum_{\alpha} V_{i\alpha}^L V_{\alpha j}^L \delta(E - \epsilon_{\alpha}^L) \quad (2.44)$$

$$\Gamma_{ij}^R(E) = 2\pi \sum_{\beta} V_{i\beta}^R V_{\beta j}^R \delta(E - \epsilon_{\beta}^R) \quad (2.45)$$

where $V^{L(R)}$ are the coupling matrices connecting the the left and right electrodes to the molecule in question. In this particular work, the indices α and β are the indices

of the left and right electrodes and the indices i and j are the indices of the extended molecule component (where we include a part of the molecule and its linker group to the electrode). Now we can define

$$d_{\alpha(\beta)}^{L(R)}(E) = \sqrt{2\pi\delta\left(E - \epsilon_{\alpha(\beta)}^{L(R)}\right)} \quad (2.46)$$

This is an unusual and well defined quantity which we will show is useful for the manipulation of the equations. Next, Γ^L and Γ^R reduce to

$$\begin{aligned} \Gamma_{ij}^L(E) &= \sum_{\alpha} V_{i\alpha}^L d_{\alpha}^L(E) d_{\alpha}^L(E) V_{\alpha j}^L \\ \Gamma_{ij}^R(E) &= \sum_{\beta} V_{i\beta}^R d_{\beta}^R(E) d_{\beta}^R(E) V_{\beta j}^R \end{aligned} \quad (2.47)$$

From this reduction, we can rewrite Equation 2.43 as

$$T(E) = \mathbf{Tr} \left[V^L d^L(E) d^L(E) V^{L\dagger} G^r(E) V^R d^R(E) d^R(E) V^{R\dagger} G^a(E) \right] \quad (2.48)$$

The \dagger denotes the conjugate transpose, or a simple transpose in the case of real matrices. From here on $V^{L(R)}$ will occur with $d^{L(R)}$ so we can simplify the expression by defining

$$\begin{aligned} \gamma^{L(R)}(E) &= V^{L(R)} d^{L(R)}(E) \\ \gamma^{L(R)\dagger}(E) &= d^{L(R)}(E) V^{L(R)\dagger} \end{aligned} \quad (2.49)$$

Equation 2.48 can then be rearranged using the equivalence of a trace to cyclic permutation and be expressed in its Hermitian form

$$\begin{aligned} T(E) &= \mathbf{Tr} \left[(\gamma^{L\dagger}(E) G^r(E) \gamma^R(E)) (\gamma^{R\dagger}(E) G^a(E) \gamma^L(E)) \right] \\ &= \mathbf{Tr} \left[(\gamma^{L\dagger}(E) G^r(E) \gamma^R(E)) (\gamma^{L\dagger}(E) G^r(E) \gamma^R(E))^{\dagger} \right] \\ &= \sum_{\alpha, \beta} \left| \sum_{i, j} \gamma_{\alpha, i}^{L\dagger}(E) G_{i, j}^r(E) \gamma_{j, \beta}^R(E) \right|^2 \end{aligned} \quad (2.50)$$

The major advantage of writing the transmission in its Hermitian form instead of in terms of $\Gamma_{L(R)}^{1/2}$ is that it allows for further simplification of the equations and also

clearly shows where the electrode and molecule couplings remain in the expression. Also, this expression for transmission can easily be converted back to the normal rate expression for electron transfer. This expression differs from standard electron transfer rates because if we follow the work of Datta and Nitzan, we assume that the effective state density for energy dissipation for an electron transfer process (in coherent junction transport), is just the electrode's density of states appearing in Γ . Briefly

$$\begin{aligned}
k_{ET} &= \frac{1}{\hbar} \int dE T(E) \\
&= \frac{2\pi}{\hbar} \int dE \sum_{\alpha,\beta} \left| \sum_{i,j} V_{\alpha,i}^{L\dagger}(E) G_{i,j}^r(E) V_{j,\beta}^R(E) \right|^2 \\
&\quad \times \delta(E - \epsilon_\alpha^L) \delta(E - \epsilon_\beta^R) \\
&= \frac{2\pi}{\hbar} \sum_{\alpha,\beta} \left| \sum_{i,j} V_{\alpha,i}^{L\dagger}(\epsilon_\alpha^L) G_{i,j}^r(\epsilon_\alpha^L) V_{j,\beta}^R(\epsilon_\alpha^L) \right|^2 \delta(\epsilon_\alpha^L - \epsilon_\beta^R) \\
&= \frac{2\pi}{\hbar} \sum_{\alpha,\beta} |t_{\alpha,\beta}(\epsilon_\alpha^L)|^2 \delta(\epsilon_\alpha^L - \epsilon_\beta^R)
\end{aligned} \tag{2.51}$$

This is now considered a ‘‘Golden Rule’’ type expression for the electron transfer rate as derived from the Landauer equation and within the domain of scattering theory. This derivation of the equation has served to transform the trace into a two-index sum over α and β (the electrode dimensions). Also, the dimension of the matrix under the trace is now left electrode by right electrode. We can use this in order to make a few more salient points.

The first point we can note is that the expression derived above for $T_{\alpha\beta}$ is equivalent to another one derived earlier for the donor-acceptor coupling through the system.

$$t_{\alpha\beta}^{DA}(E) = \sum_{i,j} V_{\alpha,i}^L G_{i,j}^r(E) V_{j,\beta}^R \tag{2.52}$$

This now conceptually provides a solid link between the Landauer equation, scattering theory, and electron transfer theory. The coupling as calculated using this method-

ology slightly differs from convention due to its inclusion of the self energy term in $G^r(E)$ which results in the self energy term being a complex number. If we consider the intramolecular electron transfer instead of electrodes, the self energy terms in $G^r(E)$ will lack a significantly large complex component and therefore more closely resemble the usual form. Also, this expression provides a relatively straightforward approach to calculate coupling components through many extended systems since the methods to calculate all the quantities in Equation 2.52 are well established in the transport literature.

If we use a basis transformation, the coupling and transmission through a molecule can be understood in terms of the contributions from different molecular conductance orbitals. We can obtain the eigenvectors C_r and C_a by using the overlap matrix S and diagonalize G^r and G^a .

$$\begin{aligned}
 G^{r'}(E) &= C_r^{-1} S^{-1} G^r(E) C_r \\
 G^{a'}(E) &= C_a^{-1} S^{-1} G^a(E) C_a \\
 &= C_r^\dagger G^a(E) S^{-1} C_r^{-1\dagger}
 \end{aligned}
 \tag{2.53}$$

We can see here that molecular orbitals differ from molecular *conductance* orbitals by diagonalizing $G^r(E)$ instead of the Hamiltonian of the isolated molecule we arrive at complex numbers. However, the dominate component of the isolated molecule is its molecular orbitals. In the case of complex coupling, the self energy terms will be such that the molecular conductance orbitals can resemble the simpler molecular orbitals than they will for a molecule in a junction bound to metal electrodes.

We can now see that the transmission matrix can be transformed to give

$$\begin{aligned}
T(E) &= \mathbf{Tr}[\gamma^L(E)\gamma^{L\dagger}(E)SC_rG^{r'}(E)C_r^{-1}\gamma^R(E) \\
&\quad \times \gamma^{R\dagger}(E)SC_aG^{a'}(E)C_a^{-1}] \\
T(E) &= \mathbf{Tr}[\gamma^L(E)\gamma^{L\dagger}(E)SC_rG^{r'}(E)C_r^{-1}\gamma^R(E)\gamma^{R\dagger}(E) \\
&\quad \times (C_r^\dagger)^{-1}G^{a'}(E)C_r^\dagger S^{-1}]
\end{aligned} \tag{2.54}$$

and can be further simplified if we define the transformed matrices

$$\begin{aligned}
\gamma^{L'}(E) &= C_r^\dagger S^{-1}\gamma^L(E) \\
\gamma^{R'}(E) &= C_r^{-1}\gamma^R(E)
\end{aligned} \tag{2.55}$$

Equation 2.54 then reduces to

$$\begin{aligned}
T(E) &= \mathbf{Tr} \left[\gamma^{L'\dagger}(E)G^{r'}(E)\gamma^{R'}(E)\gamma^{R'\dagger}(E)G^{a'}(E)\gamma^{L'}(E) \right] \\
&= \mathbf{Tr}[(\gamma^{L'\dagger}(E)G^{r'}(E)\gamma^{R'}(E)) \\
&\quad \times (\gamma^{L'\dagger}(E)G^{r'}(E)\gamma^{R'}(E))^\dagger] \\
&= \sum_{\alpha,\beta} \sum_i \left| \gamma_{\alpha,i}^{L'\dagger}(E)G_{i,i}^{r'}(E)\gamma_{i,\beta}^{R'}(E) \right|^2
\end{aligned} \tag{2.56}$$

Next, we define the couplings, $t_{\alpha\beta}$, as

$$t_{\alpha\beta}(E) \equiv \sum_i V_{\alpha,i}^{L'\dagger}(E)G_{i,i}^{r'}(E)V_{i,\beta}^{R'}(E) \tag{2.57}$$

where $V^{L(R)'}$ are transformed by the same transformations as $\gamma^{L(R)'}$. From this equation, we can define the quantity $t_{\alpha\beta i} = V_{\alpha,i}^{L'\dagger}(E)G_{i,i}^{r'}(E)V_{i,\beta}^{R'}$. This allows the coupling to be written as

$$t_{\alpha\beta}(E) = \sum_i t_{\alpha\beta i} \tag{2.58}$$

This now shows the result that the total transmission through the system is given and the sum of contributions through each of the molecular conductance orbitals can be read as each of the $t_{\alpha\beta}$ is given as a single index sum of the contributions ($t_{\alpha\beta i}$)

from each of the eigenfunctions of G^r . Due to previous interference between pairs of orbitals, such an attempt to separate the transmission into individual molecular conductance orbital contributions failed, unlike the derivation above. Also, typically the donor-acceptor coupling is given as a series of expansions, however, the main advantage of this expression is that by diagonalizing G^r the series reduces to a single index sum. Hence, through the use of these derivations, the transmission and coupling through a molecule can be ascertained by summing the contributions from each of the molecular conductance orbitals.

2.6 Quantum Interference and Fano Resonances

Similar to classical interference in which two traveling waves may interact (superpose) to form a new resultant wave of modified amplitude [63], quantum interference (QI) is a phenomenon which is caused by the superposition of wave functions (or propagating wavefunctions in nano-structures) [5]. The phenomenon of QI is not new and the effect of QI on transport has been studied in the field of mesoscopic physics [64, 65], quantum dots [66, 67], and electron transfer systems [68, 28, 69]. Due to the increasing interest in tunable electronics, the effect of QI on electron transport in molecular junctions has also benefited from an increase in attention and its possible applications in various fields [70, 71, 72, 73, 74, 75, 76]. The QI phenomenon is visualized as additional peaks or dips in transmission spectra which is easily recognizable. The understanding of this phenomena can improve the performance of molecular switches and sensors [71, 77], and thermoelectric devices [78, 79].

Figure 2.1 shows a schematic representation of four common QI effects with their respective transmission spectra of various systems connected to two electrodes. Here, due to the efforts of Nozaki and coworkers [5], it can be seen that the type of molecular junctions affects the transmission spectra of that system. Figure 2.1 also shows

how modifying the junction can give rise to interesting spectral features such as the appearance of resonance characteristics. The following equations and derivations are idealized for the making of similar diagrams and illustrate how certain types of spectral features can be described.

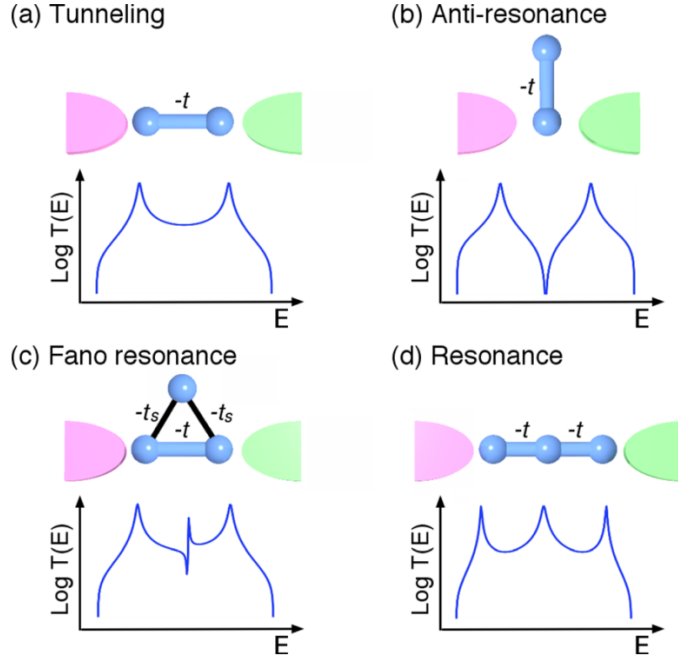


Figure 2.1: Common Types of Molecular Junctions with Transmission Profiles. (a) 2-Site, (b) T-Shaped, (c) Cyclic, and (d) Odd-membered Molecular Junctions. Figure Reproduced from Nozaki *et al.* [5]

The electronic structure of the molecular junctions can be entirely captured by a tight-binding Hamiltonian

$$H = H_L + V_L + H_M + V_R + H_R \quad (2.59)$$

where $H_{L/R}$ and H_M represent the Hamiltonian for the left and right electrodes as well as the molecule in the junction. $V_{L/R}$ defines how the molecule couples to the left and right electrodes. The electronic propagator for the entire system is defined

by a retarded Green's function defined as

$$G^{\text{R}}(E) = [(E + i\eta)I - H_{\text{M}} - \Sigma_{\text{L}} - \Sigma_{\text{R}}]^{-1} \quad (2.60)$$

where $i\eta$ is the infinitesimal imaginary value and where $\Sigma_{\text{L/R}}$ are the self-energy elements that include the influence of the electrodes on the coupling. At low bias and within the coherent regime, the conduction through a junction can be obtained using the Fisher-Lee relation

$$G = \frac{2e^2}{h} \text{Tr} [G^{\text{R}}\Gamma_{\text{L}}G^{\text{A}}\Gamma_{\text{R}}] \quad (2.61)$$

where $\Gamma_{\text{L/R}}$ represents a spectral broadening function

$$\Gamma_{\text{L/R}}(E) = i \left[\Sigma_{\text{L/R}} - \Sigma_{\text{L/R}}^{\dagger} \right] \quad (2.62)$$

The self-energies of the electrodes can be given using the Newns-Anderson model

$$\Gamma_{\text{L/R}}(E) = V_{\text{L/R}}g_{\text{L/R}}(E)V_{\text{L/R}}^{\dagger} \quad (2.63)$$

where $g_{\text{L/R}}(E)$ is the surface Green's function [80, 81, 82, 83, 84]

$$g_{\text{L/R}}(E) = \frac{ie^{ika}}{t_{\text{L/R}}} \quad (2.64)$$

where $t_{\text{L/R}}$ is the nearest-neighboring transfer integral in the left and right electrodes. All energies in t are normalized while all on-site energies are set to zero for convenience. Here, the nearest-neighbor couplings in the contacts are defined as $t_{\text{L/R}} = -t$. Tight-binding parameters used in this representation are given in units of eV (for example, the energy for carbon-based π -electron systems is $t = 2.66$ eV). These on-site energies are not always representative of the energies of atomic orbitals but rather could represent the eigenenergies of the fragment molecular orbitals [5].

One of the more interesting types of resonance is the Fano resonance, exemplified by its asymmetric line profile. As mentioned previously, in short molecular junctions,

wave propagation distances can make the phase-coherent processes a very important topic. The scattering of waves propagating along different paths can, as a consequence, result in interference where either constructive interference corresponds to resonant enhancement and destructive interference can correspond to suppression of the transmission [6]. Resonances with asymmetric line shapes were first described by Ugo Fano [85, 86] when he noticed unusual sharp peaks in the absorption spectra of noble gases in the work of Beutler [87]. Fano interpreted these spectral absorption lines based on the interaction of a discrete excited state of an atom with a continuum sharing the same energy level. Fano resonances also appear in Raman spectra and are characterized by asymmetric line broadening (expressed by the Breit-Wigner-Fano line shape) [88]. These characteristic line shapes have been observed in the Raman spectra of carbonic materials; for example, in the spectra of metallic single wall carbon nanotubes [88].

As a result of his observations of Beutler's work, Fano proposed a formula for the shape of the resonance profile [85, 86] of a scattering cross section as

$$\sigma = \frac{(\epsilon + q)^2}{\epsilon^2 + 1} \quad (2.65)$$

where q is a phenomenological shape parameter and ϵ is a reduced energy defined by $2(E - E_F)/\Gamma$. The resonant energy is E_F and Γ is the width of the spectral feature. In Equation 2.65, there exists one maximum and one minimum in the Fano profile

$$\sigma_{\min} = 0 \quad \text{at} \quad \epsilon = -q \quad (2.66)$$

$$\sigma_{\max} = 1 + q^2 \quad \text{at} \quad \epsilon = 1/q \quad (2.67)$$

Fano introduced in his original paper the asymmetry parameter q [86]. Here, q is a ratio of the transition probabilities to the mixed state and to the continuum as seen in Figure 2.2 and referred to as the asymmetry parameter. When q is on the

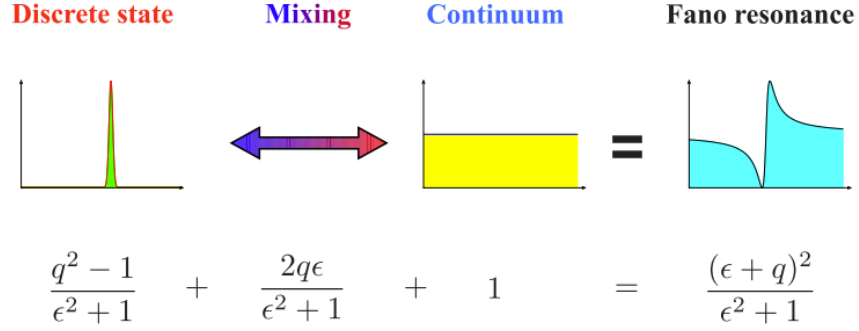


Figure 2.2: Illustration of the Fano Formula (Equation 2.65) as a Superposition of the Lorentzian Line Shape of the Discrete Level with a Flat Continuous Background. Caption and Figure Adopted From Ref. [6]

order of unity, the discrete state and continuum are of the same magnitude leading to the asymmetric profile seen in Equation 2.65. Here, the maximum value at $E_{\max} = E_F + \Gamma/(2q)$ and minimum at $E_{\min} = E_F - \Gamma q/2$. When $q = 0$ (a unique case of the Fano resonance), a symmetrical dip occurs representing an antiresonance profile (See Figure 2.3). The salient feature of the Fano resonance is the likelihood of destructive interference which leads to the asymmetric line profile [89, 90, 91, 92, 93, 94].

2.7 Polarizability

Polarizability is a property of matter that describes the ability of a system to respond to an external electric field. In the case of this study, polarizability describes specifically how a cloud of electron density will deform in the presence of an electric field. Polarizability as a property is involved in the modeling and study of dispersion and dipole-dipole interactions [95]. When we consider the size domain of molecules, polarizability is considered the first important term of the dipole moment expansion as power series (contained within a uniform electric field) and is expressed by a second-rank Cartesian tensor [96]. Polarizability has been used to understand other

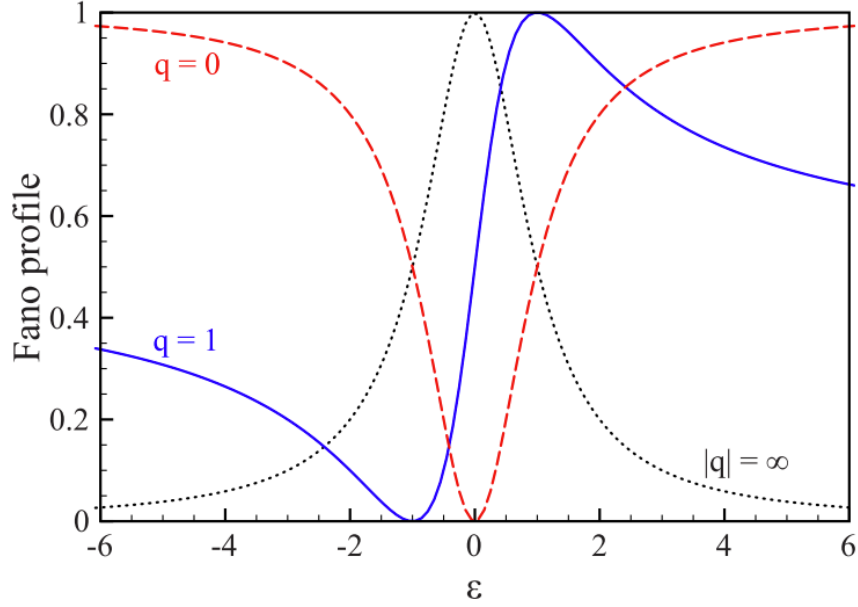


Figure 2.3: Normalized Fano Profiles (1) with the Prefactor $1/(1+q^2)$ (2) for Various Values of the Asymmetry Parameter q . Caption and Figure Adopted From Ref. [6]

properties of matter such as refraction indices and absorption coefficients while also being important in optical cooling and the trapping of atoms [96, 97], also in the use of optical tweezers [98]. In these areas, polarizability is considered a fundamental electronic property user to determine optical properties. Last, polarizability plays an important role in thermodynamic models; for instance, as an estimation of cohesive energy density models [99].

The polarizability tensor, α , is linked to density functional theory (DFT) [100, 101] through the linear response kernel ($\chi(\vec{r}, \vec{r}')$) [102]. Here, polarizability can be written exactly in terms of an integral over $\chi(\vec{r}, \vec{r}')$ as

$$\alpha = - \int d\vec{r} d\vec{r}' \chi(\vec{r}, \vec{r}') \vec{r}' \quad (2.68)$$

or by using the local polarization tensor $\alpha(\vec{r})$ [103] defined as the vector derivative

of the density over the electric field $\vec{\varepsilon}$ as

$$\alpha(\vec{r}) = - \left(\frac{\partial \rho(\vec{r})}{\partial \vec{\varepsilon}} \right) = - \int \chi(\vec{r}, \vec{r}') \vec{r}' d\vec{r}' \quad (2.69)$$

The polarizability tensor on its own does not provide an interpretation for the chemical description of the local changes in a molecule; it does not provide any information concerning which atoms or groups of atoms are most involved in contributing to the total polarizability of the molecule. Due to this, different molecular partitioning schemes have been created in order to “group or cluster” polarizabilities computed via the dependency between the trace of the polarizability tensor (pertaining either to an atom or a molecule) and its volume [104, 105]. There are typically two general approaches to partition the total polarizability tensor into atomic contributions. The first approach describes the response of an atom to the local field affected by the “closeness” of other atoms in the molecule [106, 107, 108, 109, 110, 111, 112]. The second approach examines the response of an atom to the applied field. This method carries out partitioning that does not use empirical or point-dipole models for the estimation of the induced field. Both avenues start at the atomic polarizability for their characterizations of a system.

Different uses for the atomic polarizability have been proposed combining the approach presented by Becke and Johnson [95, 113, 114] together with a Hirshfeld-type partitioning for the molecular polarizabilities into atomic contributions [115, 116, 117].

We will focus on Hirshfeld-based partitioning schemes in this work. Any Hirshfeld-based [118] partitioning scheme assumes that the electron density for each distinct point, \vec{r} , in a molecule consisting of N atoms is represented by the contribution of all atoms. The contribution of atom A to total polarizability is based on a “weight-function” ($W_A(\vec{r})$), which is formed by the ratio between the atomic density of the

isolated atom A ($\rho_A(\vec{r})$) and the sum of all other atomic contributions (promolecular density) ($\rho_{\text{mol}}(\vec{r})$)

$$W_A(\vec{r}) = \frac{\rho_A(\vec{r})}{\rho_{\text{mol}}(\vec{r})} = \frac{\rho_A(\vec{r})}{\sum_{n=1}^N \rho_n(\vec{r})} \quad (2.70)$$

and satisfies the following requirements

$$\sum_{n=1}^N W_n(\vec{r}) = 1 \quad (2.71)$$

$$0 \leq W_n(\vec{r}) \leq 1 \quad (2.72)$$

Here, the 9-component polarizability tensor α , combined with its local counterpart $\alpha(\vec{r})$ can be partitioned into atomic contributions when they are considered with respect to the first-order perturbed electron density when integrated over the molecular space

$$\alpha_{ij} = - \int \alpha_{ij}(\vec{r}) d\vec{r} = - \int i\rho^{(j)}(\vec{r}) d\vec{r} \quad (2.73)$$

where $\rho^{(j)}(\vec{r})$ is the electron density derivative with respect to an external (uniform and time-independent) electric field $\vec{\epsilon}_j$ in the j direction. This is evaluated in the limit of zero field strength where i corresponds to the Cartesian coordinate of (\vec{r}) .

Polarizability is partitioned by the introduction of the previously mentioned “weight-function” $W_A(\vec{r})$ as

$$\alpha_{ij} = \sum_{n=1}^N - \int W_n(\vec{r}) i\rho^{(j)}(\vec{r}) d\vec{r} \quad (2.74)$$

Equation 2.73 explicitly depends on an atoms position in a molecule and hinders the comparison of equivalent atoms in different molecules. For example, a methyl group attached to a small molecule vs a methyl group attached to a larger molecule will not provide the same polarizability description. This would therefore hamper the polarizability descriptor from being a reactivity index (if we were to consider a very large molecule, then the outer regions would completely overshadow any information

of the inner region). The preferred solution is then to sum and subtract the nuclear position of atom A (R_A) and then to multiply that by the corresponding atomic perturbed population in Equation 2.74.

Therefore, the atomic polarizability for atom A is given by two resulting components

$$\begin{aligned}
\alpha_{ij}^A &= - \int W_A(\vec{r}') i \rho^{(j)}(\vec{r}') d\vec{r}' + (R_A^i - R_A^j) N_A^{(j)} \\
&= - \int W_A(\vec{r}') i \rho^{(j)}(\vec{r}') d\vec{r}' + \int W_A(\vec{r}') [R_A^i - R_A^j] \rho^{(j)}(\vec{r}') d\vec{r}' \\
&= - \int W_A(\vec{r}') (i - R_A^i) \rho^{(j)}(\vec{r}') d\vec{r}' - \int W_A(\vec{r}') R_A^j \rho^{(j)}(\vec{r}') d\vec{r}' \\
&= \alpha_{ij}^{A,\text{intr}} + \alpha_{ij}^{A,\text{ct}}
\end{aligned} \tag{2.75}$$

where $\alpha_{ij}^{A,\text{intr}}$ and $\alpha_{ij}^{A,\text{ct}}$ stand for the intrinsic and charge transfer component of the polarizability, respectively.

When the polarizability is calculated by any of the many atomic partitioning schemes, the polarizability represents the response of the atoms in the molecule to the applied electric field. An important note is that the polarizability of a molecule does not correspond to the simple sum of the polarizabilities of the isolated atoms. When we consider the interactions between atoms (electrostatic, etc), the polarizability of an atom depends not only on its location within a molecule, but also on the types of bonds it makes. Therefore, the molecular polarizability is the sum of the atomic polarizabilities coupled with their charge transfer contributions (in bonds, etc).

In this study, we also use the average of the polarizability tensor trace, also referred to as isotropic polarizability

$$\alpha_{\text{iso}} = \frac{\alpha_{xx} + \alpha_{yy} + \alpha_{zz}}{3} \tag{2.76}$$

Chapter 3

CALCULATED PROPERTIES OF SELECTED MONOMERS

3.1 Introduction

Prior work by Meidanshahi *et al.* examined the effects of polarizability in molecular junctions involving hydrogen bonds [119]. A very important feature of hydrogen bonds is that they are characterized by high polarizabilities [120]. This feature is increased in the presence of external electric fields [121]. This feature is important to our study of transport through hydrogen bonds because polarizable systems have an electron cloud that will deform in direct response to any bias modulation. This bias modulation serves to modulate the tunneling current through changes in the barrier properties of the junction [122]. Meidanshahi *et al.* found that the changes in the conductance of some molecules adsorbed onto gold electrodes could be used to calculate their polarizabilities [123]. Also, they found a direct connection between conductance and polarizability that may allow for a simple descriptor of conductance. In this section we look at the polarizability of selected monomers in order to ascertain if polarizability can be used to predict simple trends in conductance. Later, in Chapter 5, we will again look at polarizability but after these monomers have entered into a hydrogen bond.

3.2 Computational Methods

Full geometry optimizations of all monomer conformations were carried out at the density functional level of theory (DFT) using the Becke gradient-corrected exchange functional and Lee-Yang-Parr correlation functional with three parameters (B3LYP)

and the 6-311++G(2d,2p) basis set. Also, the total isotropic polarizability was calculated and then partitioned into individual atomic components using an approach based on Hirshfeld population analyses [124]. Both calculations were performed using Gaussian 09.

In this method, the spherically averaged molecular static dipole polarizability $\alpha_{\gamma\gamma}$ can be partitioned over all atoms i in a molecule as,

$$\alpha_{\gamma\gamma} = \sum_i \alpha_{\gamma\gamma i} \quad (3.1)$$

using the following relation:

$$\alpha_{\gamma\gamma i} = \lim_{F_\gamma \rightarrow 0} \frac{\mu_{\gamma i}(F_\gamma) - \mu_{\gamma i}(0)}{F_\gamma} \quad (3.2)$$

In the above equation, the quantities $\mu_{\gamma i}(F_\gamma)$ and $\mu_{\gamma i}(0)$ are the distributed contributions to the dipole moment obtained from the Hirshfeld population analysis, where the $\gamma\gamma$ component of the molecular static dipole polarizability is calculated as,

$$\alpha_{\gamma\gamma} = \left(\frac{\partial \mu_\gamma}{\partial F_\gamma} \right)_0 = \lim_{F_\gamma \rightarrow 0} \frac{\mu_\gamma(F_\gamma) - \mu_\gamma(0)}{F_\gamma} \quad (3.3)$$

where μ_γ is the component of the dipole moment along the γ axis, with $\gamma = x, y, \text{ or } z$. F_γ is the magnitude of an auxiliary static electric field F used in the calculation, oriented along the γ axis, and '0' indicates $F = 0$. Averaging over α_{xx} , α_{yy} , and α_{zz} yields the spherically averaged molecular dipole polarizability α . Each component of the molecular polarizability tensor is then written as a sum of the individual atomic polarizabilities.

Electronic transport calculations were performed using the NEGF+DFT approach as implemented in the Tran-SIESTA computational package [125]. In order to appropriately capture the subtleties of the hydrogen bond in all considered systems [119], we used a double- ζ basis set in our transport calculations. The generalized gradient

approximation (GGA) was used as the exchange correlation functional. The energy cutoff for the real space grid was 200 Ry.

The theoretical model that accounts for a quantitative interpretation of an experimental setup corresponds to electron transport occurring via a one-electron tunneling mechanism under the Landauer regime. In such a model the current is well described by a dimensionless transmission coefficient, which depends on the nature of the tunneling barrier,

$$I(V) = \frac{4e}{h} \int_{\mu_R}^{\mu_L} dE \tau(E, V) \quad (3.4)$$

where E is the energy of the tunneling electron, V is the applied voltage, and μ_L , μ_R are the electrochemical potentials in the left and right electrodes, respectively. Equation 3.4 becomes the linearized expression for the current

$$I(V) = \frac{4e^2}{h} \tau(E_F) V \quad (3.5)$$

In this regime the conductance is given by the Landauer expression,

$$G = \frac{4e^2}{h} \tau(E_F) \quad (3.6)$$

where the transmission coefficient can be written as [126],

$$\tau(E_F) = T_{LMR} \xi_L(E_F) \xi_R(E_F) \quad (3.7)$$

and T_{LMR} is the effective coupling to the left (L) and right (R) electrodes mediated by the molecule M and $\xi_{L/R}(E_F)$ are the densities of states of the L/R electrode/molecule contacts at the Fermi energy. Last, we use an implementation of the NEGF formalism contained in the trans-SIESTA computational package [127] for our transport calculations.

3.3 Results and Discussion

Before we discuss the polarizability results of our calculations and how they relate to conductance, it is useful to note that the considered monomers have similar gap energies between their highest occupied molecular orbital (HOMO) and lowest unoccupied molecular orbital (LUMO). The results of these calculations can be seen in Table 3.1.

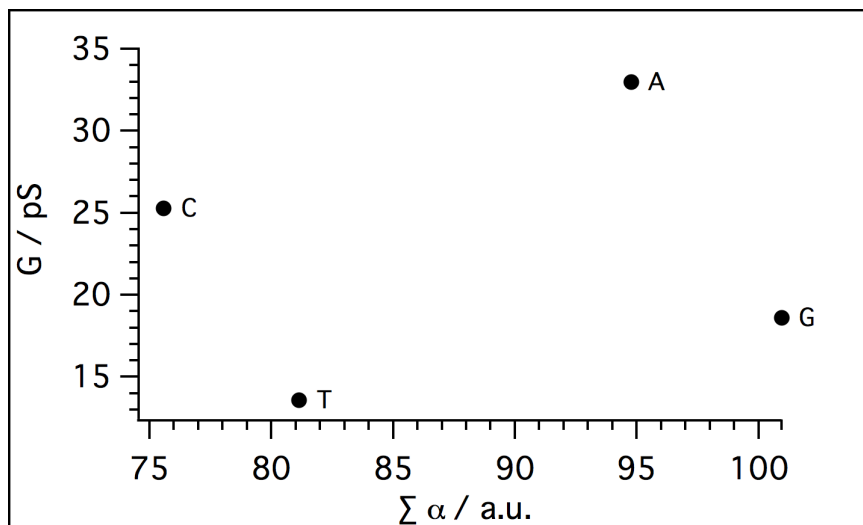
| System | HOMO (eV) | LUMO (eV) | Gap (eV) |
|--------|-----------|-----------|----------|
| A | -6.3 | -0.9 | 5.4 |
| T | -6.9 | -1.5 | 5.4 |
| U | -7.3 | -1.7 | 5.6 |
| C | -6.5 | -1.3 | 5.2 |
| G | -5.9 | -1.0 | 4.9 |

Table 3.1: HOMO-LUMO Gap Energies of Considered Systems.

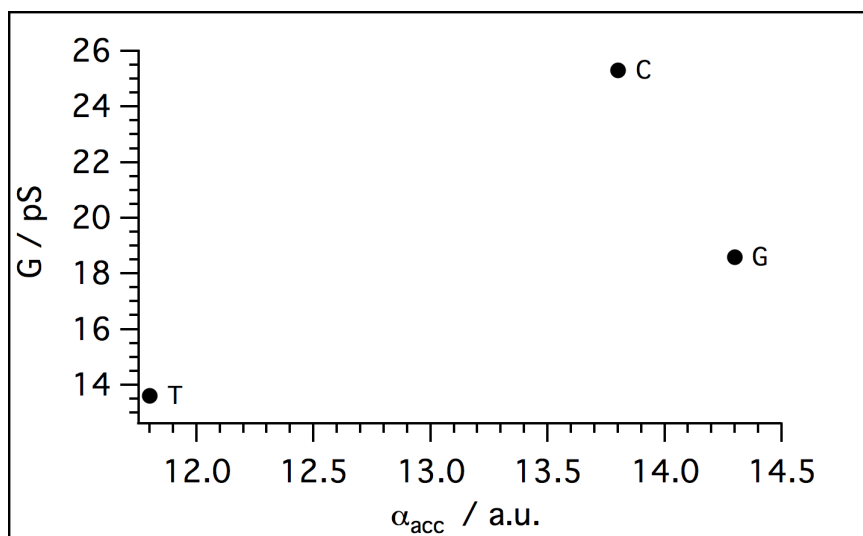
Next, we obtained conductance values from an experimental paper by Chang *et al.* [7] for the considered monomers and plotted these values against total polarizability and the proton acceptor’s atomic polarizability which can be seen in Figure 3.1. In Figure 3.1a, the measured conductance (G) was plotted against the total polarizability of the selected monomers. The measured conductance demonstrates the trend: $A > C > G > T$ while the polarizability demonstrates the trend: $G > A > T > C$. The polarizability values demonstrate a trend when comparing purine versus pyrimidine derivatives. A and G are 2-ringed purine derivatives while C and T are 1-ring pyrimidine derivatives. We can see that the polarizability is higher for A and G versus C and T. In Figure 3.1b, we have the measured conductance plotted against the atomic polarizability of the proton acceptor atom. The measured conductance

values demonstrate the trend: $C > G > T$ while the acceptor polarizability values demonstrate the trend: $G > C > T$.

Table 3.2 and Table 3.3 show the atomic polarizabilities for the atoms participating in a hydrogen bond when these systems are bound to their complement in either DNA or RNA. Table 3.2 contains the atomic polarizabilities for atoms in the $NH \cdots O$ bond while Table 3.3 contains the atomic polarizabilities for atoms in the $NH \cdots N$ bond.



(a) Measured G vs $\Sigma \alpha$ for Selected Nucleotides



(b) Measured G vs α_{acc} for Selected Nucleotides

Figure 3.1: (a) Measured Conductance (G) [7] Versus Total Polarizability. (b) Measured Conductance (G) [7] Versus the Polarizability of the Proton Acceptor Atom in the $\text{NH} \cdots \text{O}$ Bond. Here, O is the Proton Acceptor.

| System | α_N | α_H | α_O | $\sum \alpha$ | $\sum \alpha_N$ | $\sum \alpha_C$ | r_{N-H} |
|--------|------------|------------|------------|---------------|-----------------|-----------------|-----------|
| A | 5.8 | 8.6 | — | 95 | 33.4 | 20.3 | 1.003 |
| T | — | — | 11.8 | 81 | 5.2 | 10.0 | — |
| U | — | — | 13.3 | 68 | 4.9 | 12.4 | — |
| G | 7.0 | 8.0 | 14.3 | 101 | 28.3 | 18.8 | 1.007 |
| C | — | — | 13.8 | 76 | 13.9 | 13.0 | — |

Table 3.2: Calculated Atomic Polarizability and Other Geometric Parameters in Comparison to Their $NH \cdots O$ Bond.

| System | α_N | α_H | α_N | $\sum \alpha$ | $\sum \alpha_N$ | $\sum \alpha_C$ | r_{N-H} |
|--------|------------|------------|------------|---------------|-----------------|-----------------|-----------|
| A | — | — | 7.9 | 95 | 33.4 | 20.3 | — |
| T | 2.1 | 5.4 | — | 81 | 5.2 | 10.0 | 1.010 |
| U | 1.9 | 4.9 | — | 68 | 4.9 | 12.4 | 1.010 |
| G | 2.5 | 6.1 | — | 101 | 28.3 | 18.8 | 1.009 |
| C | — | — | 5.3 | 76 | 13.9 | 13.0 | — |

Table 3.3: Calculated Atomic Polarizability and Other Geometric Parameters in Comparison to Their $NH \cdots N$ Bond.

Next we investigated the atomic polarizabilities of N atoms in the family of purines to ascertain what effect, if any, neighboring electron withdrawing or electron donating groups had on the polarizability of the atoms labeled α_{N-A} , α_{N-B} , α_{N-C} , and α_{N-D} . The family of purines analyzed in this study with their labeled nitrogen atoms can be seen in Figure 3.2.

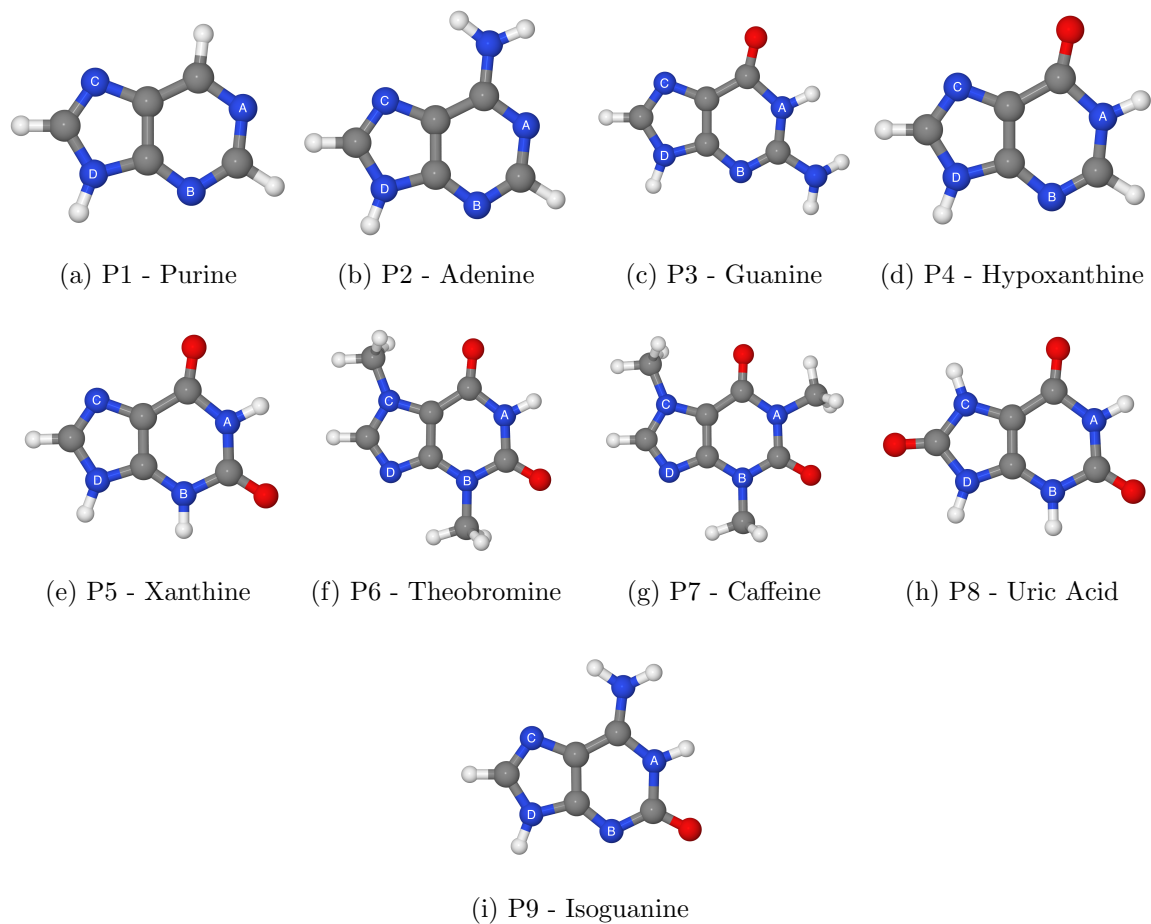


Figure 3.2: Purine and Its Derivatives. Nitrogen Atoms in the 6-Membered Ring are Labeled A and B; All Nitrogen Atoms in the 5-Membered Ring are Labeled C and D.

Table 3.4 shows the relevant information on the polarizability data calculated for the purine family.

| Label | System | $\sum \alpha$ | $\sum \alpha_N$ | $\sum \alpha_C$ | α_{N-A} | α_{N-B} | α_{N-C} | α_{N-D} |
|-------|--------------|---------------|-----------------|-----------------|----------------|----------------|----------------|----------------|
| P1 | Purine | 83 | 28.8 | 21.8 | 9.7 | 7.3 | 8.3 | 3.5 |
| P2 | Adenine | 95 | 33.5 | 20.3 | 7.8 | 8.8 | 7.0 | 4.0 |
| P3 | Guanine | 101 | 21.3 | 18.8 | 2.5 | 6.2 | 8.6 | 4.0 |
| P4 | Hypoxanthine | 89 | 22.6 | 20.2 | 3.3 | 7.7 | 7.7 | 3.9 |
| P5 | Xanthine | 92 | 16.9 | 17.2 | 2.3 | 2.6 | 8.0 | 3.9 |
| P6 | Theobromine | 118 | 14.5 | 20.9 | 2.7 | 1.8 | 2.5 | 7.4 |
| P7 | Caffeine | 131 | 14.3 | 23.7 | 1.8 | 1.9 | 2.5 | 8.0 |
| P8 | Uric Acid | 99 | 11.3 | 13.6 | 2.8 | 2.6 | 2.6 | 3.3 |
| P9 | Isoguanine | 102 | 28.6 | 18.8 | 2.8 | 8.0 | 7.6 | 4.1 |

Table 3.4: Calculated Polarizabilities of Purine and Derivatives.

Purines are a class of nitrogen-containing heterocycles that occur in natural systems. Purines consist of a pyrimidine ring fused into an imidazole ring (purine). While the atomic polarizability of the nitrogen atoms in pyrimidine is equal (7.2 bohr³), purine's nitrogen atoms (labeled as A and B in Figure 3.2 have very different atomic polarizability as a result of the breaking the C₂ symmetry due to the imidazole-like ring. The atomic polarizability of the nitrogen atoms in purines is affected by, the hybridization of nitrogen atom. The sp³ nitrogen atoms show a higher atomic polarizability in comparison to sp²s. It is interesting to note that, the N-methylation of the purines not only reduces the atomic polarizability of the nitrogen atom, but also increases the electron donating abilities of purines. It is worth noting that the sp³ nitrogens on the 5-member ring have higher atomic polarizability than their counterparts in the 6-membered ring.

Since purines occur naturally in biological systems we can use them as a probe

to interrogate electrochemical phenomenon that happens in biological systems, for instance: mitochondria’s electron transport channel.

Last, we investigated the polarizability of pyrimidines. Table 3.5 shows differing levels of theory used in our calculations as a benchmark. While all levels of theory gave excellent data, we used the B3LYP/6-311++G(2d,2p) level of theory for all of our monomer, and later, DNA base pair calculations.

| Label | System | Level of Theory | $\sum \alpha$ | α_{N-A} | α_{N-B} |
|-------|------------|-----------------------|---------------|----------------|----------------|
| Py1 | Pyrimidine | PBEh1PBE/6-31G* | 46 | 5.4 | 5.4 |
| Py2 | Pyrimidine | PBEh1PBE/6-31+G* | 54 | 6.9 | 6.9 |
| Py3 | Pyrimidine | B3LYP/6-31++G** | 56 | 7.1 | 7.1 |
| Py4 | Pyrimidine | B3LYP/6-311++G(2d,2p) | 57 | 7.2 | 7.2 |

Table 3.5: Calculated Polarizabilities of Pyrimidine - Different Levels of Theory.

Figure 3.3 shows the structures of the pyrimidine family with labeling of the nitrogen atoms under investigation.

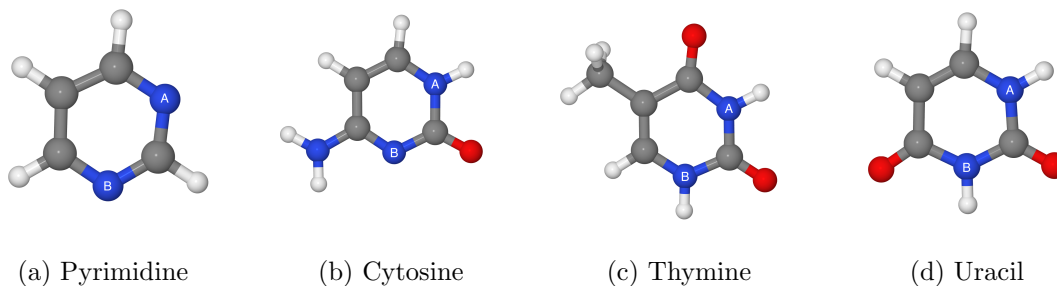


Figure 3.3: Pyrimidine and Derivatives.

Last, Table 3.6 lists the values for the different α_{N-A} , and α_{N-B} values from the pyrimidine calculations.

| System | $\sum \alpha$ | $\sum \alpha_N$ | $\sum \alpha_C$ | α_{N-A} | α_{N-B} |
|------------|---------------|-----------------|-----------------|----------------|----------------|
| Pyrimidine | 57 | 14.3 | 15.3 | 7.2 | 7.2 |
| Cytosine | 76 | 13.9 | 13.0 | 3.1 | 5.3 |
| Thymine | 81 | 5.2 | 10.0 | 2.1 | 3.1 |
| Uracil | 68 | 4.9 | 12.4 | 3.0 | 1.9 |

Table 3.6: Calculated Polarizabilities of Pyrimidine and Derivatives.

In summary, we have found that when comparing similar families of molecules, that the polarizability of the hydrogen acceptor atom is proportional to the measured conductance. Figure 3.4 shows a summary of our results. Here, we have separated the purines (black) from the pyrimidines (red). When comparing pyrimidines, cytosine demonstrates a higher conductance trend than thymine. The polarizability of the hydrogen acceptor atom is also higher for cytosine than for thymine. These initial

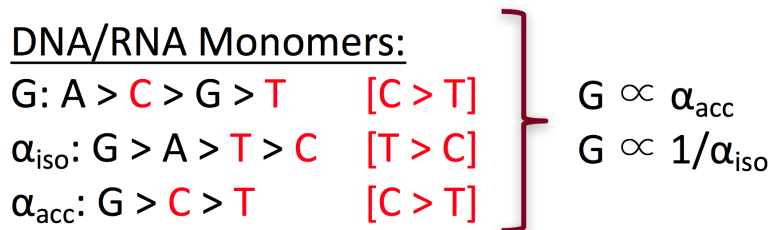


Figure 3.4: Summary of Results for Monomer Structures.

calculations suggest that the trend in conductance in DNA/RNA monomers may be ascertained by the hydrogen atom acceptors polarizability. Future work includes creating an anchoring group that works for both families of monomers and would allow us to calculate the conductance and other parameters for these systems to create a more complete picture of the correlation between conductance and atomic polarizability.

SINGLE-MOLECULE CONDUCTANCE THROUGH HYDROGEN BONDS. THE
ROLE OF RESONANCES.

4.1 Abstract

The single-molecule conductance of hydrogen-bonded and alkane systems are compared in this theoretical investigation. The results indicate that for short chains, the H-bonded molecules exhibit larger conductance than the alkanes. While earlier experimental investigations attributed this observation to a large density of states (DOS) corresponding to an occupied molecular orbital below the Fermi energy, the current work indicates the presence of a Fano resonance in the transmission function in the vicinity of the Fermi energy. The inclusion of this observation is essential in understanding the behavior of these systems. We also address the characteristics of the H-bond for transport and provide an explanation for the presence of a turnover regime wherein the conductance of the alkanes becomes larger than the H-bonded systems. Incidentally, this feature cannot be explained using a simple DOS argument.

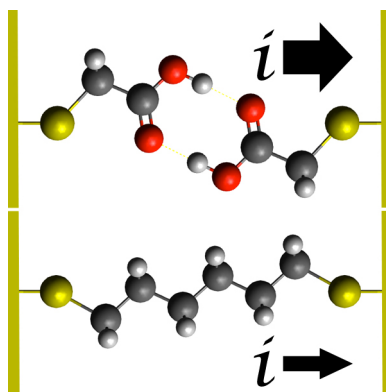


Figure 4.1: Original TOC Graphic.

4.2 Introduction

As has been emphasized in earlier studies by Kurlancheek and Cave, bond strength does not necessarily translate into better transport properties, and their calculations show modest differences between tunneling mediated by weak bonds as compared to σ and π -bonds [48]. Furthermore, it is not clear that molecular orbitals can be obviously interpreted as conduction channels, as analyzed in detail in the work of Solomon *et al* [62]. However, judging how the strength of a bond affects the transport effectiveness through a molecule is an important subject. For example, in a recent study using an STM break junction technique, Nishino et al found that nano-junctions including molecules with hydrogen bonds exhibit enhanced electron transport compared with alkanes for short inter-electrode distances ($<13 \text{ \AA}$) [128]. In both systems, the conductance behavior corresponds to tunneling transport, exhibiting exponential decay with length. This study demonstrates that under some conditions the inclusion of H-bonding in a molecular junction significantly impacts its transport property, a fact that has important implications for our understanding of transport through DNA, and biological interfaces in general. A relevant example is the use of tunneling junctions for DNA sequencing, as pioneered by Lindsay and co-workers [129, 7].

In this study we examine the DOS and transmission coefficients of H-bond systems in the neighborhood of the Fermi energy. We observe that an appropriate description of the transport properties of the H-bonded systems requires the consideration of larger basis sets, as compared to the alkanes, something that could be expected solely based on quantum chemical arguments. More importantly for the purpose of this study, the calculated conductance closely resemble the experimental results, including the exponential length decay for the two families of molecules and the turnover region at large inter-electrode separation. This conductance pattern is partly determined by

a feature of the DOS that can be interpreted as resulting from orbital resonances in the H-bonded systems that are absent in the alkane chains, and partly by the behavior of the transmission function, which differs markedly for the two systems and corresponds to what other authors have identified as a Fano resonance [5, 130]. Despite our comparison being limited to a particular set of observations, our analysis is related to the more general issue of the relative importance of the quasi-resonant tunneling regime in molecular junctions. For instance, the influence of resonance behavior in the interpretation of single-molecule experiments has been previously investigated [131].

4.3 Theory

The theoretical model that accounts for a quantitative interpretation of the experimental results corresponds to electron transport occurring via a one-electron tunneling mechanism under the Landauer regime. In such a model the current is well described by a dimensionless transmission coefficient, which depends on the nature of the tunneling barrier,

$$I(V) = \frac{4e}{h} \int_{\mu_L}^{\mu_R} dE \tau(E, V) \quad (4.1)$$

where E is the energy of the tunneling electron, V is the applied bias voltage, and μ_L , μ_R are the electrochemical potentials in the left and right electrodes, respectively. In the linear regime of low bias voltage, which is the one we are concerned with, equation 4.1 becomes,

$$I(V) = \frac{4e^2}{h} \tau(E_F) V \quad (4.2)$$

In this regime the conductance is given by the Landauer expression,

$$G = \frac{4e^2}{h} \tau(E_F) \quad (4.3)$$

where the transmission coefficient can be written as [126],

$$\tau(E_F) = T_{LMR} \xi_L(E_F) \xi_R(E_F) \quad (4.4)$$

and T_{LMR} is the effective coupling to the left (L) and (R) electrodes mediated by the molecule M and $\xi_{L/R}(E_F)$ are the densities of states of the L/R electrode/molecule contacts at the Fermi energy. The main reason to include here a discussion of the Landauer formalism, is to emphasize that even in this simple model the effective coupling is a product of a term connected to the propagation of electrons through the molecule, and the chemisorption coupling of the molecule to the electrodes. As discussed in the computational section, we use here an implementation of the NEGF formalism contained in the trans-SIESTA computational package [127].

4.4 Computational Methods

Two families of systems were considered in this study. The first consists of a set of alkanedithiols that range in length from 6 carbons to 10 carbons (A6-A10). The second consists of two carboxylated alkanedithiol dimers that range in length from 4 to 10 carbons (H4-H10) and are constructed such that each dimer results in a semi-planer cyclic ring containing two hydrogen bonds. See Figure 4.2.

All molecular geometries were optimized at the DFT/B3YLP level using the Pople style 6-31G*(d) basis set using the ORCA software package [132] in the form Au-S-Molecule-S-Au. After optimization the two gold atoms were removed and the resulting structure was covalently attached to gold electrodes in the atop position. All Au-S distances were fixed at 2.240 Å and each gold electrode was modeled after Krsti *et al* [133, 134]. Each gold unit cell contained two sub layers of either seven or three gold atoms with periodic boundary conditions along the transport direction. Since the contact geometry between the electrode and anchoring site can affect transport

calculations [42], an extra 7-atom layer was inserted between the molecule and the right lead to ensure the same attachment of the molecule to the left and right leads.

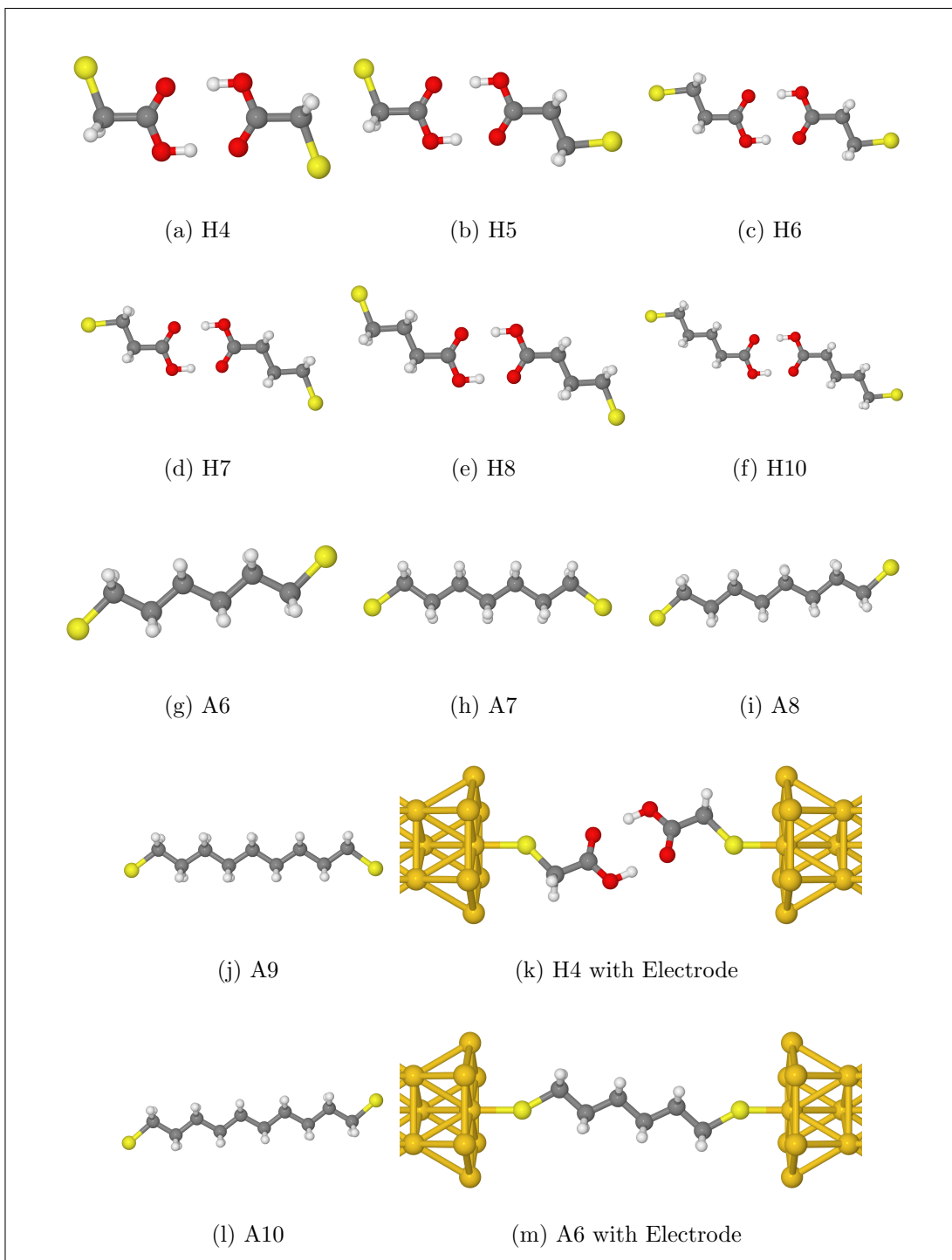


Figure 4.2: Considered Systems and Electrode Setup

Electronic transport calculations were performed using the NEGF+DFT approach

as implemented in the Tran-SIESTA computational package [127, 125]. In order to appropriately capture the subtleties of the H-bonded systems [119], we used a double- ζ basis set in our transport calculations while using single- ζ basis set for the alkanes to avoid the potential issue of ghost transmissions as discussed by Hermann *et al* [126]. The generalized gradient approximation (GGA) was used as the exchange correlation functional. The energy cutoff for the real space grid was 200 Ry.

4.5 Results and Discussion

Figure 4.3 displays a logarithmic plot of the conductance as a function of the length of the molecular bridge separating the two Au electrodes as measured by the S-S distance L . As expected for tunneling junctions, the conductance decreases exponentially as length increases. Our results agree reasonably well with the observed experimental trend regarding the value of the β parameter controlling the exponential decay. More importantly, our calculations show that the shorter H-bonded systems ($L < 16 \text{ \AA}$) have larger conductance than the alkane chains and that there is a turnover region at approximately $L \geq 17 \text{ \AA}$. Figure 4.4 (Panel A) contains the results of our calculations for the H-bonded systems. Here the dominant feature is a conspicuous peak near the Fermi energy whose shape closely resembles the profile of a Fano resonance, something that has been described in other works [5, 130, 135]. The transmission values follow an inverse ordering to that of chain length with the shortest chain exhibiting a higher transmission. This eventually decreases sharply for the H10 chain. Figure 4.4 (Panel B) displays the transmission coefficient for the alkane systems. The figure shows the peak for the HOMO but not the LUMO, which is several eV above the Fermi energy, and is not relevant for the comparison with the experiment. Here the resonant feature is absent around the Fermi energy and the transmission is consistently smaller than the corresponding one for the H-bonded system of equivalent

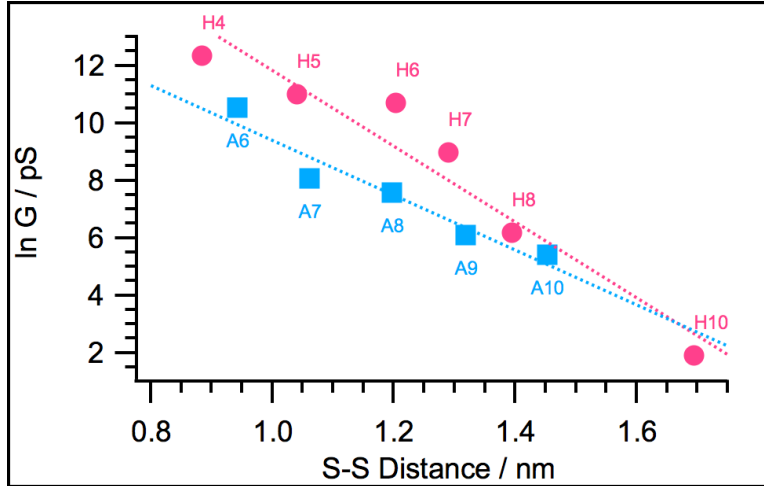


Figure 4.3: Natural Log of Conductance Verses S-S Distance of H-bonded (Pink Circles) and Alkane Systems (Blue Squares). The H-bonded Systems Have an Increased Conductance Over the Alkanes Until the Turnover Regime at Approximately 17 Å. The Beta Decay Factor is $1.32 \pm 0.18 \text{ \AA}^{-1}$ for the H-bonded Systems and $0.95 \pm 0.15 \text{ \AA}^{-1}$ for the Alkanes.

length until this trend is reversed for lengths corresponding to the A9/H8 systems. This is naturally associated with the turnover region observed in the experiment. As previously discussed, an analysis of conductance in a molecular junction based only on state availability for transport is incomplete, especially if a quasi-resonance is intervening in transport, because this feature might be difficult to identify in the DOS and is clearly visible in the transmission function. In addition to this limitation, low bias conductance involves mostly probing transmission around the Fermi energy. It is true that conductance depends on the full energy spectrum, but the linear regime is dominated by the behavior of the system close to the Fermi energy. Despite this general consideration, we include here for completeness the analysis of the DOS because it sheds complementary information about the physical mechanism involved in transport.

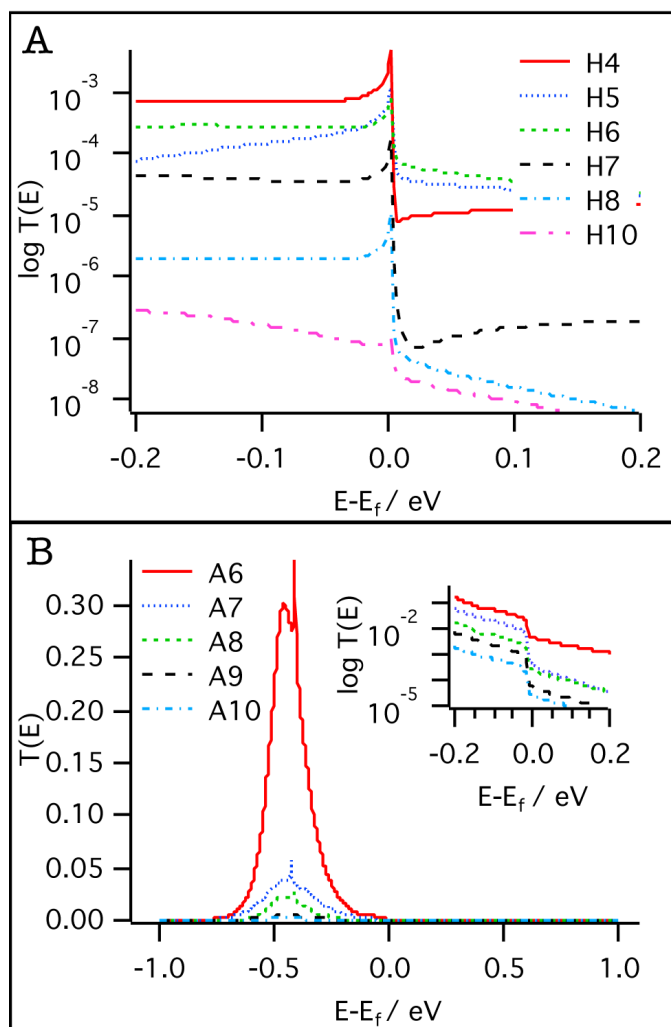


Figure 4.4: Panel A - Log of the Transmission as a Function of Energy of the H-bonded Systems Showing a Distinct Peak at the Fermi Energy. Panel B - Log of the Transmission as a Function of Energy of the Alkane Systems.

Figure 4.5 displays the total DOS for a typical H-bonded junction. For comparison we have included the results with and without the Au contacts. Once the chemical bonding between the molecule and the contact is included, the DOS is a property of the combined subsystems. However, the results indicate the presence of several features, which are important for our discussion and can be directly attributed to the presence of the molecular bridge. Since the inclusion of the much larger DOS arising

from the contacts masks the analysis of the DOS close to the Fermi energy related to the molecular electronic structure, in what follows we subtract the contribution of the contacts. Figure 4.6 shows a comparison of the DOS corresponding to the H-

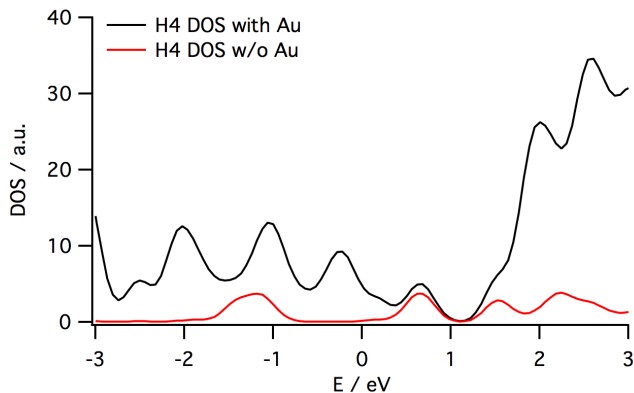


Figure 4.5: Density of States for the Shortest H-bonded Structure (H4). Red Line - DOS Including Gold Atoms of the Electrodes. Black Line - DOS Excluding Gold Atoms of the Electrodes.

bonded and alkane systems. There are two salient features. First, is the larger DOS close to the Fermi energy and within the experimental bias window of 0.2 eV, for the H-bonded systems, compared to the alkane chains. This difference would point out to a larger contribution to the conductance of the former. Second, and perhaps more important, is the fact that the large peak in the DOS for the H-bonded systems around -1.5 eV, which is much reduced for the alkane systems, is essentially invariant and therefore cannot account for the turnover region observed experimentally, as proposed in Nishinos work. The seemingly counter-intuitive result that transport through a hydrogen bond can be more efficient than through a sigma-bond, was interpreted as due to a distinctive feature in the projected density of states (PDOS) that was present for the hydrogen bonded systems only. An interpretation for the conductance behavior of a molecular junction that is solely based on a DOS argument, is not as

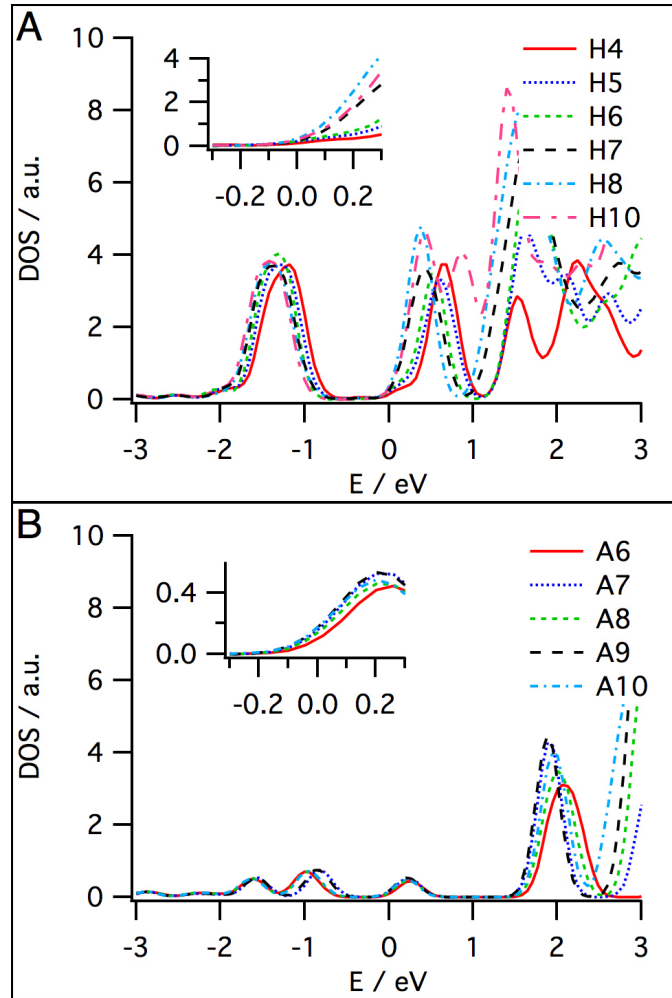


Figure 4.6: Panel A - DOS of the H-bonded Systems. Inset Shows the Region Around the Fermi Energy Magnified. Panel B - DOS of the Alkane Systems.

complete as one based of a full theory of transport, such as the NEGF approach, that in addition to state availability, takes into account the electron propagation ability of the molecular bridge. This is particularly important in a situation, such as that in the above-referred measurements, where a low bias voltage (0.2 V) is applied. This corresponds to a small window around the Fermi energy whereas the PDOS peak structure invoked to interpret the experiment lies at around -2 eV. Furthermore, even if there is a consistent correlation between PDOS and conductance, this argument

cannot explain the turnover region observed at larger electrode separation.

We have explored the implications of quasi-resonant transport in a particularly important instance of a weakly bonded molecular junction involving hydrogen bonds. This is a subject that has been almost completely ignored in McConnell-type analysis [29], which is valid only for non-resonant transport that is the dominant mechanism in most tunneling junctions studied so far. Although the possibility of quantum interference [62] to be partly responsible for the peak in the transmission function cannot be ruled out, we have identified it as a Fano resonance based on its profile. The possible role of quantum interference due to the cyclic topology of the hydrogen-bonded part of the molecule is currently under study.

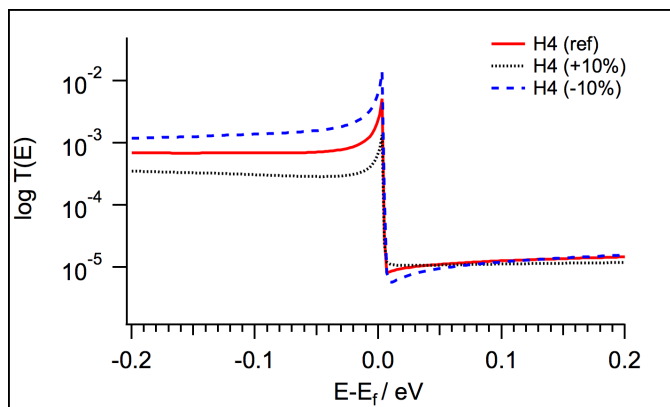


Figure 4.7: Transmission Function Comparing the Modified H-bond Lengths.

We also looked at comparing the H-bond length and its affect on the transmission function. Figure 4.7 shows the results of these calculations. After geometry optimization, the H-bond length was modified by elongating the bond by 10% and by shortening it by 10%. The resulting transmission functions are graphed together to show that when the H-bond is shortened by 10%, the transmission function peak around the corrected Fermi energy is higher as when compared to the other two systems. This directly translates into a higher conductance and shows that by phys-

ically altering the dimensions of the H-bond in the junction, tunable electronics can be realized in a practical way.

Our model provides for a comprehensive rationale for some recent experimental results that indicate that under some conditions transport through a weak bond can be more efficient than through a stronger chemical link. An alternative theoretical explanation to this finding was given by Li *et al* who took into account an explicit self-energy correction in their calculations [136]. In a more general context, our results are also relevant for the issue of understanding the role of the chemical bond in electron transfer and transport processes. In this connection, high-level calculations are required to account both for the electronic structure of weakly bonded systems and transport properties. The dependence of our results on the quality of the basis set is also highlighted by the need to examine the onset of ghost transmission for short chains.

Finally, our results may be significant for the design of devices and understanding transport in DNA [137].

Chapter 5

CALCULATED PROPERTIES OF SELECTED DIMERS AND DNA/RNA BASE PAIRS

5.1 Introduction

While electron transport through covalent bonds has been extensively studied, recent studies have shifted their focus towards hydrogen-bonded systems due to their ubiquitous presence in biological systems and their potential in forming nanojunctions between molecular electronic devices and our own biological systems. Moreover, our prior study explored the implications of quasis resonant transport in a particularly important instance of a weakly bonded molecular junction involving hydrogen bonds. This study demonstrated that under some conditions the inclusion of H-bonding in a molecular junction significantly impacts its transport property, a fact that has important implications for our understanding of transport through DNA, and biological interfaces in general [138]. The critical role of hydrogen-bonds in structure and electrical conductance of the DNA, and the possibility of using molecular conductance and the spectral features of it to characterize a base pair sequence of DNA [139, 140, 141] makes studying and characterizing of hydrogen bond in DNA of paramount importance.

Characterizing the electrical conductivity of DNA nucleotides may lead to faster and more cost effective personalized medicine and a revolution in the design and application of new drugs [142, 139]. While significant progress has been achieved in discovering more and more about electron transport through DNA, such as measuring the conductance of double helical DNA, studying of modified DNA to alter its charge

transport properties [143], the transversal conductance of DNA (i.e. conductance across the nucleotides themselves) is mostly understudied. In one case, Tao et al. recognized that long-range transport can occur along double helical DNA via the overlapping π molecular orbitals of the DNA stacked bases [143]. They furthermore replaced a DNA base with anthraquinone, a redox group, to demonstrate conductance switching in DNA [143]. In this paper, we will focus on systematic study of electron transport through DNA base pairs and will try to explore the use of polarizability as a potential descriptor.

It has been shown that for a set of biologically relevant hydrogen bonded systems that polarizability can be used as a guideline to qualitatively predict conductance through the system [60].

Since $NH \cdots O$, $OH \cdots O$, and $NH \cdots N$ are the three most widely prevalent hydrogen bonds in biological systems and organic electronics [119], DNA is a perfect system to assess the qualitative properties of using polarizability to characterize hydrogen bonds. The connection between conductance and polarizability has already been investigated in different families containing hydrogen bonds. In two studies, the measured conductance of a few experimental design motifs were compared to the molecular polarizability [60, 119]. In one paper, results show an inverse relationship between conductance and polarizability; the conductance decreases as the molecular polarizability increases [60].

5.2 Methods

Full geometry optimizations of all hydrogen bonded and DNA/RNA conformations were carried out at the density functional level of theory (DFT) using the Becke gradient-corrected exchange functional and Lee-Yang-Parr correlation functional with three parameters (B3LYP) and the 6-311++G(2d,2p) basis set. Also,

the total isotropic polarizability was calculated and then partitioned into individual atomic components using an approach based on Hirshfeld population analyses [?]. Both calculations were performed using Gaussian 09.

Electronic transport calculations were performed using the NEGF+DFT approach as implemented in the Tran-SIESTA computational package [125]. In order to appropriately capture the subtleties of the hydrogen bond in all considered systems [119], we used a double- ζ basis set in our transport calculations. The generalized gradient approximation (GGA) was used as the exchange correlation functional. The energy cutoff for the real space grid was 200 Ry.

5.3 Results & Discussion

A hydrogen bond, by definition, results from an attractive interaction between the hydrogen atom of a covalent bond containing a donor hydrogen and an electronegative acceptor atom. One important feature of a hydrogen bond is that it is highly polarizable. This feature is extremely important in the context of electron transport across hydrogen bonds. Polarizable systems have a soft electron cloud that deforms in response to bias modification which then modulates the tunneling current [119].

Figure 5.1 shows the hydrogen bonded dimers that were first investigated in order to understand conductance and polarizability trends in more complicated systems than previously studied. Here we consider the H4, H6, H8, and H10 systems.

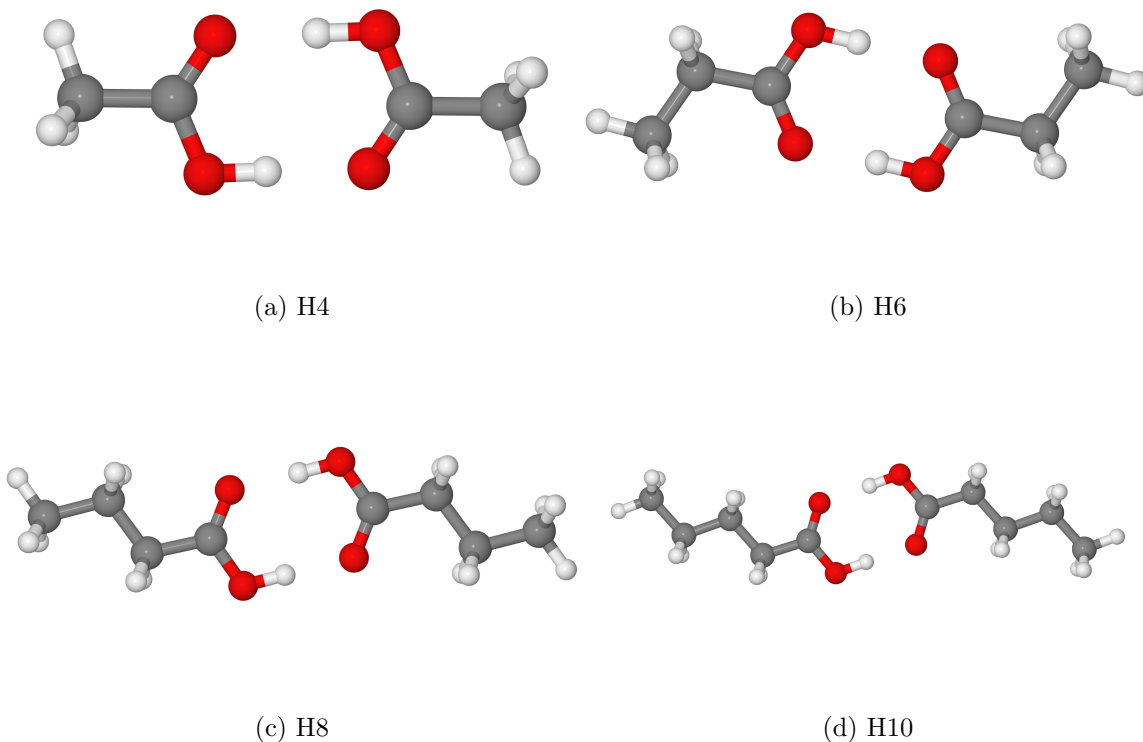
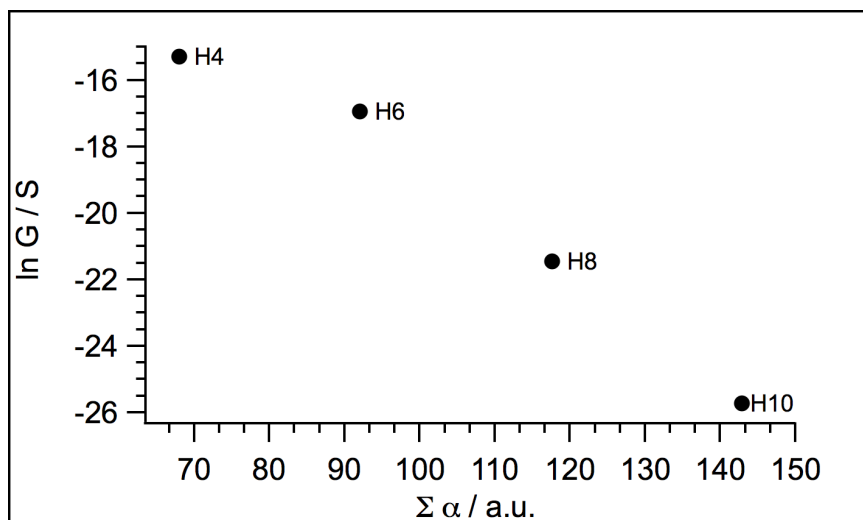
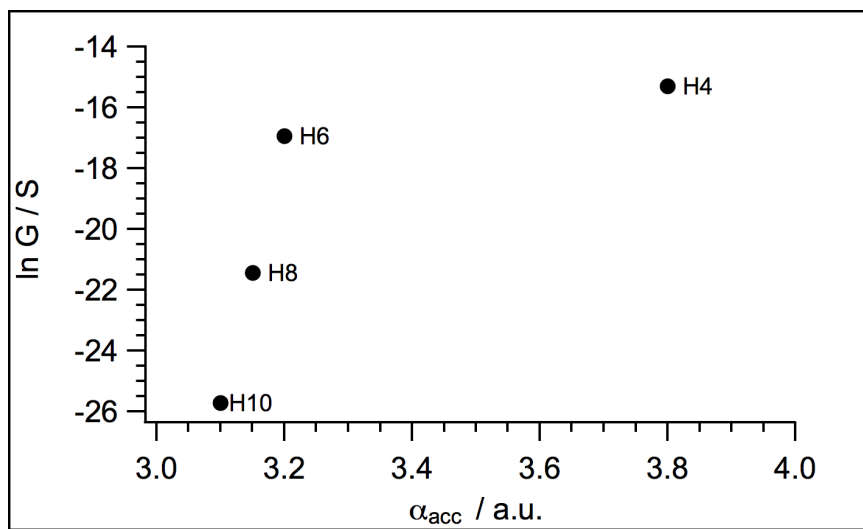


Figure 5.1: H-bonded Dimers Considered in This Section

Figure 5.2a shows the natural log of conductance versus the total polarizability of the hydrogen bonded dimers. We can see that as the total polarizability increases, the overall conductance decreases. Next, we can see in Figure 5.2b that as the polarizability of the hydrogen acceptor atom increases, so does the conductance for these simple systems; again we see a direct correlation between the polarizability of the hydrogen acceptor atom and the conductance.



(a) Avg G vs Total Polarizability



(b) Avg G vs Acc Polarizability

Figure 5.2: Conductance (G) Versus Total (a) and Acceptor Atom (b) Atomic Polarizabilities for the H-Bonded Systems.

Next, we investigated the polarizability sensitivity of the hydrogen bond acceptor atom when changing a functional group near the acceptor atom. Figure 5.3 shows the found hydrogen bonded dimer systems with a terminal methyl group changed for either an electron withdrawing or an electron donating group.

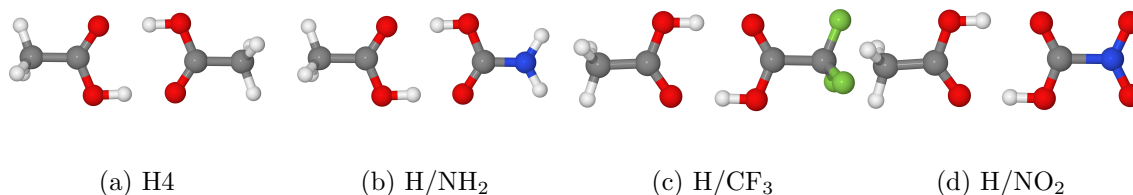


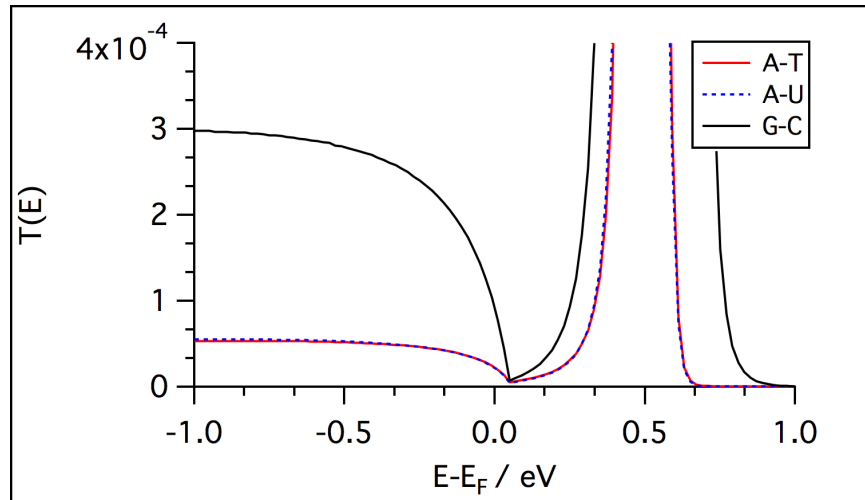
Figure 5.3: H4 and CH₃ Modified Terminal Groups.

Table 5.1 shows the results of the previous calculations. The hydrogen acceptor atom is designated as the one closest to the changed functional group (right side of each dimer in the previous image). We can see that changing the functional group does indeed change the polarizability of the acceptor atom. If we compare system H4 (Figure 5.3a) to system H/NH₂ (Figure 5.3b), the atomic polarizability increases from 3.8 to 3.9 by the addition of an electron donating group. However, when an electron withdrawing group such as CF₃ is used, then the polarizability decreases from 3.8 to 2.9. Again, we see that as an electron donating group can increase the local atomic polarizability by pushing electron density into the bond, an electron withdrawing group will decrease polarizability by decreasing electron density near the acceptor atom.

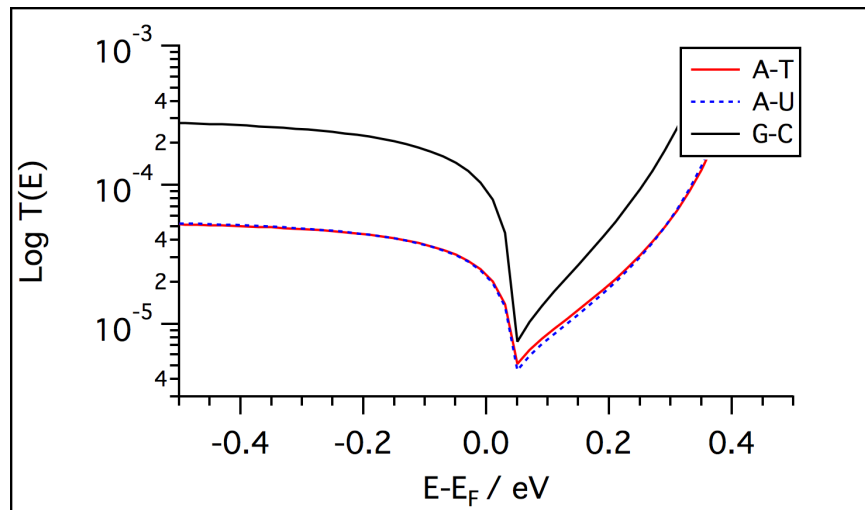
| System | α_{O1} | α_{O2} | $\bar{\alpha}_O$ | Group |
|-------------------|---------------|---------------|------------------|-------|
| H4 | 3.8 | 3.8 | 3.8 | Ref |
| H/NH ₂ | 3.9 | 3.7 | 3.8 | EDG |
| H/CF ₃ | 2.9 | 4.6 | 3.8 | EWG |
| H/NO ₂ | 3.1 | 4.2 | 3.7 | EWG |

Table 5.1: Atomic Polarizability of the Hydrogen Acceptor Atom (α_O) in the Presence of EDG and EDW Groups.

We next began to investigate the conductance and polarizability properties of DNA and RNA base pairs. Figure 5.4 shows the transmission profile for A-T, A-U, and C-G. As opposed to our hydrogen bonded work from earlier where the presence of a Fano resonance helped to explain interesting results, the transmission profiles of these base pairs show no striking features.



(a) $T(E)$ vs $E - E_F$



(b) $\text{Log } T(E)$ vs $E - E_F$

Figure 5.4: Transmission Curves for the A-T, A-U, and G-C Systems.

| System | HOMO (eV) | LUMO (eV) | Gap (eV) | $r_{N\dots N}$ | $r_{O\dots N}$ | G (nS) |
|--------|-----------|-----------|----------|----------------|----------------|--------|
| A-T | -6.2 | -1.4 | 4.7 | 2.837 | 2.911 | 1.69 |
| A-U | -6.2 | -1.5 | 4.6 | 2.836 | 2.908 | 1.65 |
| G-C | -5.4 | -1.7 | 3.8 | 2.914 | 2.894 | 6.83 |
| A | -6.3 | -0.9 | 5.4 | — | — | — |
| T | -6.9 | -1.5 | 5.4 | — | — | — |
| U | -7.3 | -1.7 | 5.6 | — | — | — |
| C | -6.5 | -1.3 | 5.2 | — | — | — |
| G | -5.9 | -1.0 | 4.9 | — | — | — |

Table 5.2: HOMO-LUMO Gap Energies of Considered Systems

Studying of A-T and A-U systems can be very illuminating since A-T is the methylated version of the A-U system. We have previously shown that for structurally similar systems we can use polarizability as a descriptor for electron transport in organic molecules. In the $NH\dots N$ and $NH\dots O$ bonds, N and O are acting as hydrogen bond acceptors. It can be seen that the higher the polarizability of the hydrogen bond acceptor the lower the conductance of the molecule. It is worth noting that while many use HOMO-LUMO gap as a measure for the tunneling barrier, A-U has a smaller HOMO-LUMO gap in comparison with A-T, but it has a weaker ability to conduct transport electrons. Once again this proves that the assuming HOMO-LUMO gap as a measure of the tunneling barrier's height fails for relatively complicated systems, particularly when weak interactions are involved. It is also important to note that the distance from the hydrogen bond donor and acceptor is slightly larger for A-T than A-U, hence intuitively one would imagine that the conductance of A-T should be smaller while the opposite is true. The inverse corre-

lation between the hydrogen bond acceptor’s atomic polarizability and conductance was previously shown for simple hydrogen bonded systems. The more polarizable an hydrogen bond acceptor atom is, the more resistance and change in the electron density is present on the electron acceptor moiety which can result in partial charge accumulation around the hydrogen bond.

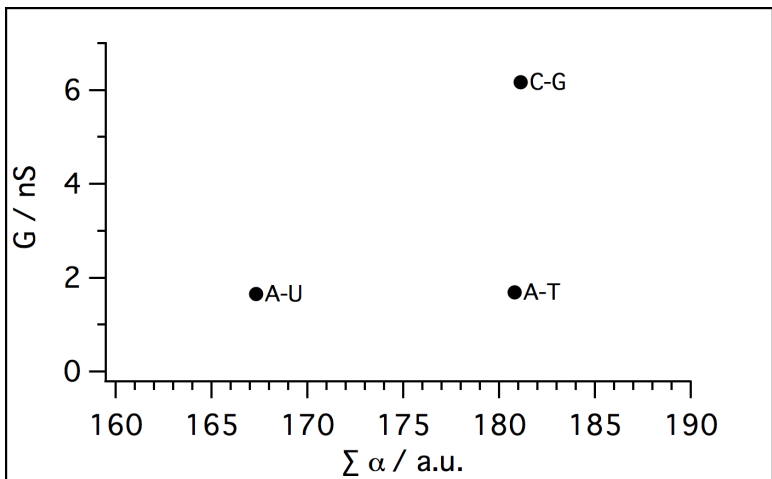


Figure 5.5: Calculated Conductance (G) Versus Total Polarizability for A-T, A-U, and C-G.

The polarizabilities of A-T, A-U, G-C, and their respective monomers were calculated using the B3LYP/6-311++G(2d,3p) level of theory. In Table 5.3 we consider the base-pairs and monomer systems from the perspective of their $NH \cdots O$ bond. We consider the $NH \cdots O$ bond as originating from the adenine and guanine molecules. In this case, nitrogen acts as the hydrogen donor while oxygen is the acceptor. We first see that the polarizability of the donor atom in adenine decreases from 5.8 to essentially zero when compared to A-T while increasing to 7.2 when compared to A-U. The polarizability of hydrogen in adenine decreases from 8.6 to 3.8 when compared to A-T and 2.7 when compared to A-U. We can also see that the N-H bond length is shortest in adenine as compared to the other two systems. Next, the polarizability

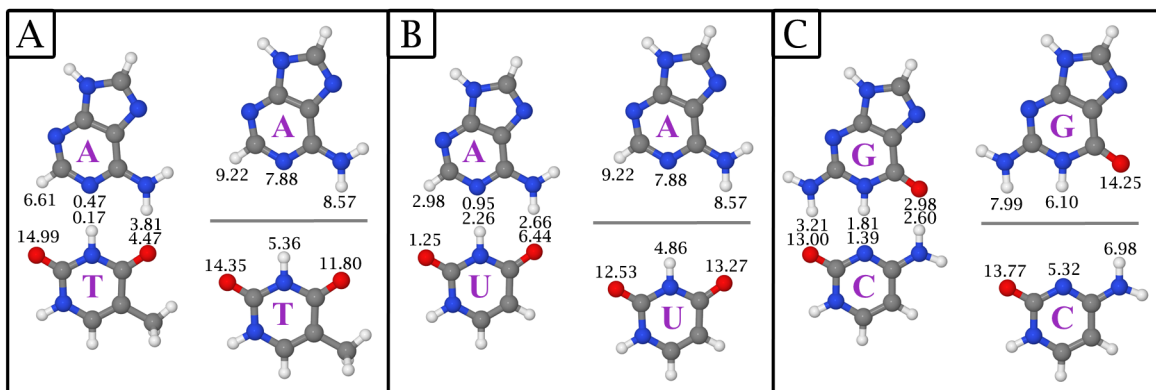


Figure 5.6: Atomic Polarizabilities of Atoms Participating in the Junction Between Nucleotides. The Images Located on the Left of each Panel Shows the Values of Each Atom in the Junction When the Base Pairs are Analyzed Together. Images on the Left of Each Panel are the Values of the Same Structures as Monomers.

| System | α_N | α_H | α_O | $\sum \alpha$ | r_{N-H} | $r_{O...H}$ | $r_{O...N}$ | G (nS) |
|--------|------------|------------|------------|---------------|-----------|-------------|-------------|--------|
| A-T | -1.3 | 3.8 | 4.5 | 178 | 1.023 | 1.891 | 2.911 | 1.69 |
| A-U | 7.2 | 2.7 | 6.4 | 170 | 1.023 | 1.887 | 2.908 | 1.65 |
| G-C | 7.4 | 3.2 | 13.0 | 177 | 1.023 | 1.871 | 2.894 | 6.83 |
| A | 5.8 | 8.6 | — | 95 | 1.003 | — | — | — |
| T | — | — | 11.8 | 81 | — | — | — | — |
| U | — | — | 13.3 | 68 | — | — | — | — |
| G | 7.0 | 8.0 | — | 101 | 1.007 | — | — | — |
| C | — | — | 13.8 | 76 | — | — | — | — |

Table 5.3: Calculated Atomic Polarizability, Conductance, and Other Geometric Parameters of Different Systems from the Perspective of Their $NH \cdots O$ Bond.

of the acceptor atom in thymine decreases from 11.8 to 4.5 when compared to A-T. Likewise, the acceptor atom in uracil also decreases from 13.3 to 6.4 when compared

to A-U. The polarizability of the donor atom in guanine increases from 7.0 to 7.4 when compared to G-C. The polarizability of the hydrogen atom in guanine decreases from 8.0 to 3.2 when compared to G-C. The N-H bond length is also shortest when guanine is a monomer. Next, the polarizability of the acceptor atom in cytosine decreases from 13.8 to 13.0 when compared to G-C. Last, the $O \cdots H$ distance is shortest in the G-C base pair as compared to the other two systems and also demonstrates the highest conductance.

| System | α_N | α_H | α_N | $\sum \alpha$ | \mathbf{r}_{N-H} | $\mathbf{r}_{H \cdots N}$ | $\mathbf{r}_{N \cdots N}$ | G (nS) |
|--------|------------|------------|------------|---------------|--------------------|---------------------------|---------------------------|--------|
| T-A | 2.4 | 0.2 | 0.5 | 178 | 1.048 | 1.790 | 2.837 | 1.69 |
| U-A | -2.0 | 2.3 | 0.9 | 170 | 1.048 | 1.788 | 2.836 | 1.65 |
| G-C | 0.5 | 1.8 | 1.4 | 177 | 1.034 | 1.881 | 2.914 | 6.83 |
| A | — | — | 7.9 | 95 | — | — | — | — |
| T | 2.1 | 5.4 | — | 81 | 1.010 | — | — | — |
| U | 1.9 | 4.9 | — | 68 | 1.010 | — | — | — |
| G | 2.5 | 6.1 | — | 101 | 1.009 | — | — | — |
| C | — | — | 5.3 | 76 | — | — | — | — |

Table 5.4: Calculated Atomic Polarizability, Conductance, and Other Geometric Parameters of Different Systems from the Perspective of Their $NH \cdots N$ Bond.

The polarizabilities of T-A, U-A, G-C, and their respective monomers were calculated using the B3LYP/6-311++G(2d,3p) level of theory. In Table 5.3 we consider the base-pairs and monomer systems from the perspective of their $NH \cdots N$ bond. We consider the $NH \cdots N$ bond as originating from the thymine, uracil, and guanine molecules. In this case, nitrogen can act as either the hydrogen bond acceptor or donor. We first see that the polarizability of the acceptor nitrogen in adenine de-

creases from 7.9 to 0.5 as compared to T-A and 0.9 as compared to U-A. Next, the polarizability of the donor atom in thymine increases from 2.1 to 2.4 when compared to T-A and the polarizability of it's hydrogen atom decreases from 5.4 to 0.2. Next, the polarizability of the donor atom in uracil decreases from 1.9 to essentially 0 when compared to U-A and the polarizability of it's hydrogen atom decreases from 4.9 to 2.3. Next, the polarizability of the donor atom in guanine decreases from 2.5 to 0.5 as compared to G-C and the polarizability of it's hydrogen atom decreases from 6.1 to 1.8. We can also see that the polarizability of the acceptor atom in cytosine decreases from 5.3 to 1.4 as compared to G-C. Last, we can see that the N-H bond in the monomer is consistently smaller than their associated base pairing.

In summary, Figure 5.7 shows the salient results from our hydrogen bonded dimer calculations. Here, we can see that again that there is a correlation between the conductance of a system and the polarizability of a hydrogen acceptor atom. Also, the total polarizability of our system is inversely proportional to the conductance. This makes intuitive sense: that the conductance would decrease as the volume increases (hence it's total polarizability increasing).

| | | |
|---|---|----------------------------|
| <u>Hydrogen Bonded Dimers:</u> | } | |
| G: H4 > H6 > H8 > H10 | | $G \propto \alpha_{acc}$ |
| α_{iso}: H4 > H6 > H8 > H10 | | $G \propto 1/\alpha_{iso}$ |
| α_{acc}: H4 > H6 > H8 > H10 | | |

Figure 5.7: Summary of Results - Hydrogen Bonded Dimers.

We then observed that we can affect the atomic polarizability of an atom by modifying a functional group close to the atom in question. In a previous section we have shown that electron accepting and electron withdrawing groups close to an atom in question affects its polarizability. In these calculations, we can modify the

polarizability by carefully choosing an appropriate functional group.

Last, in Figure 5.8 we can see the results of our DNA/RNA calculations. Again, the polarizability of the hydrogen acceptor atom correlates to the overall conductance of the systems. As a preliminary results, this is an exciting development that may lead to conductance trend analysis using a descriptor that is faster and computationally cheaper than other methods.

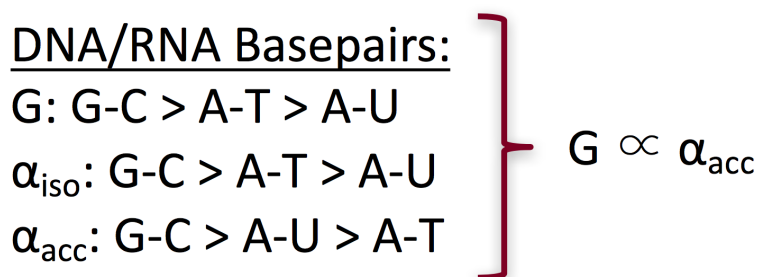


Figure 5.8: Summary of Results - DNA/RNA Basepairs.

Chapter 6

CONCLUSIONS AND FUTURE WORK

As we saw in Chapter 4, hydrogen bonds can, in some instances, exhibit greater conductance values than different systems (alkanes) of comparable size. We also found that the shorter hydrogen bonded systems were higher in conductance not due to a density of states argument as suggested by others, but by a feature contained in the transmission profile of the systems in question. We found the presence of a Fano resonance in the hydrogen bonded systems at short distance that was not present in the transmission profile of the alkanes. This Fano resonance is a striking feature that comes up in special circumstances and is the sole feature that explains the higher conductance of the hydrogen bonded systems over alkanes. Also, we found that we can artificially tune the hydrogen bond length in the shortest hydrogen bonded system to attenuate the transmission profile and hence, the conductance of the system.

In Chapter 3 we assessed the role of atomic polarizability and conductance in selected monomers. The monomers in question consisted of a set of purines and a set of pyrimidines. We chose these monomers since they compose DNA and RNA systems of interest to biological interactions. We found that the presence of electron donating and electron withdrawing groups close to the nitrogen atoms responsible for the hydrogen bonds in base pairing between these two families greatly affected the atomic polarizability of the nitrogen atoms in predictable ways. We found that when an electron donating group was in close proximity to a nitrogen atom, the atomic polarizability was increased. Also, an electron withdrawing group reduced the atomic polarizability of the atoms in question. We also found that when comparing the polarizability of the hydrogen acceptor atom across a family of molecules, that the

conductance was proportional. Figure 6.1 shows the summary of results from Chapter 3 and Chapter 5 calculations. When comparing monomers of the same family (in this case, cytosine and thymine), we can clearly see the correlation between conductance and the hydrogen acceptors atomic polarizability.

In Chapter 5, we began to explore the atomic polarizability and the relationship to conductance in more complicated hydrogen bonded networks. We started with four hydrogen bonded dimers and observed that conductance decreased with length but was proportional to the hydrogen acceptors atomic polarizability. We then chose the smallest system and modified the end-group of each H4 dimer with either an electron donating or electron withdrawing group to see how these groups would affect the atomic polarizability of the hydrogen acceptor atom. We found that by changing the group, we could affect the polarizability of the oxygen atom participating the hydrogen bond in predictable ways. By changing the terminal methyl group to an electron donating group, we observed an increase in polarizability while changing the terminal group to an electron withdrawing group caused the polarizability to decrease.

We then analyzed the conductance and polarizability (both total and atomic) of DNA/RNA base pairs. Our preliminary results indicate that as the polarizability of the hydrogen bond acceptors atom increased, the conductance of the system increased. Again, we have a direct correlation between conductance and atomic polarizability. Once more we have a correlation between the atomic polarizability of the hydrogen acceptor atom and conductance. This leads us to conclude that a connection between these two phenomena does exist and that after further study, we may be able to show that the atomic polarizability of certain atoms may reveal physical trends in a system that is both faster and computationally cheaper to acquire.

| | | |
|--|---|--|
| <u>Hydrogen Bonded Dimers:</u> | } | $G \propto \alpha_{\text{acc}}$ $G \propto 1/\alpha_{\text{iso}}$ |
| G: H4 > H6 > H8 > H10 | | |
| α_{iso} : H4 > H6 > H8 > H10 | | |
| α_{acc} : H4 > H6 > H8 > H10 | | |
| <u>DNA/RNA Monomers:</u> | } | $G \propto \alpha_{\text{acc}}$ $G \propto 1/\alpha_{\text{iso}}$ |
| G: A > C > G > T [C > T] | | |
| α_{iso} : G > A > T > C [T > C] | | |
| α_{acc} : G > C > T [C > T] | | |
| <u>DNA/RNA Basepairs:</u> | } | $G \propto \alpha_{\text{acc}}$ |
| G: G-C > A-T > A-U | | |
| α_{iso} : G-C > A-T > A-U | | |
| α_{acc} : G-C > A-U > A-T | | |

Figure 6.1: Summary of Polarizability Studies.

6.1 Future Work

While we have seen that we can attenuate the transmission profile of the shortest hydrogen bond system in Chapter 4, we would like to assess this phenomena in a more systematic way. One way to accomplish this would be to change the hydrogen bond length of each dimer in the series both by elongating the hydrogen bond and by shortening it. We think it would be interesting to see the persistence of the Fano resonance and at what configuration the resonance feature disappears. Another path of investigation is to use the computational package KWANT [144] and model the hydrogen bonded dimers and alkanes in a tight binding model. We would like to move the hydrogen bonded junction of each structure closer and further to each electrode to assess the role of topology in the conductance of these systems. We would also

like to decompose our systems based on bond currents and see the role of symmetry and quantum interference in the conductance of our systems. The main question to be addressed in this future work is to ascertain the ideal parameters for conductance in these hydrogen bonded systems.

Next, we would like to create an anchoring group to anchor the monomers from the purine and pyrimidine families in Chapter 3 to calculate the conductance of each system for a more systematic comparison to polarizability. Also, it would be interesting to include electron donating and withdrawing groups to each monomer to further elucidate the nature of conductance and polarizability in these systems. We would also like to calculate the conductance of the hydrogen bonded dimers in Chapter 5 before and after changing the terminal methyl group. We would like to see whether we can predict the changes in conductance while modifying the hydrogen acceptor atoms polarizability in a systematic way. By keeping the length of the system constant (by only modifying one group), we believe that we may see a more concrete trend between the conductance and atomic polarizability.

Last, we would like to conduct a further study into the transversal conductance through DNA base pairs (conductance across the hydrogen bond) both with and without the phosphate backbone.

REFERENCES

- [1] G. Jeffrey. *An Introduction to Hydrogen Bonding*, volume 32. Oxford University Press: New York and Oxford, 1997.
- [2] T. Steiner. The whole palette of hydrogen bonds. *Angewandte Chemie International Edition*, 48:41, 2002.
- [3] J. Bang, S. Russell, K. Rupp, and S. Claridge. Multimodal scanning probe imaging: nanoscale chemical analysis from biology to renewable energy. *Analytical Methods*, 7(17):7106–7127, 2015.
- [4] M. Ratner, B. Davis, M. Kemp, and V. Mujica. Molecular wires: Charge transport, mechanisms, and control. *Annals of the New York Academy of Sciences*, 852(1):22–37, 2006.
- [5] D. Nozaki, S. Avdoshenko, H. Sevinçli, and G. Cuniberti. Quantum interference in thermoelectric molecular junctions: A toy model perspective. *Journal of Applied Physics*, 116(7):074308, 2014.
- [6] A. Miroshnichenko, S. Flach, and Y. Kivshar. Fano resonances in nanoscale structures. *Reviews of Modern Physics*, 82(3):2257–2298, aug 2010.
- [7] S. Chang, S. Huang, J. He, F. Liang, P. Zhang, S. Li, X. Chen, O. Sankey, and S. Lindsay. Electronic signatures of all four DNA nucleosides in a tunneling gap. *Nano Letters*, 10(3):1070–1075, 2010.
- [8] M. Ratner. A brief history of molecular electronics. *Nature Nanotechnology*, 8(6):378–381, 2013.
- [9] A. Aviram and M. Ratner. Molecular rectifiers. *Chemical Physics Letters*, 29(2):277–283, 1974.
- [10] N. J. Tao. Electron transport in molecular junctions. *Nature Nanotechnology*, 1(3):173–181, 2006.
- [11] P. Muralt, D. Pohl, and W. Denk. Wide-range, low-operating-voltage, bimorph stm: application as potentiometer. *IBM journal of research and development*, 30(5):443–450, 1986.
- [12] B. Xu, X. Li, X. Xiao, H. Sakaguchi, and N.J. Tao. Electromechanical and conductance switching properties of single oligothiophene molecules. *Nano Letters*, 5(7):1491–1495, 2005.
- [13] J. Tour. Conjugated macromolecules of precise length and constitution. organic synthesis for the construction of nanoarchitectures. *Chemical Reviews*, 96(1):537–554, 1996.
- [14] D. Porath, A. Bezryadin, S. de Vries, and C. Dekker. Direct measurement of electrical transport through DNA molecules. *Nature*, 403(6770):635–638, 2000.

- [15] V. García-Suárez, A. Rocha, S. Bailey, C. Lambert, S. Sanvito, and J. Ferrer. Single-channel conductance of h 2 molecules attached to platinum or palladium electrodes. *Physical Review B*, 72(4):045437, 2005.
- [16] Y. Xue and M. Ratner. End group effect on electrical transport through individual molecules: A microscopic study. *Physical Review B*, 69(8):085403, 2004.
- [17] H. Basch, R. Cohen, and M. Ratner. Interface geometry and molecular junction conductance: Geometric fluctuation and stochastic switching. *Nano Letters*, 5(9):1668–1675, 2005.
- [18] A. Bratkovsky and P. Kornilovitch. Effects of gating and contact geometry on current through conjugated molecules covalently bonded to electrodes. *Physical Review B*, 67(11):115307, 2003.
- [19] R. McCreery, J. Dieringer, A. Solak, B. Snyder, A. Nowak, W. McGovern, and S. DuVall. Molecular rectification and conductance switching in carbon-based molecular junctions by structural rearrangement accompanying electron injection. *Journal of the American Chemical Society*, 125(35):10748–10758, 2003.
- [20] X. Guo, J. Small, J. Klare, Y. Wang, M. Purewal, I. Tam, B. Hong, R. Caldwell, L. Huang, and S. O’Brien. Covalently bridging gaps in single-walled carbon nanotubes with conducting molecules. *Science*, 311(5759):356–359, 2006.
- [21] M. Stewart, F. Maya, D. Kosynkin, S. Dirk, J. Stapleton, C. McGuinness, D. Allara, and J. Tour. Direct covalent grafting of conjugated molecules onto si, gaas, and pd surfaces from aryldiazonium salts. *Journal of the American Chemical Society*, 126(1):370–378, 2004.
- [22] C. McGuinness, A. Shaporenko, C. Mars, S. Uppili, M. Zharnikov, and D. Allara. Molecular self-assembly at bare semiconductor surfaces: Preparation and characterization of highly organized octadecanethiolate monolayers on gaas (001). *Journal of the American Chemical Society*, 128(15):5231–5243, 2006.
- [23] G. Tulevski, M. Myers, M. Hybertsen, M. Steigerwald, and C. Nuckolls. Formation of catalytic metal-molecule contacts. *Science*, 309(5734):591–594, 2005.
- [24] K. Ralls, W. Skocpol, L. Jackel, R. Howard, L. Fetter, R. Epworth, and D. Tennant. Discrete resistance switching in submicrometer silicon inversion layers: Individual interface traps and low-frequency ($1/f$) noise. *Physical Review Letters*, 52(3):228, 1984.
- [25] J. Baik, S. Lee, and M. Moskovits. Polarized surface-enhanced raman spectroscopy from molecules adsorbed in nano-gaps produced by electromigration in silver nanowires. *Nano Letters*, 9(2):672–676, 2009.
- [26] Y. Chen, M. Zwolak, and M. Di Ventra. Local heating in nanoscale conductors. *Nano Letters*, 3(12):1691–1694, 2003.

- [27] Z. Huang, B. Xu, Y. Chen, M. Ventra, and N.J. Tao. Measurement of current-induced local heating in a single molecule junction. *Nano Letters*, 6(6):1240–1244, 2006.
- [28] V. Mujica, M. Kemp, and M. Ratner. Electron conduction in molecular wires. i. a scattering formalism. *The Journal of Chemical Physics*, 101(8):6849–6855, 1994.
- [29] V. Mujica, M. Kemp, and M. Ratner. Electron conduction in molecular wires. ii. application to scanning tunneling microscopy. *The Journal of Chemical Physics*, 101(8):6856–6864, 1994.
- [30] W. Wang, T. Lee, and M. Reed. Mechanism of electron conduction in self-assembled alkanethiol monolayer devices. *Physical Review B*, 68(3):035416, 2003.
- [31] G. Gryn’ova, M. Coote, and C. Corminboeuf. Theory and practice of uncommon molecular electronic configurations. *Wiley Interdisciplinary Reviews: Computational Molecular Science*, 5(6):440–459, 2015.
- [32] Y. Imry and R. Landauer. Conductance viewed as transmission. In *More Things in Heaven and Earth*, pages 515–525. Springer, 1999.
- [33] R. Landauer. Transport as a consequence of incident carrier flux. In *Localization, Interaction, and Transport Phenomena*, pages 38–50. Springer, 1985.
- [34] B. Taylor and P. Mohr. Codata value: Conductance quantum, 2014.
- [35] S. Datta, W. Tian, S. Hong, R. Reifenberger, J. Henderson, and C. Kubiak. Current-voltage characteristics of self-assembled monolayers by scanning tunneling microscopy. *Physical Review Letters*, 79(13):2530–2533, 1997.
- [36] R. Andres, T. Bein, M. Dorogi, and S. Feng. “coulomb staircase” at room temperature in a self-assembled molecular nanostructure. *Science*, 272(5266):1323, 1996.
- [37] D. Klein, P. McEuen, J. Katari, R. Roth, and A. Alivisatos. An approach to electrical studies of single nanocrystals. *Applied Physics Letters*, 68(18):2574–2576, 1996.
- [38] A. Troisi and M. Ratner. Molecular signatures in the transport properties of molecular wire junctions: What makes a junction “molecular”? *Small*, 2(2):172–181, 2006.
- [39] H. Fink and C. Schönberger. Electrical conduction through DNA molecules. *Nature*, 398(6726):407–410, 1999.
- [40] A. Troisi and M. Ratner. Molecular transport junctions: Propensity rules for inelastic electron tunneling spectra. *Nano Letters*, 6(8):1784–1788, 2006.

- [41] M. Ng, D. Lee, and L. Yu. Molecular diodes based on conjugated diblock co-oligomers. *Journal of the American Chemical Society*, 124(40):11862–11863, 2002.
- [42] F. Chen, X. Li, J. Hihath, Z. Huang, and N.J. Tao. Effect of anchoring groups on single-molecule conductance: Comparative study of thiol-, amine-, and carboxylic-acid-terminated molecules. *Journal of the American Chemical Society*, 128(49):15874–15881, 2006.
- [43] H. Ness and A.J. Fisher. Coherent electron injection and transport in molecular wires: inelastic tunneling and electron–phonon interactions. *Chemical physics*, 281(2):279–292, 2002.
- [44] W. Wang, T. Lee, I. Kretzschmar, and M. Reed. Inelastic electron tunneling spectroscopy of an alkanedithiol self-assembled monolayer. *Nano Letters*, 4(4):643–646, 2004.
- [45] C. Joachim and M. Ratner. Molecular electronics: Some views on transport junctions and beyond. *Proceedings of the National Academy of Sciences of the United States of America*, 102(25):8801–8808, 2005.
- [46] S. Lindsay and M. Ratner. Molecular transport junctions: Clearing mists. *Advanced Materials*, 19(1):23–31, 2007.
- [47] A. Voityuk. Long-range electron transfer in biomolecules. tunneling or hopping? *The Journal of Physical Chemistry B*, 115(42):12202–12207, 2011.
- [48] W. Kurlancheek and R. Cave. Tunneling through weak interactions: Comparison of through-space-, h-bond-, and through-bond-mediated tunneling. *The Journal of Physical Chemistry A*, 110(51):14018–14028, 2006.
- [49] J. Onuchic and D. Beratan. A predictive theoretical model for electron tunneling pathways in proteins. *The Journal of Chemical Physics*, 92(1):722–733, 1990.
- [50] J. Onuchic, D. Beratan, J. Winkler, and H. Gray. Pathway analysis of protein electron-transfer reactions. *Annual review of biophysics and biomolecular structure*, 21(1):349–377, 1992.
- [51] X. Li, B. Walker, and A. Michaelides. Quantum nature of the hydrogen bond. *Proceedings of the National Academy of Sciences*, 108(16):6369–6373, 2011.
- [52] A. Buckingham, J. Del Bene, and S. McDowell. The hydrogen bond. *Chemical Physics Letters*, 463(1–3):1–10, 2008.
- [53] E. Glowacki, M. Irimia-Vladu, S. Bauer, and N. Sariciftci. Hydrogen-bonds in molecular solids - from biological systems to organic electronics. *Journal of Materials Chemistry B*, 1(31):3742–3753, 2013.
- [54] G. Pimentel and A. McClellan. *The hydrogen bond*. Freeman, 1960.

- [55] A. Reed, L. Curtiss, and F. Weinhold. Intermolecular interactions from a natural bond orbital, donor-acceptor viewpoint. *Chemical Reviews*, 88(6):899–926, 1988.
- [56] L. Lafferentz, F. Ample, H. Yu, S. Hecht, C. Joachim, and L. Grill. Conductance of a single conjugated polymer as a continuous function of its length. *Science*, 323(5918):1193–1197, 2009.
- [57] A. Nitzan. *Chemical dynamics in condensed phases: relaxation, transfer and reactions in condensed molecular systems*. Oxford university press, 2006.
- [58] G. Solomon, D. Andrews, R. Van Duyne, and M. Ratner. When things are not as they seem: Quantum interference turns molecular electron transfer “rules” upside down. *Journal of the American Chemical Society*, 130(25):7788–7789, 2008.
- [59] V. Mujica, A. Roitberg, and M. Ratner. Molecular wire conductance: Electrostatic potential spatial profile. *The Journal of Chemical Physics*, 112(15):6834–6839, 2000.
- [60] S. Mazinani, R. Meidanshahi, J. Palma, P. Tarakeshwar, T. Hansen, M. Ratner, and V. Mujica. Polarizability as a molecular descriptor for conductance in organic molecular circuits. *The Journal of Physical Chemistry C*, 120(45):26054–26060, 2016.
- [61] A. Nitzan. Electron transmission through molecules and molecular interfaces. *Annual Review of Physical Chemistry*, 52(1):681–750, 2001.
- [62] G. Solomon, D. Andrews, T. Hansen, R. Goldsmith, M. Wasielewski, R. Van Duyne, and M. Ratner. Understanding quantum interference in coherent molecular conduction. *The Journal of Chemical Physics*, 129(5):54701, 2008.
- [63] W. Ockenga. Phase contrast, 2011.
- [64] J. Barański and T. Domański. Fano-type interference in quantum dots coupled between metallic and superconducting leads. *Physical Review B*, 84(19):195424, 2011.
- [65] L. Torres, H. Pastawski, and E. Medina. Antiresonances as precursors of decoherence. *EPL (Europhysics Letters)*, 73(2):164, 2006.
- [66] P. Trocha and J. Barnaś. Dicke-like effect in spin-polarized transport through coupled quantum dots. *Journal of Physics: Condensed Matter*, 20(12):125220, 2008.
- [67] P. Trocha and J. Barnaś. Kondo-dicke resonances in electronic transport through double quantum dots. *Journal of nanoscience and nanotechnology*, 10(4):2489–2494, 2010.

- [68] P. Levstein, H. Pastawski, and J. D'amato. Tuning the through-bond interaction in a two-centre problem. *Journal of Physics: Condensed Matter*, 2(7):1781, 1990.
- [69] M. Kemp, A. Roitberg, V. Mujica, T. Wanta, and M. Ratner. Molecular wires: extended coupling and disorder effects. *The Journal of Physical Chemistry*, 100(20):8349–8355, 1996.
- [70] E. Emberly and G. Kirczenow. State orthogonalization by building a hilbert space: a new approach to electronic quantum transport in molecular wires. *Physical review letters*, 81(23):5205, 1998.
- [71] T. Tada and K. Yoshizawa. Quantum transport effects in nanosized graphite sheets. *ChemPhysChem*, 3(12):1035–1037, 2002.
- [72] K. Sasada and N. Hatano. Quantum interference effect of resonant transport in nano-scale systems. *Physica E: Low-dimensional Systems and Nanostructures*, 29(3):609–613, 2005.
- [73] D. Lovey and R. Romero. Quantum interference through gated single-molecule junctions. *Chemical Physics Letters*, 530:86–92, 2012.
- [74] J. Bergfield and C. Stafford. Thermoelectric signatures of coherent transport in single-molecule heterojunctions. *Nano Letters*, 9(8):3072–3076, 2009.
- [75] L. Zotti, E. Leary, M. Soriano, J. Cuevas, and J. Palacios. A molecular platinum cluster junction: A single-molecule switch. *Journal of the American Chemical Society*, 135(6):2052–2055, 2013.
- [76] C. Arroyo, S. Tarkuc, R. Frisenda, J. Seldenthuis, C. Woerde, R. Eelkema, F. Grozema, and H. van der Zant. Signatures of quantum interference effects on charge transport through a single benzene ring. *Angewandte Chemie International Edition*, 52(11):3152–3155, 2013.
- [77] T. Markussen, J. Schiötz, and K. Thygesen. Electrochemical control of quantum interference in anthraquinone-based molecular switches. *The Journal of Chemical Physics*, 132(22):224104, 2010.
- [78] R. Stadler and T. Markussen. Controlling the transmission line shape of molecular t-stubs and potential thermoelectric applications. *The Journal of Chemical Physics*, 135(15):154109, 2011.
- [79] J. Bergfield, G. Solomon, C. Stafford, and M. Ratner. Novel quantum interference effects in transport through molecular radicals. *Nano Letters*, 11(7):2759–2764, 2011.
- [80] E. Emberly and G. Kirczenow. Antiresonances in molecular wires. *Journal of Physics: Condensed Matter*, 11(36):6911, 1999.

- [81] D. Nozaki, H. Pastawski, and G. Cuniberti. Controlling the conductance of molecular wires by defect engineering. *New Journal of Physics*, 12(6):063004, 2010.
- [82] S. Datta. *Quantum Transport: Atom to Transistor*. Cambridge University Press, 2005.
- [83] D. Newns. Self-consistent model of hydrogen chemisorption. *Physical Review*, 178(3):1123, 1969.
- [84] P. Anderson. Localized magnetic states in metals. *Physical Review*, 124(1):41, 1961.
- [85] U. Fano. Sullo spettro di assorbimento dei gas nobili presso il limite dello spettro darco. *Il Nuovo Cimento (1924-1942)*, 12(3):154–161, 1935.
- [86] U. Fano. Effects of configuration interaction on intensities and phase shifts. *Physical Review*, 124(6):1866, 1961.
- [87] H. Beutler. Über absorptionsserien von argon, krypton und xenon zu termen zwischen den beiden ionisierungsgrenzen $2p\ 3/2$ und $2p\ 1/2$. *Zeitschrift für Physik A Hadrons and Nuclei*, 93(3):177–196, 1935.
- [88] D. Yoon, D. Jeong, H. Lee, R. Saito, Y. Son, H. Lee, and H. Cheong. Fano resonance in raman scattering of graphene. *Carbon*, 61:373–378, 2013.
- [89] G. Piao, R. Lewis, and P. Fisher. Fano resonances in the absorption spectrum of singly ionised zinc in germanium. *Solid State Communications*, 75(10):835–838, 1990.
- [90] J. Nöckel and A. Stone. Resonance line shapes in quasi-one-dimensional scattering. *Physical Review B*, 50(23):17415, 1994.
- [91] S. Lee and B. Kim. Direct evaluation of the asymmetry parameters for isolated resonances. *Journal of Physics B: Atomic, Molecular and Optical Physics*, 33(17):3441, 2000.
- [92] A. Bianconi, A. Marcelli, and N. Saini. Ugo fano and shape resonances. In *AIP Conference Proceedings*, volume 652, pages 13–18. AIP, 2003.
- [93] S. Bandopadhyay, B. Dutta-Roy, and H. Mani. Understanding the fano resonance through toy models. *American journal of physics*, 72(12):1501–1507, 2004.
- [94] A. Rau. Perspectives on the fano resonance formula. *Physica Scripta*, 69(1):C10, 2004.
- [95] A. Becke and E. Johnson. Exchange-hole dipole moment and the dispersion interaction revisited. *The Journal of Chemical Physics*, 127(15):154108, 2007.

- [96] K. Bonin and V. Kresin. *Electric-dipole polarizabilities of atoms, molecules, and clusters*. World Scientific, 1997.
- [97] C. Foot. Laser cooling and trapping of atoms. *Contemporary Physics*, 32(6):369–381, 1991.
- [98] A. Ashkin, J. Dziedzic, J. Bjorkholm, and S. Chu. Observation of a single-beam gradient force optical trap for dielectric particles. *Optics Letters*, 11(5):288–290, 1986.
- [99] M. Lazzaroni, D. Bush, C. Eckert, T. Frank, S. Gupta, and J. Olson. Revision of mosced parameters and extension to solid solubility calculations. *Industrial & engineering chemistry research*, 44(11):4075–4083, 2005.
- [100] P. Geerlings, F. De Proft, and W. Langenaeker. Conceptual density functional theory. *Chemical Reviews*, 103(5):1793–1874, 2003.
- [101] H. Chermette. Chemical reactivity indexes in density functional theory. *Journal of Computational Chemistry*, 20(1):129–154, 1999.
- [102] R. Parr and W. Yang. *Density Functional Theory of Atoms and Molecules*. Horizons of Quantum Chemistry, 1980.
- [103] L. Komorowski, J. Lipiński, and P. Szarek. Polarization justified fukui functions. *The Journal of Chemical Physics*, 131(12):124120, 2009.
- [104] K. Laidig and R. Bader. Properties of atoms in molecules: Atomic polarizabilities. *The Journal of Chemical Physics*, 93(10):7213–7224, 1990.
- [105] K. Gough. Theoretical analysis of molecular polarizabilities and polarizability derivatives in hydrocarbons. *The Journal of Chemical Physics*, 91(4):2424–2432, 1989.
- [106] J. Applequist. An atom dipole interaction model for molecular optical properties. *Accounts of Chemical Research*, 10(3):79–85, 1977.
- [107] A. Stone. Distributed polarizabilities. *Molecular Physics*, 56(5):1065–1082, 1985.
- [108] A. Stone. Distributed multipole analysis, or how to describe a molecular charge distribution. *Chemical Physics Letters*, 83(2):233–239, 1981.
- [109] C. Le Sueur and A. Stone. Practical schemes for distributed polarizabilities. *Molecular Physics*, 78(5):1267–1291, 1993.
- [110] J. Ángyán, G. Jansen, M. Loss, C. Hättig, and B. Heß. Distributed polarizabilities using the topological theory of atoms in molecules. *Chemical Physics Letters*, 219(3-4):267–273, 1994.

- [111] J. Ángyán and C. Chipot. A comprehensive approach to molecular charge density models: From distributed multipoles to fitted atomic charges. *International Journal of Quantum Chemistry*, 52(1):17–37, 1994.
- [112] M. Yang, P. Senet, and C. Van Alsenoy. Dft study of polarizabilities and dipole moments of water clusters. *International journal of quantum chemistry*, 101(5):535–542, 2005.
- [113] A. Becke and E. Johnson. Exchange-hole dipole moment and the dispersion interaction: High-order dispersion coefficients. *The Journal of Chemical Physics*, 124(1):014104, 2006.
- [114] A. Becke and E. Johnson. A density-functional model of the dispersion interaction. *The Journal of Chemical Physics*, 123(15):154101, 2005.
- [115] A. Krishtal, K. Vannomeslaeghe, D. Geldof, C. Van Alsenoy, and P. Geerlings. Importance of anisotropy in the evaluation of dispersion interactions. *Physical Review A*, 83(2):024501, 2011.
- [116] A. Krishtal, K. Vanommeslaeghe, A. Olasz, T. Veszprémi, C. Van Alsenoy, and P. Geerlings. Accurate interaction energies at density functional theory level by means of an efficient dispersion correction. *The Journal of Chemical Physics*, 130(17):174101, 2009.
- [117] A. Olasz, K. Vanommeslaeghe, A. Krishtal, T. Veszprémi, C. Van Alsenoy, and P. Geerlings. The use of atomic intrinsic polarizabilities in the evaluation of the dispersion energy. *The Journal of Chemical Physics*, 127(22):224105, 2007.
- [118] F. Hirshfeld. Bonded-atom fragments for describing molecular charge densities. *Theoretical Chemistry Accounts: Theory, Computation, and Modeling (Theoretica Chimica Acta)*, 44(2):129–138, 1977.
- [119] R. Meidanshahi, S. Mazinani, V. Mujica, and P. Tarakeshwar. Electronic transport across hydrogen bonds in organic electronics. *International Journal of Nanotechnology*, 12(3-4):297–312, 2015.
- [120] R. Janoschek, E. Weidemann, H. Pfeiffer, and G. Zundel. Extremely high polarizability of hydrogen bonds. *Journal of the American Chemical Society*, 94(7):2387–2396, 1972.
- [121] M. Eckert and G. Zundel. Proton polarizability, dipole moment, and proton transitions of an ah... b. dblharw. a-... h+ b proton-transfer hydrogen bond as a function of an external electrical field: an ab initio scf treatment. *Journal of Physical Chemistry*, 91(20):5170–5177, 1987.
- [122] A. Natan, N. Kuritz, and L. Kronik. Polarizability, susceptibility, and dielectric constant of nanometer-scale molecular films: A microscopic view. *Advanced Functional Materials*, 20(13):2077–2084, 2010.

- [123] A. Moore, S. Yeganeh, Y. Yao, S. Claridge, J. Tour, M. Ratner, and P. Weiss. Polarizabilities of adsorbed and assembled molecules: measuring the conductance through buried contacts. *ACS Nano*, 4(12):7630–7636, 2010.
- [124] A. Marenich, C. Cramer, and D. Truhlar. Reduced and quenched polarizabilities of interior atoms in molecules. *Chemical Science*, 4(6):2349–2356, 2013.
- [125] J. Sánchez-Portal, E. Artacho, J. Gale, A. García, J. Junquera, and P. Ordejón. The siesta method for ab initio order- n materials simulation. *Journal of Physics: Condensed Matter*, 14(11):2745, 2002.
- [126] C. Herrmann, G. Solomon, J. Subotnik, V. Mujica, and M. Ratner. Ghost transmission: How large basis sets can make electron transport calculations worse. *The Journal of Chemical Physics*, 132(2):024103, 2010.
- [127] M. Brandbyge, J. Mozos, P. Ordejón, J. Taylor, and K. Stokbro. Density-functional method for nonequilibrium electron transport. *Physical Review B*, 65(16):165401, 2002.
- [128] T. Nishino, N. Hayashi, and P. Bui. Direct measurement of electron transfer through a hydrogen bond between single molecules. *Journal of the American Chemical Society*, 135(12):4592–4595, 2013.
- [129] S. Lindsay, J. He, O. Sankey, P. Hapala, P. Jelinek, P. Zhang, S. Chang, and S. Huang. Recognition tunneling. *Nanotechnology*, 21(26):262001, 2010.
- [130] D. Nozaki, H. Sevincli, S. Avdoshenko, R. Gutierrez, and G. Cuniberti. A parabolic model to control quantum interference in t-shaped molecular junctions. *Physical Chemistry Chemical Physics*, 15(33):13951–13958, 2013.
- [131] M. Perrin, R. Frisenda, M. Koole, J. Seldenthuis, G. Celis, H. Valkenier, J. Hummelen, N. Renaud, F. Grozema, J. Thijssen, D. Dulić, and H. van der ZantHerre. Large negative differential conductance in single-molecule break junctions. *Nature Nanotechnology*, 9(10):830–834, 2014.
- [132] F. Neese. The orca program system. *Wiley Interdisciplinary Reviews: Computational Molecular Science*, 2(1):73–78, 2012.
- [133] P. Krstić, X. Zhang, and W. Butler. Generalized conductance formula for the multiband tight-binding model. *Physical Review B*, 66(20):205319, 2002.
- [134] W. Ding, M. Koepf, C. Koenigsmann, A. Batra, L. Venkataraman, C. Nègre, G. Brudvig, R. Crabtree, C. Schmuttenmaer, and V. Batista. Computational design of intrinsic molecular rectifiers based on asymmetric functionalization of *n*-phenylbenzamide. *Journal of Chemical Theory and Computation*, 11(12):5888–5896, 2015.
- [135] Z. Liu and J. Neaton. Energy-dependent resonance broadening in symmetric and asymmetric molecular junctions from an ab initio non-equilibrium green’s function approach. *arXiv preprint arXiv:1408.5183*, 2014.

- [136] Y. Li, X. Tu, M. Wang, H. Wang, S. Sanvito, and S. Hou. Microscopic mechanism of electron transfer through the hydrogen bonds between carboxylated alkanethiol molecules connected to gold electrodes. *The Journal of Chemical Physics*, 141(17):–, 2014.
- [137] L. Xiang, J. Palma, C. Bruot, V. Mujica, M. Ratner, and N.J. Tao. Intermediate tunnelling - hopping regime in DNA charge transport. *Nature Chemistry*, 7(3):221–226, 2015.
- [138] M. Wimmer, J. Palma, P. Tarakeshwar, and V. Mujica. Single-molecule conductance through hydrogen bonds: The role of resonances. *The Journal of Physical Chemistry Letters*, 7(15):2977–2980, 2016.
- [139] M. Tsutsui, M. Taniguchi, K. Yokota, and T. Kawai. Identifying single nucleotides by tunnelling current. *Nature Nanotechnology*, 5(4):286–290, 2010.
- [140] P. Krstić, J. Wells, M. Fuentes-Cabrera, D. Xu, and J. Lee. Toward electronic conductance characterization of DNA nucleotide bases. *Solid State Phenomena*, 121-123:1387–1390, 2007.
- [141] X. Zhang, P. Krstić, R. Zikić, J. Wells, and M. Fuentes-Cabrera. First-principles transversal DNA conductance deconstructed. *Biophysical Journal*, 91(1):L04–L06, 2006.
- [142] B. Xu, P. Zhang, X. Li, and N.J. Tao. Direct conductance measurement of single DNA molecules in aqueous solution. *Nano Letters*, 4(6):1105–1108, 2004.
- [143] L. Xiang, J. Palma, Y. Li, V. Mujica, M. Ratner, and N.J. Tao. Gate-controlled conductance switching in DNA. *Nature Communications*, 8:14471, 2017.
- [144] C. Groth, M. Wimmer, A. Akhmerov, and X. Waintal. Kwant: a software package for quantum transport. *New Journal of Physics*, 16(6):063065, 2014.

APPENDIX A
COMPUTATION: THE NITTY-GRITTY

A.1 Computational Details

All geometry optimizations were performed using either ORCA 2.9.1 (hydrogen bonded systems, alkanes) or Gaussian 09 (monomer, DNA/RNA basepairs). When using ORCA, optimizations were performed using the B3LYP/6-31G* level of theory and when using Gaussian, optimizations were performed using the B3LYP/6-311++G(2d,2p) level of theory. Electronic structure calculations were performed using the tranSIESTA computational package found in the SIESTA 3.1 computational platform. Since using large nonorthogonal atom-centered basis sets can lead to erroneous results; using basis sets of triple-zeta quality or higher can occasionally lead to artificially higher transmission results [126], we were careful in choosing appropriately large basis sets to avoid ghost transmission artifacts. Hirshfeld population analysis was employed using Gaussian 09 for our polarizability calculations. Sample image, coordinate, and input files can be found in the following sections.

A.2 Relating to the Electrode

A.2.1 Sample Structure

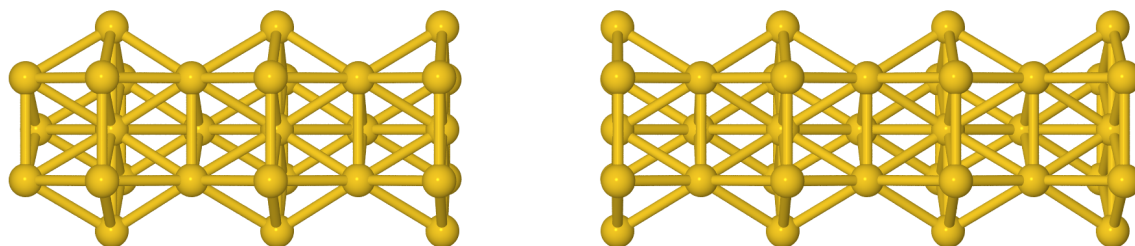


Figure A.1: Structure of the Electrode

A.2.2 XYZ Files -Electrode

| | | | | | | | | |
|----|----|-----------|-----------|-----------|-----------|-----------|-----------|-----------|
| | | | | Au | 0.000000 | 2.885000 | 11.778000 | |
| | | | | Au | 0.000000 | -2.885000 | 16.778000 | |
| | | | | Au | -2.498500 | -1.442500 | 16.778000 | |
| | | | | Au | 2.498500 | -1.442500 | 16.778000 | |
| | | | | Au | 0.000000 | 0.000000 | 16.778000 | |
| 67 | | | | Au | -2.498500 | 1.442500 | 16.778000 | |
| | Au | -0.832800 | -1.442500 | 0.000000 | Au | 2.498500 | 1.442500 | 16.778000 |
| | Au | 1.665600 | 0.000000 | 0.000000 | Au | 0.000000 | 2.885000 | 16.778000 |
| | Au | -0.832800 | 1.442500 | 0.000000 | Au | -0.832800 | -1.442500 | 19.133600 |
| | Au | 0.000000 | -2.885000 | 2.355600 | Au | 1.665600 | 0.000000 | 19.133600 |
| | Au | -2.498500 | -1.442500 | 2.355600 | Au | -0.832800 | 1.442500 | 19.133600 |
| | Au | 2.498500 | -1.442500 | 2.355600 | Au | 0.000000 | -2.885000 | 21.489200 |
| | Au | 0.000000 | 0.000000 | 2.355600 | Au | -2.498500 | -1.442500 | 21.489200 |
| | Au | -2.498500 | 1.442500 | 2.355600 | Au | 2.498500 | -1.442500 | 21.489200 |
| | Au | 2.498500 | 1.442500 | 2.355600 | Au | 0.000000 | 0.000000 | 21.489200 |
| | Au | 0.000000 | 2.885000 | 2.355600 | Au | -2.498500 | 1.442500 | 21.489200 |
| | Au | -0.832800 | -1.442500 | 4.711200 | Au | 2.498500 | 1.442500 | 21.489200 |
| | Au | 1.665600 | 0.000000 | 4.711200 | Au | 0.000000 | 2.885000 | 21.489200 |
| | Au | -0.832800 | 1.442500 | 4.711200 | Au | -0.832800 | -1.442500 | 23.844800 |
| | Au | 0.000000 | -2.885000 | 7.066800 | Au | 1.665600 | 0.000000 | 23.844800 |
| | Au | -2.498500 | -1.442500 | 7.066800 | Au | -0.832800 | 1.442500 | 23.844800 |
| | Au | 2.498500 | -1.442500 | 7.066800 | Au | 0.000000 | -2.885000 | 26.200400 |
| | Au | 0.000000 | 0.000000 | 7.066800 | Au | -2.498500 | -1.442500 | 26.200400 |
| | Au | -2.498500 | 1.442500 | 7.066800 | Au | 2.498500 | -1.442500 | 26.200400 |
| | Au | 2.498500 | 1.442500 | 7.066800 | Au | 0.000000 | 0.000000 | 26.200400 |
| | Au | 0.000000 | 2.885000 | 7.066800 | Au | -2.498500 | 1.442500 | 26.200400 |
| | Au | -0.832800 | -1.442500 | 9.422400 | Au | 2.498500 | 1.442500 | 26.200400 |
| | Au | 1.665600 | 0.000000 | 9.422400 | Au | 0.000000 | 2.885000 | 26.200400 |
| | Au | -0.832800 | 1.442500 | 9.422400 | Au | -0.832800 | -1.442500 | 28.556000 |
| | Au | 0.000000 | -2.885000 | 11.778000 | Au | 1.665600 | 0.000000 | 28.556000 |
| | Au | -2.498500 | -1.442500 | 11.778000 | Au | -0.832800 | 1.442500 | 28.556000 |
| | Au | 2.498500 | -1.442500 | 11.778000 | Au | 0.000000 | -2.885000 | 30.911600 |
| | Au | 0.000000 | 0.000000 | 11.778000 | Au | -2.498500 | -1.442500 | 30.911600 |
| | Au | -2.498500 | 1.442500 | 11.778000 | Au | 2.498500 | -1.442500 | 30.911600 |
| | Au | 2.498500 | 1.442500 | 11.778000 | Au | 0.000000 | 0.000000 | 30.911600 |
| | Au | 0.000000 | 2.885000 | 11.778000 | Au | -2.498500 | 1.442500 | 30.911600 |
| | Au | 0.000000 | -2.885000 | 16.778000 | Au | 2.498500 | 1.442500 | 30.911600 |
| | Au | -2.498500 | -1.442500 | 16.778000 | Au | 0.000000 | 2.885000 | 30.911600 |
| | Au | 2.498500 | -1.442500 | 16.778000 | | | | |

(a) Electrode XYZ File (1st Half)

(b) Electrode XYZ File (2nd Half)

Figure A.2: Electrode Structure's XYZ Files

A.3 Relating to Hydrogen Bonded Dimers

A.3.1 Sample Structure

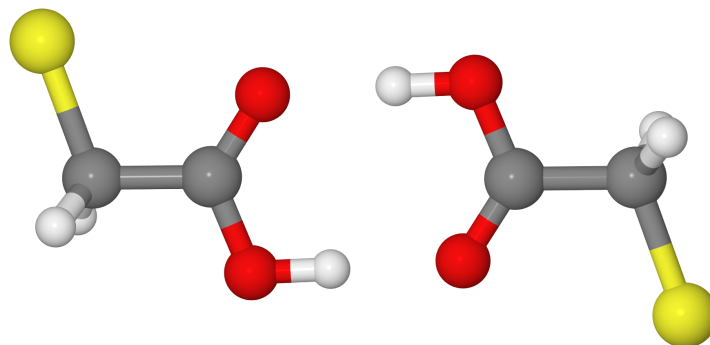


Figure A.3: Structure of H4

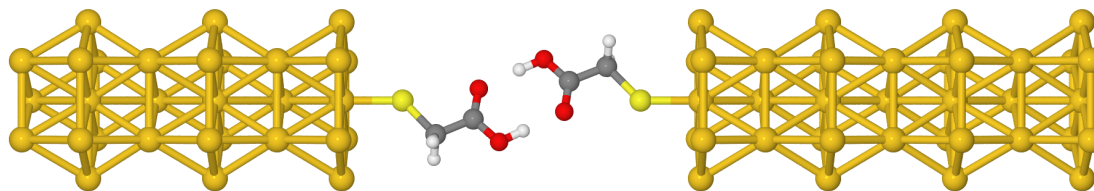


Figure A.4: H4 Between Electrodes

A.3.2 XYZ Files - H4 Dimer

| | | | | | | | | | | | |
|--|--|--|--|----|----|------------|------------|------------|---|----|----|
| | | | | 83 | | | | | | | |
| | | | | | Au | -0.8328000 | -1.4425000 | 0.0000000 | 1 | Au | 1 |
| | | | | | Au | 1.6656000 | 0.0000000 | 0.0000000 | 1 | Au | 2 |
| | | | | | Au | -0.8328000 | 1.4425000 | 0.0000000 | 1 | Au | 3 |
| | | | | | Au | 0.0000000 | -2.8850000 | 2.3556000 | 1 | Au | 4 |
| | | | | | Au | -2.4985000 | -1.4425000 | 2.3556000 | 1 | Au | 5 |
| | | | | | Au | 2.4985000 | -1.4425000 | 2.3556000 | 1 | Au | 6 |
| | | | | | Au | 0.0000000 | 0.0000000 | 2.3556000 | 1 | Au | 7 |
| | | | | | Au | -2.4985000 | 1.4425000 | 2.3556000 | 1 | Au | 8 |
| | | | | | Au | 2.4985000 | 1.4425000 | 2.3556000 | 1 | Au | 9 |
| | | | | | Au | 0.0000000 | 2.8850000 | 2.3556000 | 1 | Au | 10 |
| | | | | | Au | -0.8328000 | -1.4425000 | 4.7112000 | 1 | Au | 11 |
| | | | | | Au | 1.6656000 | 0.0000000 | 4.7112000 | 1 | Au | 12 |
| | | | | | Au | -0.8328000 | 1.4425000 | 4.7112000 | 1 | Au | 13 |
| | | | | | Au | 0.0000000 | -2.8850000 | 7.0668000 | 1 | Au | 14 |
| | | | | | Au | -2.4985000 | -1.4425000 | 7.0668000 | 1 | Au | 15 |
| | | | | | Au | 2.4985000 | -1.4425000 | 7.0668000 | 1 | Au | 16 |
| | | | | | Au | 0.0000000 | 0.0000000 | 7.0668000 | 1 | Au | 17 |
| | | | | | Au | -2.4985000 | 1.4425000 | 7.0668000 | 1 | Au | 18 |
| | | | | | Au | 2.4985000 | 1.4425000 | 7.0668000 | 1 | Au | 19 |
| | | | | | Au | 0.0000000 | 2.8850000 | 7.0668000 | 1 | Au | 20 |
| | | | | | Au | -0.8328000 | -1.4425000 | 9.4224000 | 1 | Au | 21 |
| | | | | | Au | 1.6656000 | 0.0000000 | 9.4224000 | 1 | Au | 22 |
| | | | | | Au | -0.8328000 | 1.4425000 | 9.4224000 | 1 | Au | 23 |
| | | | | | Au | 0.0000000 | -2.8850000 | 11.7780000 | 1 | Au | 24 |
| | | | | | Au | -2.4985000 | -1.4425000 | 11.7780000 | 1 | Au | 25 |
| | | | | | Au | 2.4985000 | -1.4425000 | 11.7780000 | 1 | Au | 26 |
| | | | | | Au | 0.0000000 | 0.0000000 | 11.7780000 | 1 | Au | 27 |
| | | | | | Au | -2.4985000 | 1.4425000 | 11.7780000 | 1 | Au | 28 |
| | | | | | Au | 2.4985000 | 1.4425000 | 11.7780000 | 1 | Au | 29 |
| | | | | | Au | 0.0000000 | 2.8850000 | 11.7780000 | 1 | Au | 30 |
| | | | | | S | 0.0000000 | 0.0000000 | 14.0183790 | 2 | S | 31 |
| | | | | | H | 0.0794000 | -2.1755100 | 15.1815390 | 4 | H | 32 |
| | | | | | H | -1.5594100 | -1.5180800 | 15.1825890 | 4 | H | 33 |
| | | | | | C | -0.5022100 | -1.2539200 | 15.2755290 | 3 | C | 34 |
| | | | | | C | -0.2749900 | -0.6896000 | 16.6650490 | 3 | C | 35 |
| | | | | | O | 0.1955000 | 0.4275900 | 16.8632390 | 5 | O | 36 |
| | | | | | O | -0.6392400 | -1.5353000 | 17.6099690 | 5 | O | 37 |
| | | | | | H | 0.4813000 | 1.1279700 | 18.3674490 | 4 | H | 38 |
| | | | | | H | -0.4757400 | -1.1304400 | 18.5148190 | 4 | H | 39 |
| | | | | | O | 0.6449600 | 1.5328100 | 19.2722690 | 5 | O | 40 |
| | | | | | O | -0.1925700 | -0.4288600 | 20.0190790 | 5 | O | 41 |
| | | | | | C | 0.2793500 | 0.6877900 | 20.2171690 | 3 | C | 42 |
| | | | | | C | 0.5071300 | 1.2520200 | 21.6065490 | 3 | C | 43 |
| | | | | | H | -0.0715600 | 2.1754800 | 21.7000890 | 4 | H | 44 |
| | | | | | H | 1.5651400 | 1.5126400 | 21.7005790 | 4 | H | 45 |
| | | | | | S | 0.0000000 | 0.0000000 | 22.8636990 | 2 | S | 46 |
| | | | | | Au | 0.0000000 | -2.8850000 | 25.1040780 | 1 | Au | 47 |
| | | | | | Au | -2.4985000 | -1.4425000 | 25.1040780 | 1 | Au | 48 |
| | | | | | Au | 2.4985000 | -1.4425000 | 25.1040780 | 1 | Au | 49 |
| | | | | | Au | 0.0000000 | 0.0000000 | 25.1040780 | 1 | Au | 50 |
| | | | | | Au | -2.4985000 | 1.4425000 | 25.1040780 | 1 | Au | 51 |
| | | | | | Au | 2.4985000 | 1.4425000 | 25.1040780 | 1 | Au | 52 |
| | | | | | Au | 0.0000000 | 2.8850000 | 25.1040780 | 1 | Au | 53 |
| | | | | | Au | -0.8328000 | -1.4425000 | 27.4596780 | 1 | Au | 54 |
| | | | | | Au | 1.6656000 | 0.0000000 | 27.4596780 | 1 | Au | 55 |
| | | | | | Au | -0.8328000 | 1.4425000 | 27.4596780 | 1 | Au | 56 |
| | | | | | Au | 0.0000000 | -2.8850000 | 29.8152780 | 1 | Au | 57 |
| | | | | | Au | -2.4985000 | -1.4425000 | 29.8152780 | 1 | Au | 58 |
| | | | | | Au | 2.4985000 | -1.4425000 | 29.8152780 | 1 | Au | 59 |
| | | | | | Au | 0.0000000 | 0.0000000 | 29.8152780 | 1 | Au | 60 |
| | | | | | Au | -2.4985000 | 1.4425000 | 29.8152780 | 1 | Au | 61 |
| | | | | | Au | 2.4985000 | 1.4425000 | 29.8152780 | 1 | Au | 62 |
| | | | | | Au | 0.0000000 | 2.8850000 | 29.8152780 | 1 | Au | 63 |
| | | | | | Au | -0.8328000 | -1.4425000 | 32.1708780 | 1 | Au | 64 |
| | | | | | Au | 1.6656000 | 0.0000000 | 32.1708780 | 1 | Au | 65 |
| | | | | | Au | -0.8328000 | 1.4425000 | 32.1708780 | 1 | Au | 66 |
| | | | | | Au | 0.0000000 | -2.8850000 | 34.5264780 | 1 | Au | 67 |
| | | | | | Au | -2.4985000 | -1.4425000 | 34.5264780 | 1 | Au | 68 |
| | | | | | Au | 2.4985000 | -1.4425000 | 34.5264780 | 1 | Au | 69 |
| | | | | | Au | 0.0000000 | 2.8850000 | 34.5264780 | 1 | Au | 70 |
| | | | | | Au | -0.8328000 | -1.4425000 | 34.5264780 | 1 | Au | 71 |
| | | | | | Au | 2.4985000 | 1.4425000 | 34.5264780 | 1 | Au | 72 |
| | | | | | Au | 0.0000000 | 2.8850000 | 34.5264780 | 1 | Au | 73 |
| | | | | | Au | -0.8328000 | -1.4425000 | 36.8820780 | 1 | Au | 74 |
| | | | | | Au | 1.6656000 | 0.0000000 | 36.8820780 | 1 | Au | 75 |
| | | | | | Au | -0.8328000 | 1.4425000 | 36.8820780 | 1 | Au | 76 |
| | | | | | Au | 0.0000000 | -2.8850000 | 39.2376780 | 1 | Au | 77 |
| | | | | | Au | -2.4985000 | -1.4425000 | 39.2376780 | 1 | Au | 78 |
| | | | | | Au | 2.4985000 | -1.4425000 | 39.2376780 | 1 | Au | 79 |
| | | | | | Au | 0.0000000 | 0.0000000 | 39.2376780 | 1 | Au | 80 |
| | | | | | Au | -2.4985000 | 1.4425000 | 39.2376780 | 1 | Au | 81 |
| | | | | | Au | 2.4985000 | 1.4425000 | 39.2376780 | 1 | Au | 82 |
| | | | | | Au | 0.0000000 | 2.8850000 | 39.2376780 | 1 | Au | 83 |

16

| | | | |
|---|----------|----------|---------|
| H | -0.07156 | 2.17548 | 7.68171 |
| S | 0.00000 | 0.00000 | 8.84532 |
| C | 0.50713 | 1.25202 | 7.58817 |
| C | 0.27935 | 0.68779 | 6.19879 |
| O | -0.19257 | -0.42886 | 6.00070 |
| H | 0.64496 | 1.53281 | 5.25389 |
| O | 0.48130 | 1.12797 | 4.34907 |
| H | -1.55941 | -1.51808 | 1.16421 |
| H | 1.56514 | 1.51264 | 7.68220 |
| H | -0.47574 | -1.13044 | 4.49644 |
| O | -0.63924 | -1.53530 | 3.59159 |
| O | 0.19550 | 0.42759 | 2.84486 |
| C | -0.27499 | -0.68960 | 2.64667 |
| C | -0.50221 | -1.25392 | 1.25715 |
| S | 0.00000 | -0.00000 | 0.00000 |
| H | 0.07940 | -2.17551 | 1.16316 |

(a) H4

(b) H4 with Electrode

Figure A.5: H4 Structure's XYZ Files

A.3.3 ORCA Input File - H4 Dimer Optimization

```
# =====  
# Orca input file made in Gabedit  
# =====  
! Opt tightSCF B3LYP  
! PrintBasis 6-31G*  
! ECP{TZVP=[Au]}  
  
%output  
  print[p_mos] 1  
end #output  
!PAL8  
  
* xyz 0 1  
H -3.71381 -0.34797 1.19327  
S -4.28103 1.50602 -0.15061  
C -3.44843 -0.00844 0.18222  
C -1.93749 0.00754 0.09493  
O -1.29291 1.01622 -0.19105  
O -1.39188 -1.16951 0.35921  
H -0.39240 -1.10514 0.29309  
H 3.80349 0.75463 0.53062  
H -3.78271 -0.75972 -0.54670  
H 0.39001 1.10519 -0.30167  
O 1.38942 1.16912 -0.36900  
O 1.29046 -1.01476 0.18825  
C 1.93506 -0.00718 -0.10152  
C 3.44591 0.00764 -0.19141  
S 4.19834 -1.54421 0.15961  
H 3.73251 0.32329 -1.20444  
Au -6.67120 1.36685 0.01595  
Au 6.58220 -1.33945 -0.02826  
*
```

Figure A.6: H4 ORCA Input File

A.3.4 SIESTA Input FDF File - H4 Dimer

```

SystemName H4
SystemLabel H4
=====
# SPECIES AND BASIS
# Number of species
NumberOfSpecies 5
%block ChemicalSpeciesLabel
  2 6 C
  1 1 H
  3 16 S
  4 79 Au
  5 8 O
%endblock ChemicalSpeciesLabel

%block PAO.BasisSizes
  C SZ
  H SZ
  S SZ
  Au SZ
  O SZ
%endblock PAO.BasisSizes

%block PS.lmax
  Au 2
%endblock PS.lmax
=====
# K-points
%block kgrid_Monkhorst_Pack
  3 0 0 0.0
  0 3 0 0.0
  0 0 3 0.0
%endblock kgrid_Monkhorst_Pack

T CELL AND ATOMIC POSITIONS
# UNIT CELL
LatticeConstant 1.00 Ang
%block LatticeVectors
  30.00000000 0.0000000000 0.0000000000
  0.0000000000 30.0000000000 0.0000000000
  0.0000000000 0.0000000000 41.7675000000
%endblock LatticeVectors

# Atomic coordinates
NumberOfAtoms 70
AtomicCoordinatesFormat ScaledCartesian
%block AtomicCoordinatesAndAtomicSpecies
-2.1842850000 -1.0537270000 22.9515660000 4 Au
.
<Electrode with Molecule Coordinates Here>
.
-3.5248230000 -2.0411980000 5.2837070000 4 Au
%endblock AtomicCoordinatesAndAtomicSpecies
=====
# General variables
#ElectronicTemperature 100 K
MeshCutoff 380. Ry
xc.functional LDA # Exchange-correlation functional
xc.authors CA
SpinPolarized .false.
SolutionMethod Transiesta
=====

# SCF variables
DM.MixSCF1 T
MaxSCFIterations 300 # Maximum number of SCF iter
DM.MixingWeight 0.03 # New DM amount for next SCF cycle
DM.Tolerance 1.d-4 # Tolerance in maximum difference
DM.UseSaveDM true # to use continuation files
DM.NumberPulay 5
Diag.DivideAndConquer no
Diag.ParallelOverK yes
=====
# MD variables
MD.FinalTimeStep 1
MD.TypeOfRun CG
MD.NumCGSteps 000
MD.UseSaveXV .true.
=====
# Output variables
WriteMullikenPop 1
WriteBands .false.
SaveRho .false.
SaveDeltaRho .false.
SaveHS .false.
SaveElectrostaticPotential True
SaveTotalPotential no
WriteCoorXmol .true.
WriteMDXmol .true.
WriteMDhistory .false.
WriteEigenvalues yes
=====
# Transiesta information
# GF OPTIONS
TS.ComplexContour.Emin -40.0 eV
TS.ComplexContour.NPoles 10
TS.ComplexContour.NCircle 30
TS.ComplexContour.NLine 10
# BIAS OPTIONS
TS.biasContour.NumPoints 00

# TS OPTIONS
TS.Voltage 0.000000 eV

# TBT OPTIONS
TS.TBT.Emin -5.0 eV
TS.TBT.Emax +5.0 eV
TS.TBT.NPoints 500
TS.TBT.NEigen 3
TS.TBT.Eta 0.000001 Ry

# Write hamiltonian
TS.SaveHS .true.

# LEFT ELECTRODE
TS.HSFileLeft ./au.TSHS
#TS.ReplicateA1Left 1
#TS.ReplicateA2Left 1
TS.NumUsedAtomsLeft 13
TS.BufferAtomsLeft 0

# RIGHT ELECTRODE
TS.HSFileRight ./au.TSHS
#TS.ReplicateA1Right 1
#TS.ReplicateA2Right 1
TS.NumUsedAtomsRight 13
TS.BufferAtomsRight 0
=====

```

(a) SIESTA FDF File (1st Half)

(b) SIESTA FDF File (2nd Half)

Figure A.7: H4 FDF File for Electronic Structure Calculations

A.3.5 Gaussian 09 Input File - H4 Dimer Polarizability

```
$ RunGauss
%chk=AcW4.chk
# B3LYP/6-311++G(2d,2p) OPT scf=tight integral=ultrafine Pop=Hirshfeld
H4; calculation 1: Fx=Fy=Fz=0 a.u.
0 1
H      -1.03022      -0.05575      -0.36204
C       0.00000       0.00000       0.00000
C       0.00284       0.01263       1.49828
O       0.40884       0.90567       2.22611
O      -0.52094      -1.12356       1.99737
H      -0.50537      -1.08936       2.98756
H      -0.56808       0.88968       7.19870
H       0.57661      -0.85731      -0.35771
H       0.45088       0.98889       3.88315
O       0.46844       1.02639       4.87306
O      -0.46898      -1.01250       4.71065
C      -0.05000      -0.09790       5.41280
C      -0.00000      -0.00000       6.91290
H       1.05155       0.08514       7.20111
H      -0.42195      -0.83626       7.47836
H       0.46077       0.90994      -0.39422

--link1--
%chk=AcW4.chk
# B3LYP chkbasis geom=check guess=check scf=tight integral=ultrafine Field=X+10
Pop=Hirshfeld
H4; calculation 2: Fx=-0.001 a.u.
0 1

--link1--
%chk=AcW4.chk
# B3LYP chkbasis geom=check guess=check scf=tight integral=ultrafine Field=Y+10
Pop=Hirshfeld
H4; calculation 3: Fy=-0.001 a.u.
0 1

--link1--
%chk=AcW4.chk
# B3LYP chkbasis geom=check guess=check scf=tight integral=ultrafine Field=Z+10
Pop=Hirshfeld
H4; calculation 4: Fz=-0.001 a.u.
0 1
```

Figure A.8: H4 Gaussian 09 Input File

A.4 Relating to Alkanes

A.4.1 *Sample Structure*

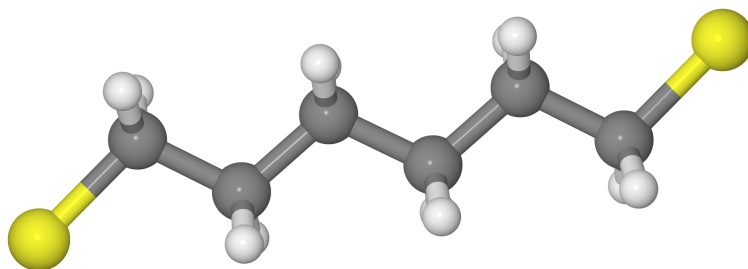


Figure A.9: Structure of A6

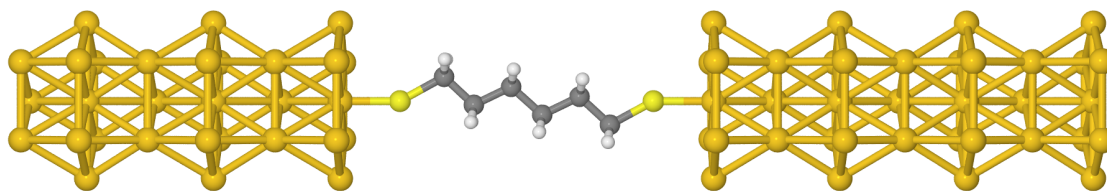


Figure A.10: A6 Between Electrodes

A.4.2 XYZ Files - A6 Alkane

20

```

C      -0.00450      0.89886      1.61943
C      0.00095     -0.14285      2.74632
H      -0.89673      1.52860      1.68789
H      0.88143      1.53731      1.68826
S      0.00000      0.00000     -0.00000
C      -0.00329      0.51249      4.13678
H      -0.87705     -0.79562      2.64413
H      0.88655     -0.78524      2.64456
C      0.00479     -0.51273      5.27901
H      0.87246      1.17148      4.23294
H      -0.88853      1.15856      4.23373
C      -0.00008      0.14264      6.66944
H      -0.87074     -1.17200      5.18261
H      0.89024     -1.15853      5.18230
C      0.00590     -0.89900      7.79639
H      0.87746      0.79602      6.77175
H      -0.88614      0.78444      6.77102
H      0.89871     -1.52793      7.72828
S      0.00000      0.00000      9.41573
H      -0.87943     -1.53824      7.72730
    
```

(a) A6

87

| | | | | | | | |
|----|------------|------------|------------|----|------------|------------|------------|
| Au | -0.8328000 | -1.4425000 | 0.0000000 | H | -0.8861400 | 0.7844400 | 20.7893990 |
| Au | 1.6656000 | 0.0000000 | 0.0000000 | H | 0.8774600 | 0.7960200 | 20.7901290 |
| Au | -0.8328000 | 1.4425000 | 0.0000000 | H | -0.8794300 | -1.5382400 | 21.7456790 |
| Au | 0.0000000 | -2.8850000 | 2.3556000 | H | 0.8987100 | -1.5279300 | 21.7466590 |
| Au | -2.4985000 | -1.4425000 | 2.3556000 | C | 0.0059000 | -0.8990000 | 21.8147690 |
| Au | 2.4985000 | -1.4425000 | 2.3556000 | S | 0.0000000 | 0.0000000 | 23.4341090 |
| Au | 0.0000000 | 0.0000000 | 2.3556000 | Au | 0.0000000 | -2.8850000 | 25.6744880 |
| Au | -2.4985000 | 1.4425000 | 2.3556000 | Au | -2.4985000 | -1.4425000 | 25.6744880 |
| Au | 2.4985000 | 1.4425000 | 2.3556000 | Au | 2.4985000 | -1.4425000 | 25.6744880 |
| Au | 0.0000000 | 2.8850000 | 2.3556000 | Au | 0.0000000 | 0.0000000 | 25.6744880 |
| Au | -0.8328000 | -1.4425000 | 4.7112000 | Au | -2.4985000 | 1.4425000 | 25.6744880 |
| Au | 1.6656000 | 0.0000000 | 4.7112000 | Au | 2.4985000 | 1.4425000 | 25.6744880 |
| Au | -0.8328000 | 1.4425000 | 4.7112000 | Au | 0.0000000 | 2.8850000 | 25.6744880 |
| Au | 0.0000000 | -2.8850000 | 7.0668000 | Au | -0.8328000 | -1.4425000 | 28.0300880 |
| Au | -2.4985000 | -1.4425000 | 7.0668000 | Au | 1.6656000 | 0.0000000 | 28.0300880 |
| Au | 2.4985000 | -1.4425000 | 7.0668000 | Au | -0.8328000 | 1.4425000 | 28.0300880 |
| Au | 0.0000000 | 0.0000000 | 7.0668000 | Au | 0.0000000 | -2.8850000 | 30.3856880 |
| Au | -2.4985000 | 1.4425000 | 7.0668000 | Au | -2.4985000 | -1.4425000 | 30.3856880 |
| Au | 2.4985000 | 1.4425000 | 7.0668000 | Au | 2.4985000 | -1.4425000 | 30.3856880 |
| Au | 0.0000000 | 2.8850000 | 7.0668000 | Au | 0.0000000 | 0.0000000 | 30.3856880 |
| Au | -0.8328000 | -1.4425000 | 9.4224000 | Au | -2.4985000 | 1.4425000 | 30.3856880 |
| Au | 1.6656000 | 0.0000000 | 9.4224000 | Au | 2.4985000 | 1.4425000 | 30.3856880 |
| Au | -0.8328000 | 1.4425000 | 9.4224000 | Au | 0.0000000 | 2.8850000 | 30.3856880 |
| Au | 0.0000000 | -2.8850000 | 11.7780000 | Au | -0.8328000 | -1.4425000 | 32.7412880 |
| Au | -2.4985000 | -1.4425000 | 11.7780000 | Au | 1.6656000 | 0.0000000 | 32.7412880 |
| Au | 2.4985000 | -1.4425000 | 11.7780000 | Au | -0.8328000 | 1.4425000 | 32.7412880 |
| Au | 0.0000000 | 0.0000000 | 11.7780000 | Au | 0.0000000 | -2.8850000 | 35.0968880 |
| Au | -2.4985000 | 1.4425000 | 11.7780000 | Au | -2.4985000 | -1.4425000 | 35.0968880 |
| Au | 2.4985000 | 1.4425000 | 11.7780000 | Au | 2.4985000 | -1.4425000 | 35.0968880 |
| Au | 0.0000000 | 2.8850000 | 11.7780000 | Au | 0.0000000 | 0.0000000 | 35.0968880 |
| S | 0.0000000 | 0.0000000 | 14.0183790 | Au | -2.4985000 | 1.4425000 | 35.0968880 |
| C | -0.0045000 | 0.8988600 | 15.6378090 | Au | 2.4985000 | 1.4425000 | 35.0968880 |
| H | -0.8967300 | 1.5286000 | 15.7062690 | Au | 0.0000000 | 2.8850000 | 35.0968880 |
| H | 0.8814300 | 1.5373100 | 15.7066390 | Au | -0.8328000 | -1.4425000 | 37.4524880 |
| H | -0.8770500 | -0.7956200 | 16.6625090 | Au | 1.6656000 | 0.0000000 | 37.4524880 |
| H | 0.8865500 | -0.7852400 | 16.6629390 | Au | -0.8328000 | 1.4425000 | 37.4524880 |
| C | 0.0009500 | -0.1428500 | 16.7646990 | Au | 0.0000000 | -2.8850000 | 39.8080880 |
| C | -0.0032900 | 0.5124900 | 18.1551590 | Au | -2.4985000 | -1.4425000 | 39.8080880 |
| H | 0.8724600 | 1.1714800 | 18.2513190 | Au | 2.4985000 | -1.4425000 | 39.8080880 |
| H | -0.8885300 | 1.1585600 | 18.2521090 | Au | 0.0000000 | 0.0000000 | 39.8080880 |
| H | 0.8902400 | -1.1585300 | 19.2006790 | Au | -2.4985000 | 1.4425000 | 39.8080880 |
| H | -0.8707400 | -1.1720000 | 19.2009890 | Au | 2.4985000 | 1.4425000 | 39.8080880 |
| C | 0.0047900 | -0.5127300 | 19.2973890 | Au | 0.0000000 | 2.8850000 | 39.8080880 |
| C | -0.0000800 | 0.1426400 | 20.6878190 | | | | |

(b) A6 with Electrode - Part 1

(c) A6 with Electrode - Part 2

Figure A.11: A6 Structure's XYZ Files

A.4.3 ORCA Input File - A6 Optimization

```
# =====  
# Orca input file made in Gabedit  
# =====  
! Opt tightSCF B3LYP  
! PrintBasis 6-31G*  
! ECP{TZVP=[Au]}  
  
%output  
  print[p_mos] 1  
end #output  
!PALB  
  
* xyz 0 1  
C -1.58494 4.04447 -0.04014  
C -0.35085 3.13473 -0.04739  
H -1.60432 4.69314 -0.92536  
H -1.59339 4.69383 0.84437  
S -3.07472 3.10744 -0.02947  
C 0.97381 3.91043 -0.05681  
H -0.38904 2.47263 -0.92459  
H -0.37774 2.47466 0.83190  
C 2.21501 3.00770 -0.06109  
H 1.01047 4.57501 0.81984  
H 1.00078 4.57024 -0.93746  
C 3.53963 3.78341 -0.07282  
H 2.17753 2.34184 -0.93674  
H 2.18885 2.34919 0.82055  
C 4.77377 2.87372 -0.07698  
H 3.57768 4.44822 0.80235  
H 3.56660 4.44075 -0.95415  
H 4.79281 2.22757 0.81009  
S 6.26351 3.81080 -0.08969  
H 4.78260 2.22187 -0.95966  
Au -5.07031 4.44068 -0.01762  
Au 8.25916 2.47764 -0.09695  
*
```

Figure A.12: A6 ORCA Input File

A.4.4 SIESTA Input FDF File - A6 Alkane

```

# SCF variables
DM.MixSCF1 T
MaxSCFIterations 300 # Maximum number of SCF iter
DM.MixingWeight 0.03 # New DM amount for next SCF cycle
DM.Tolerance 1.d-4 # Tolerance in maximum difference
DM.UseSaveDM true # to use continuation files
DM.NumberPulay 5
Diag.DivideAndConquer no
Diag.ParallelOverK yes

SystemName A6
SystemLabel A6

=====
# SPECIES AND BASIS
# Number of species
NumberOfSpecies 4
%block ChemicalSpeciesLabel
  2 6 C
  1 1 H
  3 16 S
  4 79 Au
%endblock ChemicalSpeciesLabel

%block PAO.BasisSizes
  C SZ
  H SZ
  S SZ
  Au SZ
%endblock PAO.BasisSizes

%block PS.lmax
  Au 2
%endblock PS.lmax

=====
# K-points
%block kgrid_Monkhorst_Pack
  3 0 0 0.0
  0 3 0 0.0
  0 0 3 0.0
%endblock kgrid_Monkhorst_Pack

T CELL AND ATOMIC POSITIONS

# UNIT CELL
LatticeConstant 1.00 Ang
%block LatticeVectors
  30.00000000 0.0000000000 0.0000000000
  0.00000000 30.0000000000 0.0000000000
  0.00000000 0.0000000000 41.7975000000
%endblock LatticeVectors

# Atomic coordinates
NumberOfAtoms 74
AtomicCoordinatesFormat ScaledCartesian
%block AtomicCoordinatesAndAtomicSpecies
-3.9443470000 -1.7688930000 34.6039780000 4 Au
.<Electrode with Molecule Coordinates Here>
-2.5985910000 -0.7974370000 -6.6090180000 4 Au
%endblock AtomicCoordinatesAndAtomicSpecies

=====
# General variables
#ElectronicTemperature 100 K
MeshCutoff 380. Ry
xc.functional LDA # Exchange-correlation functional
xc.authors CA
SpinPolarized .false.
SolutionMethod Transiesta

=====
# MD variables
MD.FinalTimeStep 1
MD.TypeOfRun CG
MD.NumGSteps 000
MD.UseSaveXV .true.

=====
# Output variables
WriteMullikenPop 1
WriteBands .false.
SaveRho .false.
SaveDeltaRho .false.
SaveHS .false.
SaveElectrostaticPotential True
SaveTotalPotential no
WriteCoordmol .true.
WriteMDXmol .true.
WriteMDhistory .false.
WriteEigenvalues yes

=====
# Transiesta information
# GF OPTIONS
TS.ComplexContour.Emin -40.0 eV
TS.ComplexContour.NPoles 10
TS.ComplexContour.NCircle 30
TS.ComplexContour.NLine 10
# BIAS OPTIONS
TS.biasContour.NumPoints 00

# TS OPTIONS
TS.Voltage 0.000000 eV

# TBT OPTIONS
TS.TBT.Emin -5.0 eV
TS.TBT.Emax +5.0 eV
TS.TBT.NPoints 500
TS.TBT.NEigen 3
TS.TBT.Eta 0.000001 Ry

# Write hamiltonian
TS.SaveHS .true.

# LEFT ELECTRODE
TS.HSFileLeft ./au.TSHS
#TS.ReplicateA1Left 1
#TS.ReplicateA2Left 1
TS.NumUsedAtomsLeft 13
TS.BufferAtomsLeft 0

# RIGHT ELECTRODE
TS.HSFileRight ./au.TSHS
#TS.ReplicateA1Right 1
#TS.ReplicateA2Right 1
TS.NumUsedAtomsRight 13
TS.BufferAtomsRight 0

=====

```

(a) SIESTA FDF File (1st Half)

(b) SIESTA FDF File (2nd Half)

Figure A.13: A6 FDF File for Electronic Structure Calculations

A.5 Relating to Monomers

A.5.1 Sample Structure

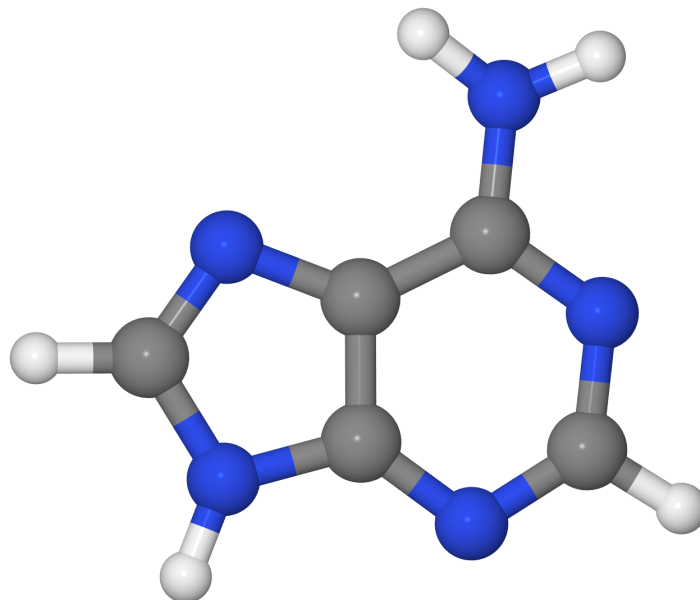


Figure A.14: Structure of Adenine

A.5.2 XYZ File - Adenine

15

```
N      -0.18033      -0.38583      -4.40176
C      -0.46459      -1.10169      -3.30559
C      -0.22052      -0.52833      -2.04542
C       0.31475       0.75875      -2.05047
N       0.61371       1.49205      -3.12441
C       0.33321       0.84287      -4.25326
N      -0.41118      -0.98515      -0.75287
N       0.45249       1.08331      -0.72091
C       0.00000       0.00000       0.00000
N      -0.95179      -2.35783      -3.45007
H       0.54461       1.37331      -5.17336
H       0.00000      -0.00000       1.07743
H       0.81312       1.94910      -0.35871
H      -1.31769      -2.83588      -2.64642
H      -1.24752      -2.64530      -4.36607
```

Figure A.15: Adenine Structure's XYZ File

A.5.3 Gaussian 09 Input File - Adenine

```
$ RunGauss

%chk=AcW2.chk

# B3LYP/6-311++G(2d,2p) OPT scf=tight integral=ultrafine Pop=Hirshfeld

P2; calculation 1: Fx=Fy=Fz=0 a.u.

0 1
N      -0.91736      0.11995      0.32230
C       0.11763      0.99080      0.26870
C       1.41745      0.47696      0.12635
C       1.53448     -0.90148      0.08555
N       0.55309     -1.81166      0.15383
C      -0.64637     -1.20402      0.26961
N       2.65811      1.07396      0.00840
N       2.87204     -1.14156     -0.03347
C       3.50641      0.07052     -0.08052
N      -0.16082      2.34905      0.34834
H      -1.50807     -1.86312      0.32881
H       4.58090      0.15679     -0.17754
H       3.29909     -2.05456     -0.07503
H       0.57498      2.93722     -0.02577
H      -1.11593      2.56215      0.09479

--link1--
%chk=AcW2.chk
# B3LYP chkbasis geom=check guess=check scf=tight integral=ultrafine Field=X+10
Pop=Hirshfeld

P2; calculation 2: Fx=-0.001 a.u.

0 1

--link1--
%chk=AcW2.chk
# B3LYP chkbasis geom=check guess=check scf=tight integral=ultrafine Field=Y+10
Pop=Hirshfeld

P2; calculation 3: Fy=-0.001 a.u.

0 1

--link1--
%chk=AcW2.chk
# B3LYP chkbasis geom=check guess=check scf=tight integral=ultrafine Field=Z+10
Pop=Hirshfeld

P2; calculation 4: Fz=-0.001 a.u.

0 1
```

Figure A.16: Adenine Optimization and Polarizability Input File

A.6 Relating to DNA/RNA Base Pairs

A.6.1 Sample Structure

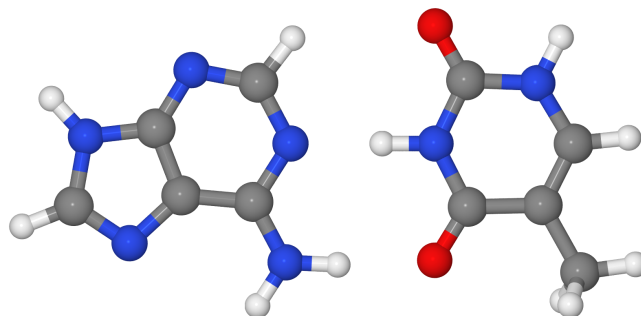


Figure A.17: Structure of Adenine-Thymine

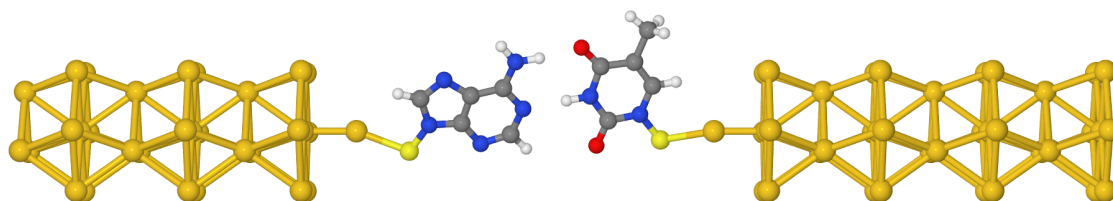


Figure A.18: A-T Between Electrodes

A.6.2 XYZ File - A-T Base Pair

```
30
H      4.313730      2.470889      0.001102
N      3.846692      1.576744      0.000495
C      2.461761      1.636745      0.000164
O      1.856349      2.691838      0.000165
N      1.864067      0.399138      -0.000164
C      2.492708      -0.830802     -0.000296
O      1.842318      -1.876171     -0.000894
C      3.952452      -0.803564     0.000344
C      4.682549      -2.106122     0.000423
C      4.555223      0.404750     0.000731
H      0.816146      0.402313     -0.000589
H      5.635344      0.514002     0.001172
H      4.413782      -2.703356     -0.877560
H      4.413144      -2.703617     0.878020
H      5.765972      -1.954482     0.000826
H      -5.641738     1.278720     0.000879
N      -0.973371     0.403405     -0.001104
C      -1.597803     1.590738     -0.000978
N      -2.901421     1.834036     -0.000437
C      -3.601544     0.694553     0.000043
C      -3.101743     -0.606312     0.000027
C      -1.696314     -0.733302     -0.000567
N      -1.068284     -1.912278     -0.000652
N      -4.114420     -1.539236     0.000687
C      -5.203133     -0.817658     0.001059
N      -4.962160     0.533873     0.000694
H      -0.932987     2.452235     -0.001371
H      -1.617731     -2.755993     0.000021
H      -0.046480     -1.958435     -0.000607
H      -6.211176     -1.211548     0.001598
```

Figure A.19: A-T Structure's XYZ File

| | | | | | | | |
|----|------------|------------|------------|----|------------|------------|------------|
| | | | | O | -2.9314300 | 2.3393400 | 23.5289690 |
| | | | | N | -1.0827200 | 1.0764100 | 23.9010390 |
| | | | | O | 0.7159000 | -0.2793600 | 24.1902090 |
| 99 | | | | C | -2.0742200 | 1.9272200 | 24.3465290 |
| | | | | C | -0.1222200 | 0.4586700 | 24.6769890 |
| | | | | H | -3.6892300 | 3.4042500 | 25.6044190 |
| Au | -0.8328000 | -1.4425000 | 0.0000000 | C | -2.0564600 | 2.1566400 | 25.7718490 |
| Au | 1.6656000 | 0.0000000 | 0.0000000 | N | -0.1831700 | 0.7357800 | 26.0219790 |
| Au | -0.8328000 | 1.4425000 | 0.0000000 | C | -3.1014600 | 3.0703500 | 26.3406990 |
| Au | 0.0000000 | -2.8850000 | 2.3556000 | C | -1.1338800 | 1.5686800 | 26.5500490 |
| Au | -2.4985000 | -1.4425000 | 2.3556000 | H | -2.6580400 | 3.8462000 | 26.7897590 |
| Au | 2.4985000 | -1.4425000 | 2.3556000 | S | 0.8363900 | 0.0878700 | 26.8938490 |
| Au | 0.0000000 | 0.0000000 | 2.3556000 | H | -3.6540800 | 2.5705100 | 27.0079390 |
| Au | -2.4985000 | 1.4425000 | 2.3556000 | H | -1.1399200 | 1.7425400 | 27.5351590 |
| Au | 2.4985000 | 1.4425000 | 2.3556000 | Au | 0.0000000 | 0.0000000 | 29.1416790 |
| Au | 0.0000000 | 2.8850000 | 2.3556000 | Au | 0.0000000 | -2.8850000 | 31.3820580 |
| Au | -0.8328000 | -1.4425000 | 4.7112000 | Au | -2.4985000 | -1.4425000 | 31.3820580 |
| Au | 1.6656000 | 0.0000000 | 4.7112000 | Au | 2.4985000 | -1.4425000 | 31.3820580 |
| Au | -0.8328000 | 1.4425000 | 4.7112000 | Au | 0.0000000 | 0.0000000 | 31.3820580 |
| Au | 0.0000000 | -2.8850000 | 7.0668000 | Au | -2.4985000 | 1.4425000 | 31.3820580 |
| Au | -2.4985000 | -1.4425000 | 7.0668000 | Au | 2.4985000 | 1.4425000 | 31.3820580 |
| Au | 2.4985000 | -1.4425000 | 7.0668000 | Au | 0.0000000 | 2.8850000 | 31.3820580 |
| Au | 0.0000000 | 0.0000000 | 7.0668000 | Au | -0.8328000 | -1.4425000 | 33.7376580 |
| Au | -2.4985000 | 1.4425000 | 7.0668000 | Au | 1.6656000 | 0.0000000 | 33.7376580 |
| Au | 2.4985000 | 1.4425000 | 7.0668000 | Au | -0.8328000 | 1.4425000 | 33.7376580 |
| Au | 0.0000000 | 2.8850000 | 7.0668000 | Au | 0.0000000 | -2.8850000 | 36.0932580 |
| Au | -0.8328000 | -1.4425000 | 9.4224000 | Au | -2.4985000 | -1.4425000 | 36.0932580 |
| Au | 1.6656000 | 0.0000000 | 9.4224000 | Au | 2.4985000 | -1.4425000 | 36.0932580 |
| Au | -0.8328000 | 1.4425000 | 9.4224000 | Au | 0.0000000 | 0.0000000 | 36.0932580 |
| Au | 0.0000000 | -2.8850000 | 11.7780000 | Au | -2.4985000 | 1.4425000 | 36.0932580 |
| Au | -2.4985000 | -1.4425000 | 11.7780000 | Au | 2.4985000 | 1.4425000 | 36.0932580 |
| Au | 2.4985000 | -1.4425000 | 11.7780000 | Au | 0.0000000 | 2.8850000 | 36.0932580 |
| Au | 0.0000000 | 0.0000000 | 11.7780000 | Au | -0.8328000 | -1.4425000 | 38.4488580 |
| Au | -2.4985000 | 1.4425000 | 11.7780000 | Au | 1.6656000 | 0.0000000 | 38.4488580 |
| Au | 2.4985000 | 1.4425000 | 11.7780000 | Au | -0.8328000 | 1.4425000 | 38.4488580 |
| Au | 0.0000000 | 2.8850000 | 11.7780000 | Au | 0.0000000 | -2.8850000 | 40.8044580 |
| Au | 0.0000000 | 0.0000000 | 14.0183790 | Au | -2.4985000 | -1.4425000 | 40.8044580 |
| H | -2.2849700 | 0.4624100 | 15.8498390 | Au | 2.4985000 | -1.4425000 | 40.8044580 |
| S | 0.2682800 | -0.7970500 | 16.2662090 | Au | 0.0000000 | 0.0000000 | 40.8044580 |
| C | -1.9483100 | 0.4315000 | 16.7907490 | Au | -2.4985000 | 1.4425000 | 40.8044580 |
| N | -0.7452500 | -0.1397500 | 17.1380790 | Au | 2.4985000 | 1.4425000 | 40.8044580 |
| N | -2.6061800 | 0.9246200 | 17.7939590 | Au | 0.0000000 | 2.8850000 | 40.8044580 |
| C | -0.6568300 | 0.0201900 | 18.4958890 | Au | -0.8328000 | -1.4425000 | 43.1600580 |
| C | -1.7918500 | 0.6678100 | 18.8875290 | Au | 1.6656000 | 0.0000000 | 43.1600580 |
| N | 0.3563200 | -0.3841100 | 19.2910890 | Au | -0.8328000 | 1.4425000 | 43.1600580 |
| H | -3.7385100 | 1.8744300 | 20.1880890 | Au | 0.0000000 | -2.8850000 | 45.5156580 |
| C | -1.9297800 | 0.9471900 | 20.2571290 | Au | -2.4985000 | -1.4425000 | 45.5156580 |
| C | 0.1189800 | -0.0707700 | 20.5453190 | Au | 2.4985000 | -1.4425000 | 45.5156580 |
| N | -2.9909100 | 1.5766200 | 20.7816090 | Au | 0.0000000 | 0.0000000 | 45.5156580 |
| N | -0.9329700 | 0.5544500 | 21.0722390 | Au | -2.4985000 | 1.4425000 | 45.5156580 |
| H | 0.8279300 | -0.3399400 | 21.1966190 | Au | 2.4985000 | 1.4425000 | 45.5156580 |
| H | -3.0345500 | 1.7492800 | 21.7651690 | Au | 0.0000000 | 2.8850000 | 45.5156580 |
| H | -1.0582700 | 0.8886700 | 22.9185790 | Au | 0.0000000 | 2.8850000 | 45.5156580 |

(a) A-T with Electrode - Part 1

(b) A-T with Electrode - Part 2

Figure A.20: A-T Structure's XYZ Files

A.6.3 Gaussian 09 Input File - A-T Base Pair

```
$ RunGauss
%chk=AcW8.chk
# B3LYP/6-311++G(2d,2p) OPT FREQ scf=tight integral=ultrafine
A Base; calculation 1: Fx=Fy=Fz=0 a.u.
0 1
H      4.3137300      2.4708890      0.0011020
N      3.8466920      1.5767440      0.0004950
C      2.4617610      1.6367450      0.0001640
O      1.8563490      2.6918380      0.0001650
N      1.8640670      0.3991380     -0.0001640
C      2.4927080     -0.8308020     -0.0002960
O      1.8423180     -1.8761710     -0.0008940
C      3.9524520     -0.8035640      0.0003440
C      4.6825490     -2.1061220      0.0004230
C      4.5552230      0.4047500      0.0007310
H      0.8161460      0.4023130     -0.0005890
H      5.6353440      0.5140020      0.0011720
H      4.4137820     -2.7033560     -0.8775600
H      4.4131440     -2.7036170      0.8780200
H      5.7659720     -1.9544820      0.0008260
H      -5.6417380      1.2787200      0.0008790
N      -0.9733710      0.4034050     -0.0011040
C      -1.5978030      1.5907380     -0.0009780
N      -2.9014210      1.8340360     -0.0004370
C      -3.6015440      0.6945530      0.0000430
C      -3.1017430     -0.6063120      0.0000270
C      -1.6963140     -0.7333020     -0.0005670
N      -1.0682840     -1.9122780     -0.0006520
N      -4.1144200     -1.5392360      0.0006870
C      -5.2031330     -0.8176580      0.0010590
N      -4.9621600      0.5338730      0.0006940
H      -0.9329870      2.4522350     -0.0013710
H      -1.6177310     -2.7559930      0.0000210
H      -0.0464800     -1.9584350     -0.0006070
H      -6.2111760     -1.2115480      0.0015980
```

Figure A.21: A-T Optimization Input File

A.6.4 SIESTA Input FDF File - A-T Base Pair

```

SystemName A-T
SystemLabel A-T

=====
# SPECIES AND BASIS
# Number of species
NumberOfSpecies 6
%block ChemicalSpeciesLabel
  1 79 Au
  2 16 S
  3 6 C
  4 1 H
  5 8 O
  6 7 N
%endblock ChemicalSpeciesLabel

%block PAO.BasisSizes
  Au DZ
  S DZ
  C DZ
  H DZP
  O DZ
  N DZ
%endblock PAO.BasisSizes

PAO.BasisType split
PAO.SplitNorm 0.15
PAO.EnergyShift 0.01 eV

%block PS.lmax
  Au 2
%endblock PS.lmax
=====
# K-points

%block kgrid_Monkhorst_Pack
  1 0 0 0.0
  0 1 0 0.0
  0 0 1 0.0
%endblock kgrid_Monkhorst_Pack
BandLinesScale ReciprocalLatticeVectors

T CELL AND ATOMIC POSITIONS

# UNIT CELL
LatticeConstant 1.00 Ang
%block LatticeVectors
  30.00000000 0.0000000000 0.0000000000
  0.00000000 30.0000000000 0.0000000000
  0.00000000 0.0000000000 50.2265000000
%endblock LatticeVectors

# Atomic coordinates
NumberOfAtoms 99
AtomicCoordinatesFormat ScaledCartesian
%block AtomicCoordinatesAndAtomicSpecies
  -0.8328000 -1.4425000 0.0000000 1 Au 1
  .
  <Electrode with Molecule Coordinates Here>
  .
  0.0000000 2.8850000 45.5156500 1 Au 99
%endblock AtomicCoordinatesAndAtomicSpecies
=====
# General variables

#ElectronicTemperature 300 K
MeshCutoff 200.0 Ry
xc.functional GGA # Exchange-correlation functional
xc.authors PBE
SpinPolarized .false.
SolutionMethod Transiesta
=====
# SCF variables

DM.MixSCF1 T
MaxSCFIterations 30000 # Maximum number of SCF iter
DM.MixingWeight 0.02 # New DM amount for next SCF cycle
DM.Tolerance 1.00-5 # Tolerance in maximum difference
DM.UseSaveDM T # to use continuation files
DM.NumberPulay 4
Diag.DivideAndConquer no
Diag.ParallelOverK yes

=====
# MD variables

MD.FinalTimeStep 1
MD.TypeOfRun CG
MD.NumCGsteps 000
MD.UseSaveXV .true.

=====
# Output variables

WriteMullikenPop 1
WriteBands .false.
SaveRho .false.
SaveDeltaRho .false.
SaveHS .false.
SaveElectrostaticPotential True
SaveTotalPotential no
WriteCoorXmol .true.
WriteMDXmol .true.
WriteMDhistory .false.
WriteEigenvalues yes

=====
# Transiesta information

# GF OPTIONS
TS.ComplexContour.Emin -20.0 Ry
TS.ComplexContour.NumPoles 10
TS.ComplexContour.NumCircle 100
TS.ComplexContour.NumLine 20
# BIAS OPTIONS
TS.BiasContour.NumPoints 100
TS.BiasContour.Eta 100-4 Ry

# TS OPTIONS
TS.Voltage 0.000000 eV

# TBT OPTIONS
TS.TBT.Emin -1.0 eV
TS.TBT.Emax +1.0 eV
TS.TBT.NPoints 1000
TS.TBT.NEigen 3
TS.TBT.Eta 0.000001 Ry
TS.TBT.OutputRegionData False

# Write hamiltonian
TS.SaveHS .true.

# LEFT ELECTRODE
TS.HSFileLeft ./Auleads.TSHS
#TS.ReplicateA1Left 1
#TS.ReplicateA2Left 1
TS.NumUsedAtomsLeft 20
TS.BufferAtomsLeft 0

# RIGHT ELECTRODE
TS.HSFileRight ./Auleads.TSHS
#TS.ReplicateA1Right 1
#TS.ReplicateA2Right 1
TS.NumUsedAtomsRight 20
TS.BufferAtomsRight 0
=====

```

(a) SIESTA FDF File (1st Half)

(b) SIESTA FDF File (2nd Half)

Figure A.22: A-T FDF File for Electronic Structure Calculations

A.6.5 Gaussian 09 Input File - A-T Base Pair

```

$ RunGauss

%chk=AcW5.chk

# B3LYP/6-311++G(2d,2p) scf=tight integral=ultrafine Pop=Hirshfeld

A-T Base; calculation 1: Fx=Fy=Fz=0 a.u.

0 1
H 4.3137300 2.4708890 0.0011020
N 3.8466920 1.5767440 0.0004950
C 2.4617610 1.6367450 0.0001640
O 1.8563490 2.6918380 0.0001650
N 1.8640670 0.3991380 -0.0001640
C 2.4927080 -0.8300020 -0.0002960
O 1.8423180 -1.8761710 -0.0008940
C 3.9524520 -0.8035640 0.0003440
C 4.6825490 -2.1061220 0.0004230
C 4.5552230 0.4047500 0.0007310
H 0.8161460 0.4023130 -0.0005890
H 5.6353440 0.5140020 0.0011720
H 4.4137820 -2.7033560 -0.8775600
H 4.4131440 -2.7036170 0.8780200
H 5.7659720 -1.9544820 0.0008260
H -5.6417380 1.2787200 0.0008790
N -0.9733710 0.4034050 -0.0011040
C -1.5978030 1.5907380 -0.0009780
N -2.9014210 1.8340360 -0.0004370
C -3.6015440 0.6945530 0.0000430
C -3.1017430 -0.6063120 0.0000270
C -1.6963140 -0.7333020 -0.0005670
N -1.0682840 -1.9122780 -0.0006520
N -4.1144200 -1.5392360 0.0006870
C -5.2031330 -0.8176580 0.0010590
N -4.9621600 0.5338730 0.0006940
H -0.9329870 2.4522350 -0.0013710
H -1.6177310 -2.7559930 0.0000210
H -0.0464800 -1.9584350 -0.0006070
H -6.2111760 -1.2115480 0.0015980

--link1--
%chk=AcW5.chk
# B3LYP/6-311++G(2d,2p) chkbasis geom=check guess=check scf=tight integral=ultrafine Field=X+10
Pop=Hirshfeld

A-T Base; calculation 2: Fx=-0.001 a.u.

0 1

--link1--
%chk=AcW5.chk
# B3LYP/6-311++G(2d,2p) chkbasis geom=check guess=check scf=tight integral=ultrafine Field=Y+10
Pop=Hirshfeld

A-T Base; calculation 3: Fy=-0.001 a.u.

0 1

--link1--
%chk=AcW5.chk
# B3LYP/6-311++G(2d,2p) chkbasis geom=check guess=check scf=tight integral=ultrafine Field=Z+10
Pop=Hirshfeld

A-T Base; calculation 4: Fz=-0.001 a.u.

0 1

```

Figure A.23: A-T Polarizability Input File

APPENDIX B
REPRINT PERMISSIONS

B.1 Chapter 1

| ROYAL SOCIETY OF CHEMISTRY LICENSE TERMS AND CONDITIONS | |
|--|---|
| Apr 18, 2017 | |
| <hr/> | |
| This Agreement between Micah Wimmer ("You") and Royal Society of Chemistry ("Royal Society of Chemistry") consists of your license details and the terms and conditions provided by Royal Society of Chemistry and Copyright Clearance Center. | |
| License Number | 4092081292030 |
| License date | |
| Licensed Content Publisher | Royal Society of Chemistry |
| Licensed Content Publication | Analytical Methods |
| Licensed Content Title | Multimodal scanning probe imaging: nanoscale chemical analysis from biology to renewable energy |
| Licensed Content Author | J. J. Bang, S. R. Russell, K. K. Rupp, S. A. Claridge |
| Licensed Content Date | Jul 6, 2015 |
| Licensed Content Volume | 7 |
| Licensed Content Issue | 17 |
| Type of Use | Thesis/Dissertation |
| Requestor type | academic/educational |
| Portion | figures/tables/images |
| Number of figures/tables/images | 1 |
| Format | print and electronic |
| Distribution quantity | 100 |
| Will you be translating? | no |
| Order reference number | |
| Title of the thesis/dissertation | A Computational and Theoretical Study of Conductance in Hydrogen-bonded Molecular Junctions |
| Expected completion date | Apr 2017 |
| Estimated size | 110 |
| Requestor Location | Micah Wimmer |
| | Attn: Micah Wimmer |
| Billing Type | Invoice |
| Billing Address | Micah Wimmer |
| | ----- Attn: Micah Wimmer |
| Total | 0.00 USD |

Figure B.1: Reprint Permission for Used Figure

JOHN WILEY AND SONS LICENSE TERMS AND CONDITIONS

Mar 27, 2017

This Agreement between Micah Wimmer ("You") and John Wiley and Sons ("John Wiley and Sons") consists of your license details and the terms and conditions provided by John Wiley and Sons and Copyright Clearance Center.

| | |
|---------------------------------------|---|
| License Number | 4077220802863 |
| License date | Mar 27, 2017 |
| Licensed Content Publisher | John Wiley and Sons |
| Licensed Content Publication | Annals of the New York Academy of Sciences |
| Licensed Content Title | Molecular Wires: Charge Transport, Mechanisms, and Control |
| Licensed Content Author | MARK A. RATNER,BILL DAVIS,MATHIEU KEMP,VLADIMIRO MUJICA,ADRIAN ROITBERG,SOPHIA YALIRAKI |
| Licensed Content Date | Feb 7, 2006 |
| Licensed Content Pages | 16 |
| Type of Use | Dissertation/Thesis |
| Requestor type | University/Academic |
| Format | Print and electronic |
| Portion | Figure/table |
| Number of figures/tables | 1 |
| Original Wiley figure/table number(s) | Table 1 |
| Will you be translating? | No |
| Title of your thesis / dissertation | A Computational and Theoretical Study of Conductance in Hydrogen-bonded Molecular Junctions |
| Expected completion date | Apr 2017 |
| Expected size (number of pages) | 110 |
| Requestor Location | Micah Wimmer |
| | United States |
| | Attn: Micah Wimmer |
| Publisher Tax ID | EU826007151 |
| Billing Type | Invoice |
| Billing Address | Micah Wimmer |
| | United States |
| | Attn: Micah Wimmer |
| Total | 0.00 USD |

Figure B.2: Reprint Permission for Used Table

B.2 Chapter 2

AIP PUBLISHING LLC LICENSE TERMS AND CONDITIONS

Apr 04, 2017

This Agreement between Micah Wimmer ("You") and AIP Publishing LLC ("AIP Publishing LLC") consists of your license details and the terms and conditions provided by AIP Publishing LLC and Copyright Clearance Center.

| | |
|-------------------------------------|---|
| License Number | 4082030466475 |
| License date | Apr 04, 2017 |
| Licensed Content Publisher | AIP Publishing LLC |
| Licensed Content Publication | Journal of Applied Physics |
| Licensed Content Title | Quantum interference in thermoelectric molecular junctions: A toy model perspective |
| Licensed Content Author | |
| Licensed Content Date | Aug 21, 2014 |
| Licensed Content Volume | 116 |
| Licensed Content Issue | 7 |
| Type of Use | Thesis/Dissertation |
| Requestor type | Student |
| Format | Print and electronic |
| Portion | Figure/Table |
| Number of figures/tables | 1 |
| Title of your thesis / dissertation | A Computational and Theoretical Study of Conductance in Hydrogen-bonded Molecular Junctions |
| Expected completion date | Apr 2017 |
| Estimated size (number of pages) | 110 |
| Requestor Location | Micah Wimmer |
| | United States |
| | Attn: Micah Wimmer |
| Billing Type | Invoice |
| Billing Address | Micah Wimmer |
| | United States |
| | Attn: Micah Wimmer |
| Total | 0.00 USD |

Figure B.3: Reprint Permission for Used Figure

**AMERICAN PHYSICAL SOCIETY LICENSE
TERMS AND CONDITIONS**

Apr 12, 2017

This Agreement between Micah Wimmer ("You") and American Physical Society ("American Physical Society") consists of your license details and the terms and conditions provided by American Physical Society and Copyright Clearance Center.

| | |
|---|---|
| License Number | 4086661480151 |
| License date | Apr 12, 2017 |
| Licensed Content Publisher | American Physical Society |
| Licensed Content Publication | Reviews of Modern Physics |
| Licensed Content Title | Fano resonances in nanoscale structures |
| Licensed Content Author | Andrey E. Miroshnichenko, Sergej Flach, and Yuri S. Kivshar |
| Licensed Content Date | Aug 11, 2010 |
| Licensed Content Volume | 82 |
| Type of Use | Thesis/Dissertation |
| Requestor type | Student |
| Format | Print, Electronic |
| Portion | chart/graph/table/figure |
| Number of charts/graphs/tables/figures | 2 |
| Portion description | Figure 4, Figure 5 |
| Rights for | Main product |
| Duration of use | Life of Current Edition |
| Creation of copies for the disabled | no |
| With minor editing privileges | no |
| For distribution to | Worldwide |
| In the following language(s) | Original language of publication |
| With incidental promotional use | no |
| The lifetime unit quantity of new product | 0 to 499 |
| The requesting person/organization is: | Micah Wimmer |
| Order reference number | |
| Title of your thesis / dissertation | A Computational and Theoretical Study of Conductance in Hydrogen-bonded Molecular Junctions |
| Expected completion date | Apr 2017 |
| Expected size (number of pages) | 110 |
| Requestor Location | Micah Wimmer |

Figure B.4: Reprint Permission for Used Figures

B.3 Chapter 4

The screenshot displays the Copyright Clearance Center RightsLink interface. At the top left is the Copyright Clearance Center logo. To its right is the RightsLink logo. Further right are navigation buttons for Home, Account Info, Help, and an email icon. Below the logo is the ACS Publications logo with the tagline "Most Trusted. Most Cited. Most Read." The main content area lists the following details:

- Title:** Single-Molecule Conductance through Hydrogen Bonds: The Role of Resonances
- Author:** Micah Wimmer, Julio L. Palma, Pilarisetty Tarakeshwar, et al
- Publication:** Journal of Physical Chemistry Letters
- Publisher:** American Chemical Society
- Date:** Aug 1, 2016

Below the article details, it states "Copyright © 2016, American Chemical Society". To the right of the article details, a box indicates the user is logged in as "Micah Wimmer" with a "LOGOUT" button.

PERMISSION/LICENSE IS GRANTED FOR YOUR ORDER AT NO CHARGE

This type of permission/license, instead of the standard Terms & Conditions, is sent to you because no fee is being charged for your order. Please note the following:

- Permission is granted for your request in both print and electronic formats, and translations.
- If figures and/or tables were requested, they may be adapted or used in part.
- Please print this page for your records and send a copy of it to your publisher/graduate school.
- Appropriate credit for the requested material should be given as follows: "Reprinted (adapted) with permission from (COMPLETE REFERENCE CITATION). Copyright (YEAR) American Chemical Society." Insert appropriate information in place of the capitalized words.
- One-time permission is granted only for the use specified in your request. No additional uses are granted (such as derivative works or other editions). For any other uses, please submit a new request.

At the bottom of the main content area are two buttons: "BACK" and "CLOSE WINDOW".

At the very bottom of the page, there is a footer with the following text: "Copyright © 2017 Copyright Clearance Center, Inc. All Rights Reserved. [Privacy statement](#). [Terms and Conditions](#). Comments? We would like to hear from you. E-mail us at customer@copyright.com"

Figure B.5: Reprint Permission for Original Work